SEISMIC DESIGN AND PERFORMANCE ASSESSMENT OF POST-TENSIONED CROSS-LAMINATED TIMBER SHEAR WALL BUILDINGS

By

Huanru ZHU

Department of Civil Engineering

McGill University, Montréal, Québec, Canada

July 2024

A thesis submitted to McGill University in partial fulfillment of the requirements of the degree of Master of Science

ABSTRACT

Traditional mass timber lateral systems dissipate energy during seismic excitation primarily depending on the inelastic deformation of metal connectors. Under large drift, permanent damage to conventional connectors could result in significant residual drift of buildings and subsequent high repair costs, potential necessity for building demolishment, as well as a risk of aftershock collapse. A post-tensioned rocking wall system incorporating Cross-laminated timber panels (PT-CLT) and replaceable energy dissipation devices can produce self-centring and ductile seismic force-resisting systems (SFRSs) that are resilient, economical, and easily constructible. Global efforts have been made to explore the applicability of PT-CLT walls as primary SFRSs in mass timber buildings. Nonetheless, most studies have evaluated either low to moderate seismicity or simple seismotectonics (e.g., shallow crustal). In this thesis, to further promote the applicability of this system, the seismic performance of mass timber buildings with PT-CLT shear walls has been assessed in high seismic regions in Canada. The performance assessment considered the increased seismic hazard resulting from the sixth-generation seismic hazard model in the 2020 version of the National Building Code of Canada.

At first, performance assessments were conducted for six-, nine-, and twelve-storey prototype mass timber buildings with PT-CLT shear walls equipped with buckling-restrained axial fuses (BRAFs), which are hypothetically located in the city of Vancouver, Canada. A fibre-based numerical modelling strategy was adopted in *OpenSeesPy*, calibrated with component-level testing and validated with system-level quasi-static reversed cyclic experiments. The direct displacement-based design (DDBD) approach was used to design prototype buildings, and thirty-three ground motions reflecting three damage sources from earthquakes in Vancouver were selected and scaled. Post-earthquake performance indicators (i.e., storey shear and drift responses) based on nonlinear response history analyses (NLRHA) demonstrated the acceptability of the DDBD method and the adequate performance of the lateral system under the maximum credible earthquake (MCE) (2% in 50 years). Incremental dynamic analyses (IDAs) were carried out to examine the buildings' collapse and drift-exceedance fragilities and concluded satisfactory buildings performance.

Next, performance evaluations were similarly carried out for three-, six-, and nine-storey PT-CLT shear wall buildings with coupling U-shaped flexural plates (UFPs) in Vancouver designed using DDBD. The fibre-based models were adopted and further validated with a shaking table test of a two-storey PT-CLT shear wall building. Nonlinear static analyses yielded the backbone curves of prototype buildings, which indicated that buildings at the design target drift are not likely to be damaged due to CLT crushing. Besides using the same ground motions records employed in the previous section for NLRHA, additional ensembles of records were selected for each building and scaled to each seismotectonic regime's Conditional Spectra for IDA. Based on fragility analysis, the collapse probabilities for all buildings were significantly lower than 10% under MCE. Overall, this study demonstrated that PT-CLT walls with BRAFs and coupling UFPs are a potential SFRS alternative in Canada's high seismic-risk regions.

RESUME

Les systèmes latéraux traditionnels en bois massif dissipent l'énergie lors d'une excitation sismique principalement en fonction de la déformation inélastique des connecteurs métalliques. En cas de dérive importante, des dommages permanents aux connecteurs conventionnels pourraient entraîner une dérive résiduelle importante des bâtiments et des coûts de réparation élevés qui en résulteraient, ainsi qu'un risque d'effondrement par réplique. Un système de mur à bascule post-tendu intégrant des panneaux CLT (PT-CLT) et des dispositifs de dissipation d'énergie remplaçables peut produire des systèmes de résistance aux forces sismiques (SFRS) auto-centrants et ductiles qui sont résilients, économiques et faciles à construire. Des efforts mondiaux ont été déployés pour explorer l'applicabilité des murs PT-CLT comme principaux SFRS dans les bâtiments en bois massif. Néanmoins, la plupart des études ont évalué soit une sismicité faible à modérée, soit une sismotectonique simple (par exemple, croûte peu profonde). Dans cette thèse, afin de promouvoir davantage l'applicabilité de ce système, la performance sismique de bâtiments en bois massif avec murs de contreventement PT-CLT a été évaluée dans des régions sismiques élevées au Canada. L'évaluation des performances a pris en compte le risque sismique accru résultant du modèle de risque sismique de sixième génération dans la version 2020 du Code national du bâtiment du Canada.

Dans un premier temps, des évaluations des performances ont été réalisées pour des bâtiments prototypes en bois massif de six, neuf et douze étages dotés de murs de contreventement en PT-CLT équipés de fusibles axiaux à retenue de flambage (BRAF), qui sont hypothétiquement situés dans la ville de Vancouver, au Canada. . Une stratégie de modélisation numérique basée sur les fibres a été adoptée dans OpenSeesPy, calibrée avec des tests au niveau des composants et validée avec des expériences cycliques inversées quasi-statiques au niveau du système. L'approche de conception basée sur le déplacement direct (DDBD) a été utilisée pour concevoir des bâtiments prototypes, et trente-trois mouvements du sol reflétant trois sources de dommages causés par les tremblements de terre à Vancouver ont été sélectionnés et mis à l'échelle. Les indicateurs de performance post-séisme (c'est-à-dire les réponses au cisaillement et à la dérive des étages) basés sur des analyses d'historique de réponse non linéaire (NLRHA) ont démontré l'acceptabilité de la méthode DDBD et la performance adéquate du système latéral sous le séisme maximum crédible

(MCE) (2 % en 50 ans). Des analyses dynamiques incrémentales (IDA) ont été réalisées pour examiner les fragilités en matière d'effondrement et de dépassement de dérive des bâtiments et ont conclu que les performances des bâtiments étaient satisfaisantes.

Ensuite, des évaluations de performance ont été réalisées de la même manière pour des bâtiments à murs de cisaillement en PT-CLT de trois, six et neuf étages avec des plaques de flexion en forme de U (UFP) de couplage conçues à l'aide du DDBD à Vancouver. Les modèles à base de fibres ont été adoptés et validés par un essai sur table vibrante d'un bâtiment à murs de contreventement en PT-CLT de deux étages. Des analyses statiques non linéaires ont donné les courbes de base des bâtiments prototypes, ce qui indique que les bâtiments situés à la dérive cible de conception ne sont pas susceptibles d'être endommagés en raison de l'écrasement du CLT. En plus d'utiliser les mêmes enregistrements de mouvements du sol utilisés dans la section précédente pour NLRHA, des ensembles supplémentaires d'enregistrements ont été sélectionnés pour chaque bâtiment et adaptés aux spectres conditionnels de chaque régime sismotectonique pour l'IDA. Sur la base de l'analyse de fragilité, les probabilités d'effondrement de tous les bâtiments étaient nettement inférieures à 10 % dans le cadre du MCE. Dans l'ensemble, cette étude a démontré que les murs PT-CLT avec BRAF et UFP de couplage constituent une alternative potentielle au SFRS dans les régions à haut risque sismique du Canada.

PREFACE

The research work presented in this thesis was conducted at McGill University under the supervision of Professor Matiyas Bezabeh. The author is responsible for the literature review, development and validation of numerical models, design calculations, result analysis from simulations, and the write-up. The research outcomes, which have been published or submitted to journal publications and conference presentations, are summarised below.

Journal Papers

- Zhu, H., Bezabeh, M., Iqbal, A., Popovski, M., Chen, Z., (2024). Seismic Performance Assessment of Post-Tensioned CLT Shear Wall Buildings with Buckling-Restrained Axial Fuses. Can. J. Civ. Eng. cjce-2023-0448. https://doi.org/10.1139/cjce-2023-0448 (Chapter 3).

- Zhu, H., Bezabeh, M., Iqbal, A., Popovski, M., and Chen, Z. (2024). Seismic Design and Performance Evaluation of Post-Tensioned CLT Shear Walls with Coupling U-Shaped Flexural Plates in Canada. *Earthquake Spectra*, Under Review (*submitted on May 18, 2024* and *received first round peer review feedback on July 12, 2024*) (Chapter 4).

Conference Papers

- Zhu, H., Bezabeh, M., Iqbal, A., Popovski, M., and Chen, Z. (2024). Seismic Performance Assessment of Post-Tensioned CLT Shear Wall Buildings with Buckling-Restrained Axial Fuses. *Proceeding of the 18th World Conference on Earthquake Engineering (WCEE)*, Milan, Italy. (Chapter 3).

- Zhu, H., Bezabeh, M., Iqbal, A., Popovski, M., and Chen, Z. (2024). Seismic performance assessment of post-tensioned CLT shear wall buildings equipped with U-shaped flexural plate damper. *Proceeding of the Canadian Society of Civil Engineering Annual Conference (CSCE) 2024,* Niagara Falls, ON. Paper 685. (Chapter 4).

ACKNOWLEDGEMENTS

DEDICATION

To all the giants upon whose shoulders I am standing.

TABLE OF CONTENTS

LIST OF TABLES

LIST OF FIGURES

Chapter 1 INTRODUCTION

1.1 General Overview

In mass timber buildings, most of a building's flexibility, ductility, and energy dissipation depends on connections between wood members (Pei et al., 2013; Ceccotti et al., 2013; Gavric et al., 2015). Under large drift, permanent damage to conventional connectors could result in a significant residual drift of buildings and subsequent high repair costs, potential necessity for building demolishment, as well as a risk of aftershock collapse. To enhance seismic performance and reduce residual damage, various low-damage mass timber seismic force-resisting systems (SFRSs) have been proposed (Palermo et al., 2006; Pei et al., 2019; Hashemi et al., 2020; Lepine-Lacroix and Yang, 2023). Among them, post-tensioned (PT) Cross-laminated timber (CLT) (PT-CLT) walls (Figure 1-1) have gained global attention and public awareness due to their self-centring and stable energy dissipation capabilities (Ganey et al., 2017; Chen et al., 2018; Pei et al., 2019; Pei et al., 2023).
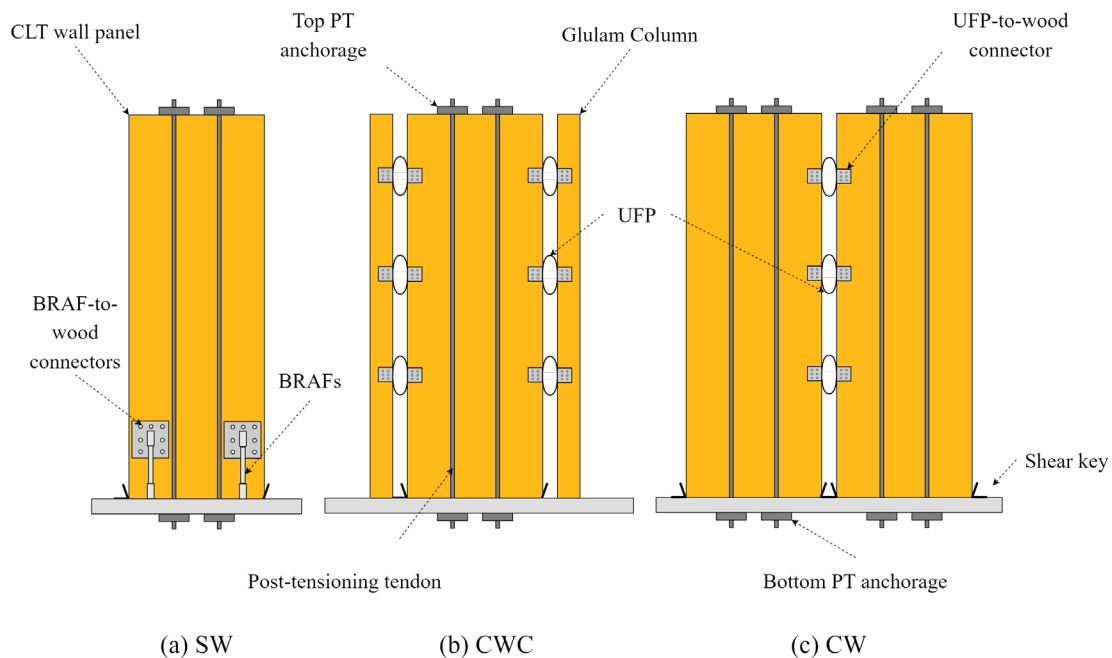
Figure 1-1. PT-CLT walls with EDDs: (a) PT-CLT wall with buckling-restrained axial fuses; (b) PT-CLT wall with Glulam boundary columns and UFPs; (c) PT-CLT coupled walls with UFPs.

PT-CLT walls integrate CLT panels with post-tensioned high-strength steel strands or threaded bars along the centerline of each panel to develop moment-resisting connections. CLT panels are allowed to undergo controlled rocking instead of being rigidly fixed to the wall-to-foundation interface. Although CLT panels can resist lateral loading, post-tensioning bars exert a restoring moment when elongated, attaining self-centring. External energy dissipation devices (EDDs) such as buckling-restrained axial fuses (BRAFs) and U-shaped Flexural Plates (UFPs) are often used to couple PT-CLT walls and provide energy dissipation (Figure 1-1). The sacrificial EDDs are designed to be activated during seismic excitation and therefore to capacity-protect primary structural components (Chen et al., 2020). With limited or negligible residual damage, such a system is economically appealing because building downtime can be significantly reduced, and post-earthquake building repairs will mainly focus on replacing the EDDs (Furley et al., 2021).

1.2 Problem Statement

Canada has regions with complex seismotectonics, such as Southwestern British Columbia (BC), where three sources of damaging earthquakes coexist: shallow crustal, deep-in-slab, and interface sources (Goda, 2019). In addition, adoption of the sixth-generation Seismic Hazard Model (SHM6) (Kolaj et al., 2020a; Kolaj et al., 2020b) by NBCC 2020 (NRCC, 2020) resulted in a nationwide increase in seismic hazard. As a result, seismic design and performance of buildings are anticipated to be greatly impacted (Popovski et al., 2021; Odikamnoro et al., 2022). Although PT-CLT shear wall buildings feature a low-damage system with ductile response, most existing studies (e.g., Ganey, 2015; Akbas, 2016; Sarti et al., 2017; Kovacs and Wiebe, 2019; Wilson et al., 2020; Furley et al., 2021; Ho et al., 2023) evaluated either low to moderate seismicity or simple seismotectonics (e.g., shallow crustal). Moreover, performance objectives during assessments were not examined in a probabilistic manner. For instance, the collapse probability was not examined. Hence, it remains unclear whether PT-CLT shear wall buildings possess adequate seismic performance and safety margin in high seismic zones in Canada.

1.3 Research Objectives

This thesis aims to address the research gap mentioned in the previous section to promote the applicability of PT-CLT walls as mass timber SFRS in Canada. The three sub-objectives of this thesis are:

1) Review the seismic response of PT-CLT walls reported in the literature, which are based on experimental and numerical studies.

2) Develop robust numerical models for PT-CLT walls. This includes component-level calibration for energy dissipation devices and model validation with system-level quasi-static cyclic and building-level shaking table tests.

3) Conduct seismic performance assessment for PT-CLT shear wall buildings equipped with BRAFs and UFPs in Southwestern BC, a high seismic zone in Canada with complex tectonic regimes.

1.4 Research Scope and Organization of the Thesis

In this thesis, efforts were made to design and assess the seismic performance of PT-CLT shear wall buildings in high seismic regions in Canada. The thesis is divided into five chapters and presented in the following structure:

Chapter 1 provides an overview of the PT-CLT wall as SFRS, identifies the research gap, highlights this thesis's research objectives, and outlines the organization of the thesis.

Chapter 2 provides a comprehensive literature review of mass timber buildings in Canada and PT-CLT walls. The latter further includes the structural mechanics and limit states of PT-CLT walls and existing studies related to experimental testing, numerical modelling, seismic design approaches, and seismic performance assessment. This chapter also incorporates a brief review of seismic hazards in Canada and SHM6.

Chapter 3 includes a seismic performance assessment for prototype six-, nine-, and twelve-storey PT-CLT shear wall buildings equipped with BRAFs. Prototype buildings hypothetically located in Vancouver are designed using the direct displacement-based design approach. Fibre-based numerical models are developed and validated with system-level quasi-static cyclic testing. A suite

of ground motions is selected and scaled to the uniform hazard spectrum prescribed in NBCC 2020 based on SHM6. NLRHA and IDA are carried out for performance examination.

Chapter 4 presents a seismic performance assessment for PT-CLT shear wall buildings with coupling UFPs. Prototype three-, six-, and nine-storey buildings hypothetically located in Vancouver are designed using the DDBD method. A fibre-based numerical modelling strategy is adopted and further validated with building-level full-scale shaking table testing. Nonlinear static, response history, and incremental dynamic analyses are conducted to verify the DDBD procedure and system performance at the maximum credible earthquake. To perform a collapse fragility assessment, IDA is conducted using eighty ground motion records that were selected for each building and scaled to each seismotectonic regime's Conditional Spectrum.

Chapter 5 summarises the key findings of the research program and makes recommendations for future work.

Chapter 2 LITERATURE REVIEW

2.1 CLT-based Mass Timber Building in Canada

Mass timber buildings have gained popularity in North America due to their attractive architectural appearance, reduced construction time, and inherent material sustainability. In Canada, the adoption of mass timber building can help address three critical domestic needs: (1) achieve net-zero carbon emissions by 2050; (2) address the housing crisis; and (3) create employment opportunities in rural and indigenous communities (Allan and Eaton, 2024). Due to these needs, a notable surge in attention towards mass timber buildings has been witnessed in Canada, as demonstrated by the rapid growth of mass timber construction and the advancements in building codes, for instance, the construction of notable tall timber and hybrid buildings under the Tall Wood Building Demonstration Initiative (TWBDI) (Figure 2-1) (NRC & CFS, 2021). The latest version of the National Building Code of Canada (NBCC 2020) has extended the encapsulated mass timber construction height limit to 12 storeys. The British Columbia and Ontario Building Code (BCBC, 2024; Meta, 2024) recently permitted mass timber construction up to 18 storeys for residential and office buildings, up from 2020's 12-storey limit. Approximately 700 mass timber buildings have been constructed, and 140 more projects have been under construction or planning in Canada since 2007, and this number is growing exponentially (NRC & CFS, 2021).
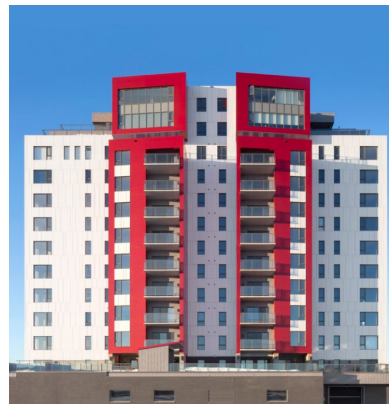
(a)   (b)

Figure 2-1.Tall timber and hybrid buildings in Tall Wood Building Demonstration Initiative (TWBDI) projects in Canada: (a) the 18-storey Brock Commons in Vancouver (Source: CTBUH). (b) the 13-storey Origine in Québec (Source: CTBUH).

Mass timber buildings use engineered wood products (EWPs) for load-bearing walls, columns, beams, floors, and roofs. Common EWPs include Cross-laminated timber (CLT), Glulam Laminated Timber (Glulam), Nail Laminated Timber (NLT), Dowel Laminated Timber (DLT), Mass Plywood Panel (MPP), and Laminated Veneer Lumber (LVL). CLT consists of an odd number of kiln-dried dimensional lumber boards (commonly three, five, seven, and nine layers), and adjacent layers are positioned in a crosswise manner and glued together on the wide face (Figure 2-2). Rigorous manufacturing standards must be complied with for CLT production, such as ANSI/APA PRG 320-2019- Standard (APA, 2017) for performance-rated CLT in North America. In Canada, CSA O86-19 (CSA, 2019) provides CLT design provisions only to APA PRGA 320 certified CLT and adopts various stress grades based on species combinations and grades of laminations. CLT features dimensional stability, demonstrated sound and thermal insulation and fire resistance, usage of low-grade timber for inner layers, higher strength-to-weight ratio compared to masonry or concrete, and higher in-plane strength and stiffness compared to sawn lumber (Ceccotti et al., 2013; Assadi et al., 2023; Teweldebrhan et al., 2023).
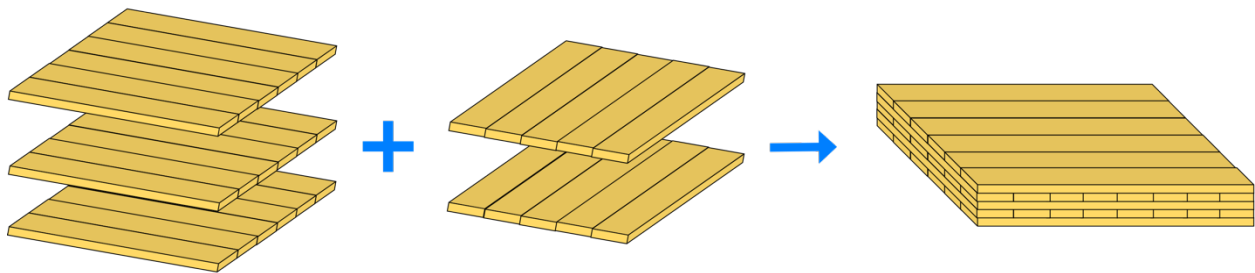
Figure 2-2. Composition of a 5-ply CLT panel.

CLT-based mass timber buildings can be built as a platform or balloon-type construction (Karacabeyli and Lum, 2022) (Figure 2-3). In platform construction, each CLT floor panel serves as a platform for the wall panel above. Therefore, gravity load is cumulatively transferred to the lowest storey, and such a design is typically governed by the perpendicular-to-grain compressive resistance of the floor panels at the base storey. The 2020 version of the National Building Code of Canada (NBCC 2020) (NRCC, 2022) prescribes seismic performance factors for moderately

ductile and limited-ductility CLT shear walls for platform-type construction. The building height limit for such SRFSs is 30 m for Seismic Categories 1 to 3 (low to medium seismicity) and 20 m for Seismic Category 4 (high seismicity). In balloon-type construction, vertical CLT panels or Glulam columns extend continuously from the foundation to the top of the building. Several studies have investigated the application and performance of balloon-type CLT walls (Chen and Popovski, 2020a; Shahnewaz et al., 2021; Hayes et al., 2023; Xing et al., 2023). Currently, balloon framing CLT shear walls as SFRSs have not yet been included in NBCC. Apart from the considered SFRSs in NBCC 2020, the variability in mass timber construction techniques and available engineered wood products and connections can lead to a wide range of possible alternative building solutions (e.g., the 18-storey Brock Commons in Vancouver). To realize these special projects, buildings must be demonstrated to possess an equivalent level of performance similar to the ones following or complying with the acceptable solutions defined in Division B in NBCC, in which performance-based seismic design can be applied.
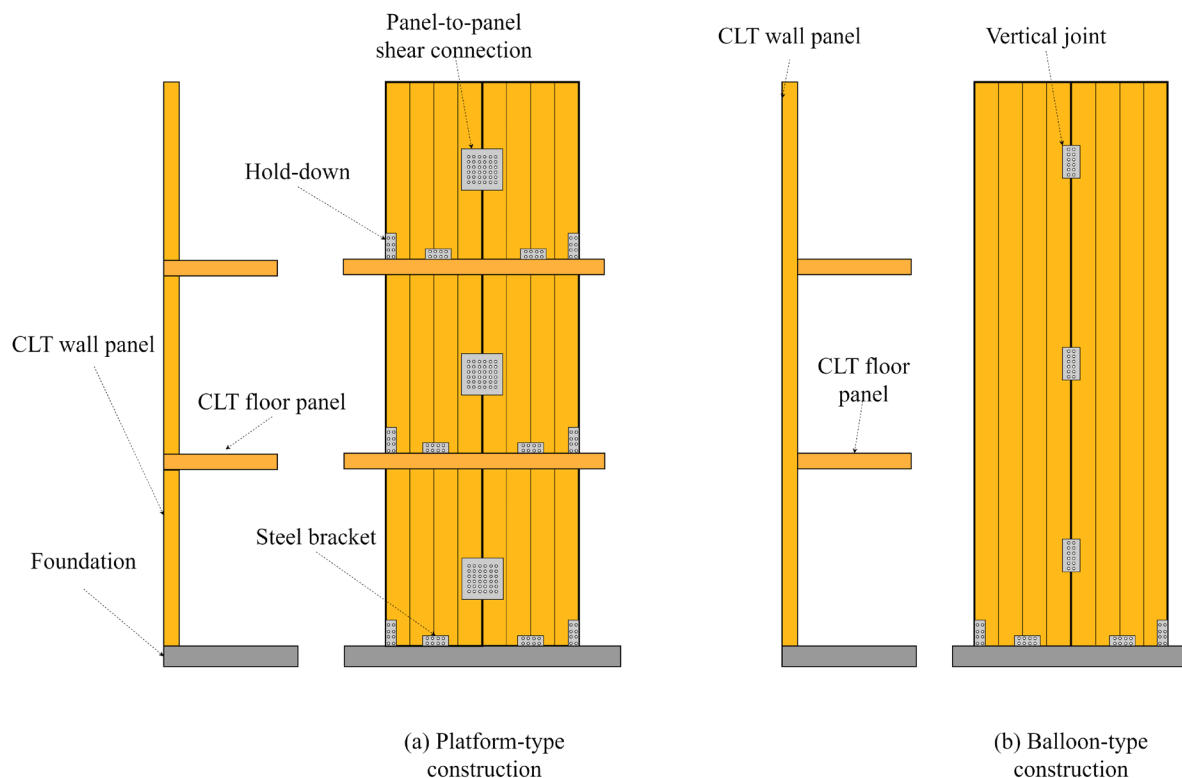
Figure 2-3. Conventional CLT-based SFRS: (a) Platform-type CLT shear wall; (b) Balloon-type CLT shear wall.

2.2 PT-CLT Walls with Energy Dissipation Devices

PT-CLT walls adopt the post-tensioned rocking dissipative connections from the PREcast Seismic Structural Systems (PRESSS) program (Priestley et al., 1991) and belong to a broad category of prestressed-laminated timber (Pres-Lam) systems (Palermo et al. 2006). When subjected to lateral loadings, such as seismic excitation, a composite deformation of the SFRS can be resulted with contributions from flexure and shear deformation, as well as rigid-body rocking (Figure 2-4). Sliding can be prevented by shear keys.
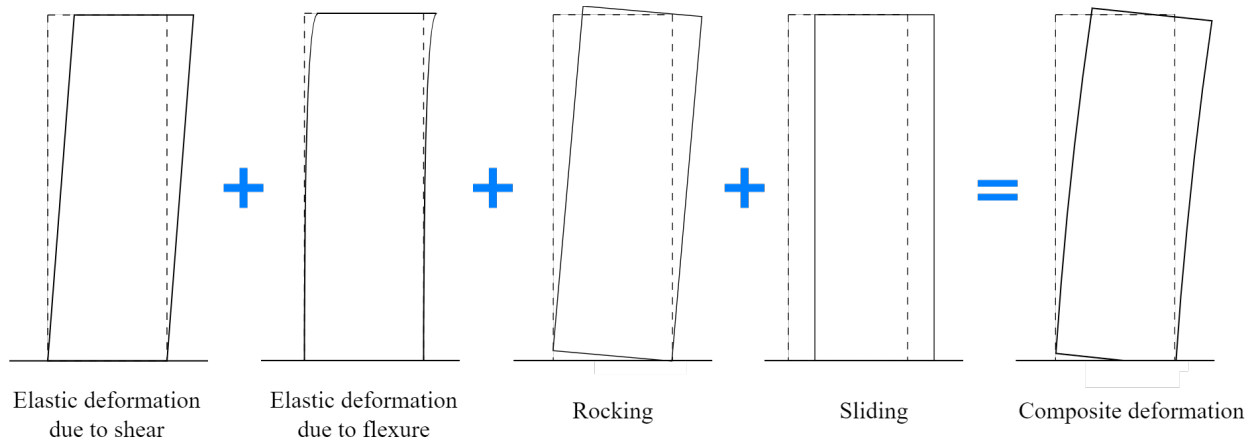
Figure 2-4.Composite deformation of PT-CLT wall under lateral loading.

Figure 2-5a shows a typical base shear versus roof displacement relationship of PT-CLT walls with EDD under monotonic pushover analysis. Initially, the overturning moment in PT-CLT walls is resisted by the panel's self-weight (W) and initial post-tensioning force ($T_{pt,ini}$) until reaching the decompression (DEC) limit state. Such a limit state corresponds to the decompression moment (M_{dec}) [Equation 2-1], where d is the moment arm between centerline of the panel and wall edge.

$$M_{dec} = \left(T_{pt,ini} + W\right)d \qquad \text{Equation 2-1}$$

Prior to DEC, the wall behaves as a fixed-end cantilever and exhibits exclusively elastic deformation due to flexure and shear (Figure 2-4). As the DEC is exceeded, rigid body rocking of the panel commences. The base uplift or gap opening at one side of the CLT wall will accumulate compressive stress on the opposite side. Meanwhile, EDDs could reach the yielding limit state

(YEDD) depending on their relative position with respect to the rocking interface and start dissipating energy with increasing imposed rotation at the wall-to-foundation interface. However, the initial geometric and material nonlinearity is limited, and the wall still behaves quasi-elastically until the effective linear limit (ELL). Akbas et al. (2017) quantitatively associated ELL with the contact length between the wall and foundation, defining it as three-eighths of the panel length. As the contact length further reduces due to rocking, the rest of the EDDs yield consecutively, and the yielding of CLT (YCLT) can occur at the compressive toe of the wall, followed by the splitting of CLT (SCLT), crushing of CLT (CCLT), and the eventual yielding of PT tendons (YPT). Under reversed cyclic loading, PT-CLT walls achieve self-centring due to the restoring moment from PT elements. When coupled with EDDs, energy dissipation can be provided through their inelastic deformation, and the system exhibits, hence, an overall flag-shaped force-deformation (F-d) hysteresis (Figure 2-5b).
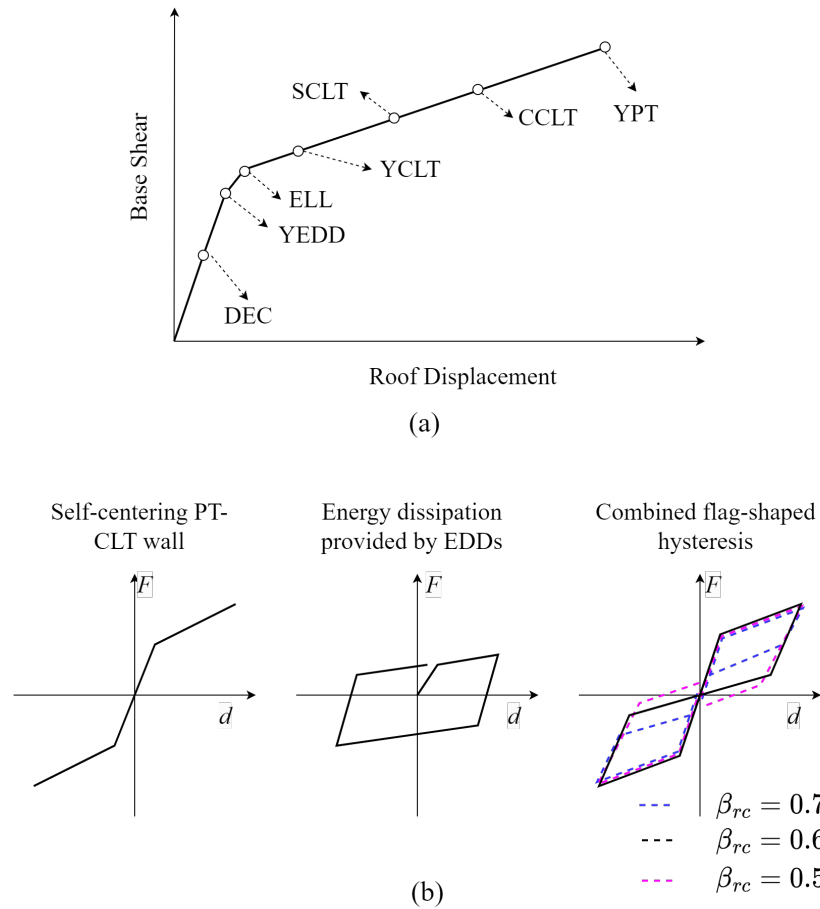
Figure 2-5. (a) Typical force-deformation relationship of PT-CLT walls with EDDs under monotonic pushover analysis; (b) System's flag-shaped force-deformation hysteretic behaviour.

22

A balanced resistance distribution between the PT elements and EDDs is crucial to attain self-centring and energy dissipation simultaneously, and such distribution can be described by three interchangeable design parameters, which are energy dissipation ratio (β_{ed}) [Equation 2-2], re-centring ratio(β_{rc}) [Equation 2-3], and restoring ratio (λ) [Equation 2-4] (Chen et al., 2024). Sarti (2015) recommends β_{rc} to be greater than 0.55. To ensure a minimum amount of energy dissipation, a lower-bound β_{ed} of 0.25 was adopted by Busch et al. (2022). The conversion among the three factors is shown in Table 2-1.

$$\beta_{ed} = \frac{M_{EDD}}{M_{tot}} \qquad\qquad \text{Equation 2-2}$$

$$\beta_{rc} = \frac{M_{PT}}{M_{tot}} = 1 - \beta_{ed} \qquad\qquad \text{Equation 2-3}$$

$$\lambda = \frac{M_{PT}}{M_{EDD}} = \frac{1}{\beta_{ed}} - 1 \qquad\qquad \text{Equation 2-4}$$

where M_{EDD} , M_{PT} are the moment resisted by EDDs and PT elements respectively. Ignoring the contribution from gravity load, M_{tot} is the sum of M_{EDD} and M_{PT}.

Table 2-1. Conversion among factors prescribing moment resisted by PT and EDD elements.

β_{rc}	β_{ed}	λ
0.75	0.25	3.00
0.70	0.30	2.33
0.65	0.35	1.86
0.60	0.40	1.50
0.55	0.45	1.22

The structural damage states of the PT-CLT walls mentioned previously can be related to different seismic performance objectives (POs) to facilitate resilient design. Note that some limit states are either difficult to detect during experiments (e.g., ELL and YCLT) (Furley et al. 2021) or computationally demanding to record the time histories of all component-level responses in numerical analysis. Therefore, inter-storey drift ratios (ISDR) are typically used as a proxy for damage (limit) states based on existing experimental observations (Ho et al., 2023). The relationship between various POs and the component and system limit states employed in the literature is summarised in Table 2-2. Wichman (2023) proposed that the 1%, 2%, and 3% ISDR can be adopted in designing PT-CLT shear wall building to achieve POs of immediate occupancy (IO), limited repair (LP), and collapse prevention (CP-W). To satisfy the PO of IO, the residual ISDR should be limited to 0.2%, and the wall and PT elements should remain elastic. For PO of LP, CLT yielding is permitted at the compressive toe of the wall panel, but yielding of PT elements is not allowed. At CP, PT yielding and CLT crushing at the wall base are expected, but lateral connections (i.e., embedded epoxy road splice connections used to connect CLT segments) should remain elastic. Note that NBCC 2020 identifies 2.5% ISDR as a collapse prevention criterion under MCE. Hence, in this thesis, CP-NBCC is employed to be distinguished from the CP PO proposed in Wichman (2023), denoted as CP-W.

Table 2-2. Summary of seismic POs and corresponding limit states for PT rocking timber walls.

Reference	System configuration	PO	Hazard level	Component limit states	System limit states
Akbas (2016)	PT-CLT walls	IO	DBE	DEC, YUFP, ELL, YCLT [1]	-
	(CW)	LS	MCE	DEC, YUFP, ELL, YCLT, SCLT [1]	-
Sarti et al.	PT-LVL walls	-	SLE	DEC, YUFP [1]	-
(2017)	(SW, CWC, CW)	-	DBE	DEC, YUFP, YCLT [1]	-
		CP	MCE	DEC, YUFP, YCLT, failure of UFP, and YPT [1]	5% roof drift
Ho et al.	PT-MPP walls	IO	SLE	Effective yielding of any component [2]	1% ISDR
(2023)	(CW)	LS	DBE	Crushing of MPP wall and YPT [2]	2% ISDR
		CP	MCE	Ultimate capacity PT element and MPP wall [2]	a) 4% ISDR b) 1.5% residual ISDR
Wichman	PT-CLT walls	OC	SLE	All components remain elastic	-
(2023)		IO	DBE	DEC, YUFP [1]	a) 1% ISDR b) 0.2% residual ISDR
		LR	5% in 50 years	DEC, YUFP, YCLT [1]	2% ISDR
		CP-W	MCE	DEC, YUFP, YCLT, CCLT, YPT [1]	3% ISDR

Note that in Table 2-2, SLE stands for a service level earthquake (50% in 30 years). Superscripts [1] and [2] denote that the system is allowed to reach and not exceed the specified component limit states respectively.

2.3 Experimental Testing for Pres-Lam Walls and EDDs

Global efforts have been made to experimentally investigate the lateral behaviour of Pres-Lam walls. This section consists of two parts: a review with emphasis on experimental testing of Pres-Lam walls (Section 2.3.1) and energy dissipation devices (Section 2.3.2). The Pres-Lam wall testing based on continental regions is categorized in Section 2.3.1, with early testing in New Zealand focusing on PT-LVL walls, more recent testing in North America targeting PT-CLT walls, and other testing from Euro-Asia. The timeline of experimental test of Pres-Lam walls is depicted in Figure 2-6. Two types of EDDs are focused on Section 2.3.2. i.e., buckling-restrained axial fuses (BRAFs) and U-shaped flexure plates (UFPs).

2.3.1 Experimental Testing for Pres-Lam Walls

2.3.1.1 Tests Conducted in New Zealand

Palermo et al. (2006) reported quasi-static cyclic and pseudo-dynamic testing of three PT-LVL walls with internal or external dissipaters. The results confirmed the enhanced performance of PT-LVL walls featuring high-level ductility, negligible residual deformations, and no damage to structural elements. Furthermore, external dissipaters are preferred based on the tests due to their easy replacement. Smith et al. (2007) conducted quasi-static cyclic and pseudo-dynamic testing of coupled wall systems. Three configurations were explored: PT-LVL coupled wall with post-tensioned solutions only, with fuse-type dissipaters at the base, and with external attachment of plywood sheet dissipaters. The test campaign further validated the low-damage nature of Pres-Lam walls. Iqbal et al. (2007) tested coupled PT-LVL walls with UFPs and concluded the stable and predictable behaviour of UFPs as EDD. Sarti et al. (2016) carried out quasi-static cyclic testing of a two-thirds scale PT-LVL wall, aiming to examine the system connection details, the anchorage of post-tensioning elements, and the fastening of the dissipation devices and shear keys. Several design recommendations were provided based on the testing results. Generally, the peak timber compressive stress at the ultimate limit state (ULS) should remain below 40-50% of the nominal compressive strength, with an expected increase to 70-80% during MCE events. The recommended initial post-tensioning stress in the tendons should not surpass 0.4-0.5 times the yield strength to avoid yielding in the post-tensioning tendons during seismic excitations.
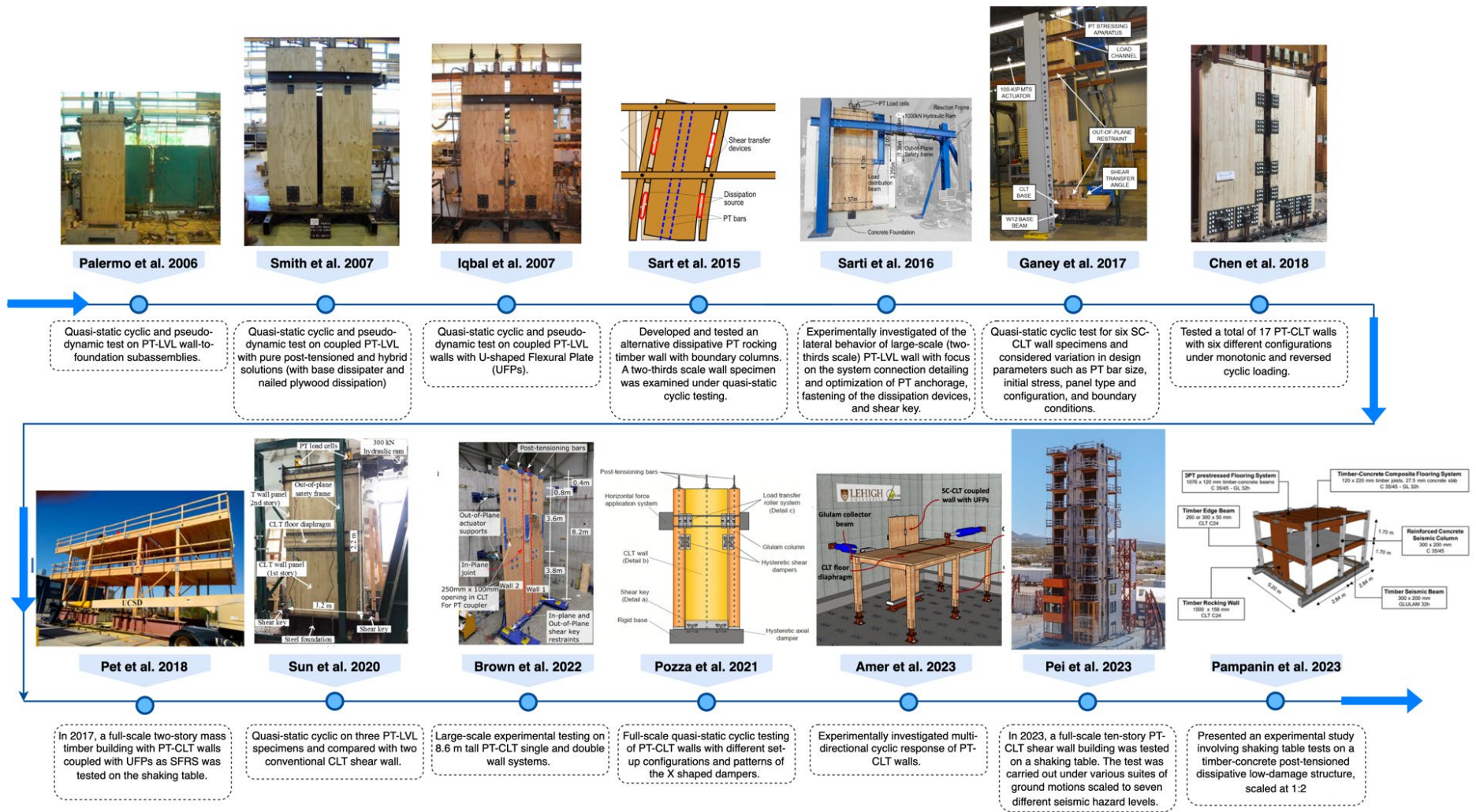
Figure 2-6. Overview of major experimental tests of Pres-Lam walls.

Sarti et al. (2016b) designed and experimentally investigated an alternative Pres-Lams wall configuration, where LVL boundary columns were coupled to the wall panel using UFPs to mitigate vertical displacement incompatibilities between the SFRS and the diaphragm. Brown et al. (2022) conducted cyclic testing of single and double PT-CLT walls with double wall systems coupled with self-tapping screws. It was demonstrated that double wall systems possessed increased shear wall strength and stiffness, as well as satisfactory energy dissipation. It was also reported that the Modified Monolithic Beam Analogy (MMBA) method for PT-LVL walls could underpredict the peak compressive strain in CLT walls because of material variability and complexity.

2.3.1.2 Tests Conducted in North America

In Canada, major testing of PT-CLT walls was initiated and led by FPInnovations (Chen et al., 2018; Chen et al., 2020a)(Figure 2-7). In 2018, seventeen full-scale PT-CLT wall specimens in six configurations were tested under monotonic and reversed cyclic loading protocols. The test campaign parametrically considered design parameters such as initial post-tensioned stress in PT elements, the relative position of BRAFs at the wall-to-foundation interface, and the number of UFPs. The individual CLT panel had a length of 1 m, a thickness of 0.143 m (5-ply), and a height of 3 m and complied with ANSI/APA PRG 320 Standard E1 grade. Cyclic loading was exerted at the actuator height of 2.9 m. The test results indicated four major failure modes of PT-CLT walls, including the yield and buckling of BRAFs, CLT splitting and crushing at the compressive edge of the wall toe, and buckling of the exterior layer of lumber of the CLT wall.
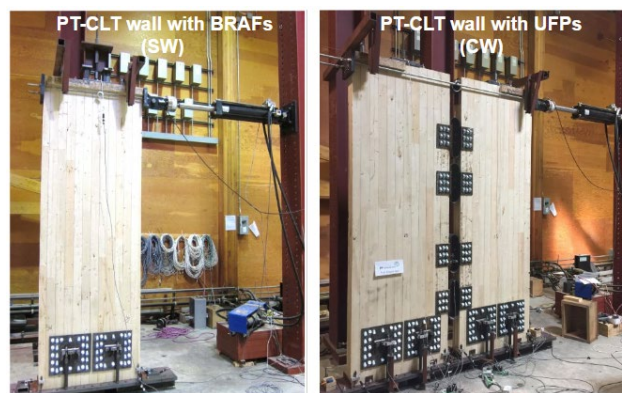
Figure 2-7. Experiment test setup for quasi-static cyclic testing of PT-CLT walls at FPInnovations (Picture courtesy of Zhiyong Chen from FPInnovations).

In the United States, the National Science Foundation funded a multi-year research project, the NHERI Tallwood Project (Pei, 2017), which aimed to develop and validate a seismic design methodology for tall wood buildings. Ganey et al. (2017) conducted full-scale quasi-static testing for six PT-CLT wall specimens (five single walls and one coupled wall) under reversed cyclic loading. Considering the design parameters such as area and initial stress of PT bar and wall boundary conditions, the study concluded that CLT wall damage did not impede the system's re-centring until 5% drift. In 2017, a full-scale two-storey mass timber building with PT-CLT walls coupled with UFPs as SFRS was tested on the shaking table at the University of California San Diego (Pei et al. 2019; Barbosa et al., 2021; Mugabo et al., 2021) (Figure 2-8). The building was tested under fourteen ground motions scaled to three hazard intensity levels, namely SLE (50% in 30 years), DBE (10% in 50 years), and MCE (2% in 50 years). After the test building was subjected to a suite of ground motions, the performance goal of no major structural damage was achieved. The test also demonstrated it is possible to accommodate the deformation compatibility between SFRS and the gravity system. Nonetheless, it should be noted that the unexpected foundation flexibility effect during the test significantly impacted the structural dynamics of PT-CLT walls.

Figure 2-8. Shaking table testing of two-storey (left) and ten-storey (right) PT-CLT shear wall buildings. (Picture source: https://leverarchitecture.com/innovation).

In 2023, a full-scale ten-storey PT-CLT shear wall building designed using a performance-based approach was tested on a shaking table (Pei et al., 2023) (Figure 2-8). The design criteria aimed to achieve an essentially elastic performance apart from the allowable deformations, including the gap opening of rocking walls and minor yielding at compressive edges of wall panels and yielding of EDDs. The test was carried out under various suites of ground motions scaled to seven different seismic hazard levels. Preliminary results indicated that building performance exceeded code minimum requirements and that the ISDR was limited to 1.5% at MCE (Wichman, 2023). Amer et al. (2023) experimentally investigated the lateral response of PT-CLT walls on a five-eighths scale timber test subassembly under bi-directional cyclic loading. Four damage states were first qualitatively defined and described based on CLT and PT damage at various levels. Based on CLT compressive testing, the damage states were further quantitively associated with different CLT strain levels. The experimental results facilitated a fragility assessment providing probabilities of exceedance of each damage state at both component- and system-levels.

2.3.1.3 Tests Conducted in Euro-Asia

Sun et al. (2020) conducted reversed cyclic loading on three PT-CLT wall specimens, including the CLT floor diaphragm. The responses were compared with traditional platform CLT shear wall, and PT-CLT walls featured re-centring behaviour and negligible damages. Pozza et al. (2021) employed X-shaped dampers in cyclic testing of PT-CLT single and coupled walls, and the satisfactory performance of the SFRS was also validated. Under the EU-funded SERA project (Seismology and Earthquake Engineering Research Infrastructure Alliance for Europe Project), Pampanin et al. (2023) presented an experimental study involving shaking table tests on a reduced-scaled timber-concrete post-tensioned dissipative low-damage structure. After more than 150 seismic excitations, damages were concentrated on external EDDs and the low-damage nature of the system was further validated.

2.3.2 Experimental and Numerical Investigations of EDDs

In post-tensioned rocking wall systems, various energy dissipation devices can be applied to absorb energy during seismic events. These include steel angles (Smith et al., 2014), X-shaped dampers (Pozza et al., 2021), bucking-restrained axis fuses (Palermo et al. 2005; Sarti et al. 2013; Sarti et al. 2016a; Rahmzadeh and Iqbal, 2018; Chen et al. 2020), U-shaped flexural plates (Ganey et al. 2017; Pei et al. 2019 ; Chen et al. 2020; Pei et al. 2023), O-shaped damper (Hossain et al., 2021), and self-taping screws (Brown et al., 2022) (Figure 2-9). This section focuses on two particular EDDs, BRAFs and UFPs, due to their extensive use in Pres-Lams wall systems.
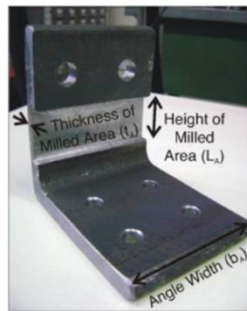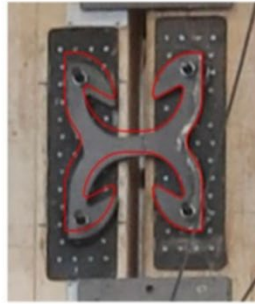
(a) Steel angles   (b) X-shaped dampers   (c) Buckling-restrained axial fuses

(d) U-shaped flexural plates   (e) O-shaped damper

Figure 2-9.Various types of energy dissipation devices: (a) steel angles (Smith et al., 2014); (b) X-shaped dampers (Pozza et al., 2021); (c) buckling-restrained axial fuses (Chen et al., 2018); (d) U-shaped flexural plates (Iqbal et al., 2007); (e) O-shaped damper (Hossain et al., 2021).

BRAFs are typically mild steel bars with reduced diameter in the centre where concentrated and localized tensile and compressive yielding occurs (Figure 2-10). The bars are usually encased in hollow steel tubes filled with epoxy or grout to prevent buckling. An alternative way to prevent buckling is to employ two steel half-tubes to cover the portion with reduced diameter (Chen et al., 2018) (Figure 2-9c).
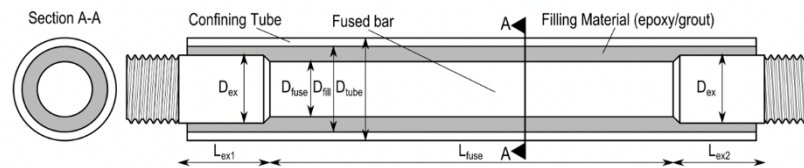
Figure 2-10. Buckling-restrained axial fuse (Sarti, 2015).

The concept of BRAFs traces back to the early application of buckling-restrained braces (BRBs) (Sabelli et al. 2003; Black et al. 2004), which effectively enhanced seismic performance for conventional braced frames. In such a system, a steel core encased in a steel tube filled with concrete was utilized, and it can produce ductile and stable hysteretic behaviour. More recently, replaceable BRAFs were adopted as EDD coupled with self-centring rocking walls to increase energy dissipation. Marriott (2009) tested three tension-compression-yielding dissipaters with varying fuse diameters, and experimental results revealed stable and distinct energy dissipation. Amaris (2010) conducted cyclic testing for three fuses of three diameters: 7 mm, 10 mm, 13mm and with a common unbonded length of 80mm. A 34mm steel tube with a thickness of 2mm was employed as an anti-buckling system. In these two studies, cyclic tests showed a sudden increase in BRAF's stiffness and strength when subjected to negative displacement (compressive range). This is due to the inner fuse being forced into contact with the confining epoxy or confining tube under compression, contributing to the overall stiffness. A decreased energy dissipation capacity was also found in the negative range. Sarti et al. (2013 and 2016) investigated the failure mechanism of BRAFs by testing samples with various dissipator slenderness, geometry, and differences in fuse versus external diameters. An infill material of either cement grout or epoxy was used. Based on the results, two failure mechanisms were identified. For specimens with a low slenderness ratio, axial low-cycle fatigue led to fracture after repetitive loading. The second failure mode is associated with a buckling/sway mechanism, where localized plasticization of the confining tube occurs due to increased unloading force and causes the entire device to sway (Sarti

32

et al., 2016). A simplified model to capture fuse-tube interaction was also provided, in which the total stiffness of a BRAF with infill material is given by [Equation 2-5]:

$$k_{comp} = k_{fuse,t} + \left(\frac{1}{k_{contact}} + \frac{1}{k_{anti-buck.}}\right)^{-1}$$

Equation 2-5

where $k_{fuse,t}$, $k_{anti-buck.}$, and $k_{contact}$ are the stiffnesses of the fuse bar, the anti-buckling system, and the contact between the fuse and infill material and are given by [Equation 2-6 and 2-7]:

$$k_{fuse,t} = \frac{E_{s,t}A_{fuse}}{L_{fuse}}$$

Equation 2-6

$$k_{anti-buck.} = \frac{E_s A_{tube}}{L_{tube}} + \frac{E_{fill}A_{fill}}{L_{tube}}$$

Equation 2-7

where $k_{contact}$ is assumed to be 6 kN/m based on experimental observation.

Smith (2014) tested seventeen BRAF specimens on six dissipative reinforcing geometries. The testing pinpointed that an underestimation of yield displacement can be resulted from using analytical relationships based on Sarti et al. (2013), because the yield displacement was assumed to concentrate in the reduced diameter portion of BRAF with only. Further refinement and a series of design recommendations for BRAFs were given. Kramer et al. (2016) performed panel tension and cyclic tests in which BRAFs were embedded in the CLT panel. In addition to validating the stable energy dissipation of the system, the study showed that no damage occurred to the CLT panel and that the fasteners remained rigidly attached as per the design. An experiment test on a two-thirds scale PT-LVL walls equipped with BRAFs (Sarti et al. 2016a) showed that BRAFs developed a maximum strain of 6% at the MCE level. Hence, it was recommended that BRAFs should be designed to achieve a maximum tensile strain within the range of 2.5-4% at ULS while limiting to 5-6% at MCE level. Such design limits ensure energy dissipation and mitigate the risk of premature low-cycle fatigue failure of the BRAFs. Rahmzadeh and Iqbal (2018) studied the cyclic behaviour of BRAFs using the numerical approach to capture the interaction between the fuse bar and the anti-buckling system. A 3D continuum and 2D fibre-based finite element model were developed

and calibrated with experimental testing. Both models were able to capture the cyclic response of BRAFs, especially in the negative range, although it should be noted that in the post-tensioned rocking system, BRAFs undergo primarily positive displacement (i.e., in the tension range) (Sarti, 2015; Rahmzadeh and Iqbal, 2018). Chen et al. (2018) conducted two BRAF tests. One was covered by an anti-buckling steel tube and filled with epoxy; the other applied two steel half-tubes in the reduced diameter portion of the inner fuse. The responses of both BRAFs had a similar shape and energy dissipation. A maximum strain of 6% can be achieved in BRAFs using either method (Chen et al., 2018).

UFPs serve as coupling links and offer energy dissipation in the event of relative vertical movement between adjacent wall panels in coupled PT-CLT walls. Bending a piece of mild steel plate of a certain thickness (t) about a certain diameter (D) can produce a UFP with a semicircle and two equal side plates (Figure 2-11). The side plates of UFPs can be connected to CLT walls to create coupling. The connection can be either bolted saddle connections for simple post-earthquake replacement of damaged UFPs (Wichman et al., 2022) or metal inert gas welding (Iqbal et al., 2015).
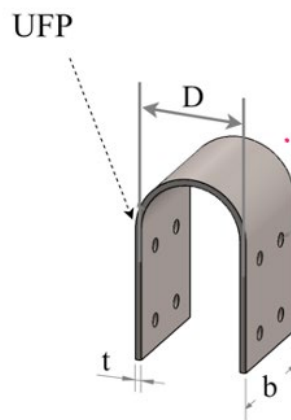
Figure 2-11.U-shaped flexural plates.

Kelly et al. (1972) indicated that the failure mode of UFPs is dominated by a localized kinking of the plate followed by a complete transverse fracture. Furthermore, UFPs, under cyclic loading, exhibit a distinct strain-hardening effect. Iqbal et al. (2007) conducted component-level testing for three UFPs under reversed cyclic loading. A 5-mm thickness and a 15-mm radius of curvature were chosen for all UFPs, with widths of 50 mm, 65 mm, and 100 mm, respectively. The test setup and UFP specimens are shown in Figure 4-2. The experiment revealed that UFP hysteresis remained stable without distinct stiffness and strength degradation. The number of cycles leading to UFP failure decreased as the strain increased, especially for strokes greater than double the initial bend length. Baird et al. (2014) reported factors governing the failure of UFPs, including stroke and maximum strain. The stroke is related to the dynamic bending deformation of UFPs, whereas the maximum strain is determined by geometry and taken as the ratio between t and D. Based on experimental testing and numerical simulation, Baird et al. (2014) further provided formulations for UFP yield force and initial stiffness with geometrical parameters (t, b, D) as inputs, given in [Equation 2-8 and 2-9]:

$$F_y = \frac{\sigma_y b t^2}{2D} \qquad \text{Equation 2-8}$$

$$k_0 = \frac{16Eb}{27\pi}\left(\frac{t}{D}\right)^3 \qquad \text{Equation 2-9}$$

where σ_y and E are the yield stress and Young's modulus of mild steel.

2.4 Numerical Modelling of Pres-Lam Walls

Various numerical modelling strategies have been proposed for Pres-Lam walls to predict their structural responses under lateral loading and perform parametric analyses (Figure 2-12). Wilson et al. (2019) categorized the models into high-order and reduced-order approaches. The former enables a detailed assessment of locally developed CLT stress and strain for damage evaluation (i.e., yielding, splitting, and crushing) and parameters determining the moment-curvature relationship (i.e., the PT element and EDDs) at the expense of high computational cost. The latter tends to focus more on the global hysteretic response, thus featuring simplicity and efficiency. While the high-order modelling strategies include the multi-spring model (Ganey 2015; Sarti et al. 2017; Massari et al, 2017; Kovacs and Wiebe 2019; Wichman et al. 2022; Qureshi et al. 2023, Ho et al. 2023, Wichman 2023), the fibre-based model (Akbas et al. 2017; Slotboom 2020; Zhu et al. 2024), and the detailed finite-element model (Wilson et al. 2019; Chen and Popovski 2020; Tomei et al. 2023), the reduced-order approach typically refers to the lumped plasticity model (Iqbal et al. 2015; Sarti et al 2015; Slotboom 2020).
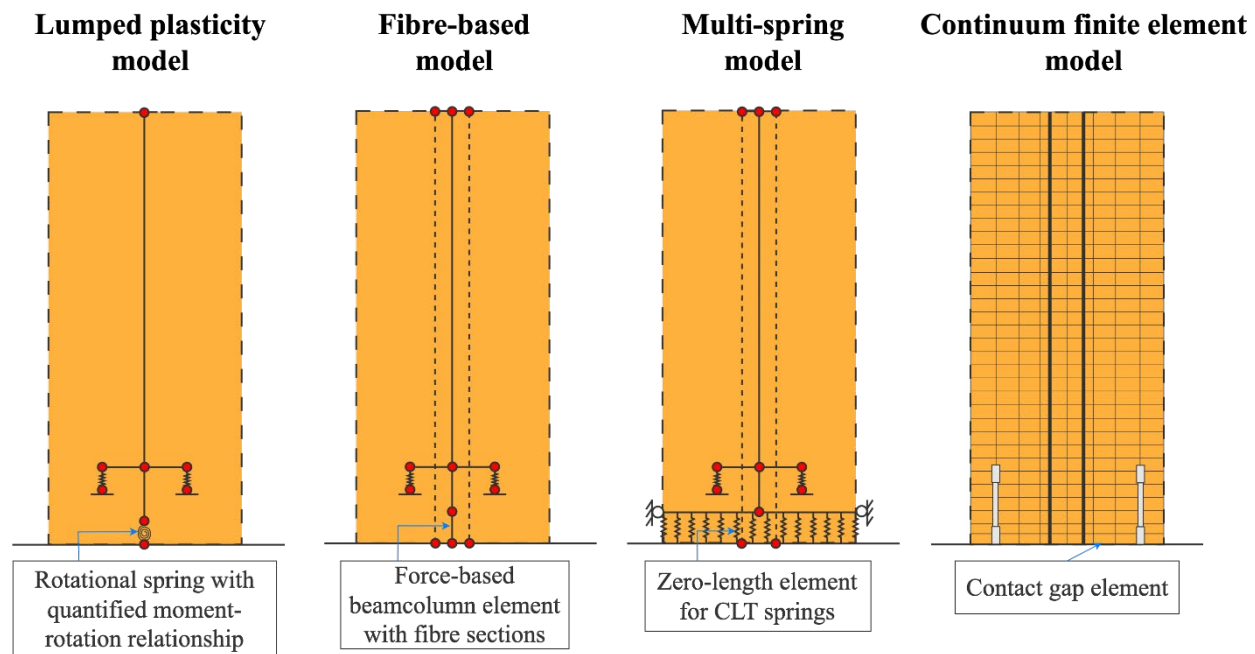
Figure 2-12. Numerical modelling strategies for PT-CLT walls.

In the fibre-based model (FBM), force-based beam-column elements with fibre sections are used to capture the base uplift and deformation at the plastic zone of the CLT panel, in which the plastic hinge length is taken as two times the wall panel thickness (Akbas et al., 2017). Each section is discretized into vertically oriented fibres across the length of the wall and assigned with representative constitutive law of CLT material. The material has a zero tensile strength to physically simulate the base uplift behaviour. The multi-spring model (MSM) employs a series of zero-length elements (ZLEs) at the wall-to-foundation interface. ZLEs can be vertically distributed across the length of the wall using a Labatto Integration method. The top of each ZLE is connected to the bottom node of the CLT panel by a rigid link element, while the bottom is fully fixed. Horizontal restraint is imposed on the elements at the two extreme wall edges to prevent sliding. To convert CLT's stress-strain relationship to force-deformation of each ZLE, the concept of contact stiffness was used, and further details can be found elsewhere (Wichman et al., 2022). Both FBM and MSM feature a relatively simple development process, computational robustness, and capability to capture the response of PT-CLT walls. They further balance accuracy and computational cost and are favourable when performance assessment involves nonlinear response history analysis (NLRHA) and incremental dynamic analysis (IDA) (Vamvatsikos and Cornell 2002).

Compared to FBM and MSM, the lumped plasticity model (LPM) is simple and efficient. It concentrates the panel's nonlinear behaviour at the bottom of the wall using a ZLE assigned with a system-specific moment-curvature relationship at the wall base. The relationship can be derived from either an experimental observation or an analytical prediction based on a monolithic beam analogy (MBA). The simplicity of LPM leads to its incapability to capture progress damage in the structure. Slotboom (2020) concluded that LPM cannot accurately describe the system's response beyond the CLT yielding and has difficulty predicting the post-tensioning force. The detailed finite-element model using finer meshing or discretization allows for considering details such as EDD-to-wall connection and PT-to-wall anchorage, as well as capturing the local and global responses of CLT. While they are accurate in nature, the computational time and modeling challenges make them less favourable for nonlinear analysis.

2.5 Seismic Design of Pres-Lam Walls

Seismic design for Pres-Lam walls typically consists of two major steps. In step one, the specified base shear force or overturning moment should be quantified, and this can be achieved by using either a code-compatible force-based design or a performance-based design. The former requires the seismic force modification factors to reduce the elastic base shear to the specified lateral earthquake force. The modification factors can vary among building codes. Several studies have adopted different seismic force modification factors for Pres-Lams walls. For instance, the Expan design guide (Pampanin et al. 2013) followed seismic design consideration in NZS1170.5:2004 and assumed the design ductility demand for PT-LVL walls at Ultimate Limit State (10 % in 50 years) to be 3. Sarti et al. (2017) concluded a response modification coefficient (R) value of 7 and a system over-strength factor of 3.5 (Ω_s) for ASCE 7 (ASCE, 2016). An R value of 6 was assumed and used in designing the 2-storey and 10-storey PT-CLT shear wall buildings for the shaking table test (Pei et al., 2019; Wichman, 2023), which was the same value also recommended by Busch et al. (2023) for Pres-Lams walls. Ho et al. (2023) reported a lower bound and mean values for R factor to be 6.48 and 11, and 1.49 and 1.91 for Ω_s for PT-MPP.

In Canada, when performing seismic design using equivalent static force procedure (ESFP) or modal response spectrum analysis (MRSA), the product of R_o and R_d is used to reduce the elastic base shear force (NRCC, 2020). R_o accounts for the overstrength arising from the difference between nominal and factored resistance, conservative selection and rounding of member and element sizes, the ratio of actual yield strength to the minimum specified yield strength, and overstrength due to strain hardening and from mobilizing the full capacity of the structural such that a collapse mechanism is formed (Mitchell et al., 2003). R_d is employed to reflect the degree of ductility associated with SFRS. Currently, PT-CLT walls can be designed only as an alternative solution in Canada due to the absence of R_d and R_o for PT-CLT walls in NBCC.

A performance-based design (e.g., a direct displacement-based design (DDBD)) can be used as an alternative to design the prototype buildings. In DDBD, the lateral displacement, inter-storey drift ratio, and material strain limit under seismic loading are considered design criteria and are set at the beginning of the design process (Priestley et al., 2007). DDBD has been applied to PT-LVL (Newcombe, 2011; Sarti, 2015) and PT-CLT walls (Sun et al., 2019; Zhu et al. 2024). DDBD is

based on the substitute structure concept, which requires transforming Multi-Degree-Of-Freedom (MDOF) system to an equivalent Single-Degree-Of-Freedom (SDOF) system. The procedure requires accurate estimation of the building's design displacement, inelastic displacement profile, and effective damping to calculate the design shear forces (Pennucci et al., 2009; Sarti, 2015).

Once design base shear forces or moments are determined based on the FBD or DDBD, the next step consists of associating the design overturning moment (M_b) with the maximum imposed rotation (θ_{imp}) (i.e., the design target). Knowing the moment resistance contributions of the PT and EDD in resisting M_b, adequate sizing can be performed, and the initial post-tensioning force, as well as the required capacity and number of EDDs, can be calculated. Notice that strain compatibility at the wall-to-foundation interface is lost during rocking of the CLT panel, making it challenging to find the section equilibrium. Therefore, a sectional analysis (Pampanin et al. 2001) can be used to quantify the system's moment resistance at θ_{imp}. The analysis starts with a trial value of the neutral axis depth, after which deformation in the post-tensioned cable and the UFPs can be evaluated based on the section geometry. To estimate the CLT strain, the Monolithic Beam Analogy (MBA) concept was used (Pampanin et al. 2001). The analogy considers the displacement of a post-tensioned connection equal to that of an equivalent monolithic connection under the same lateral load. Equating the rigid body rotation with the known rotation of a plastic hinge region makes it possible to estimate the CLT's compressive strain (ε_t), given by Equation [2-10] (Newcombe et al., 2008; Wichman, 2023):

$$\varepsilon_t = c \left(\frac{L_{cant}\, \theta_{imp}}{l_p (L_{cant} - \frac{l_p}{2})} + \phi_e \right)$$

Equation 2-10

where L_{cant} is the effective cantilever height of the wall, l_p is the plastic hinge height, taken as two times the CLT wall thickness (Akbas et al., 2017) and ϕ_e is the elastic curvature. Section equilibrium can be checked based on component deformations by determining whether the net force exceeds the tolerance. If not, iterative adjustment of the neutral axis is required until section equilibrium is achieved. Additional checks shall be performed, such as the strain in the post-tensioned tendon at the design drift. The flexural and shear resistance of the CLT walls shall also be verified following CLT manufacturing standards.

2.6 Performance Assessment of Pres-Lam Walls

Several studies have also assessed the seismic performance of Pres-Lams walls using numerical approaches (Table 2-3). Ganey (2015) applied a performance-based design procedure to design eight- and fourteen-storey archetype buildings. Besides a single rocking segment, a second rocking storey was introduced and placed at the 5th storey for 8-storey prototypes and at either the 6th, 8th, or 10th storey for 14-storey prototypes (i.e., in total, six designs). The parametric analysis using NLRHA demonstrates that multi-rocking segments can reduce storey drifts and component damage. However, the reduced stiffness of higher rocking storeys needs to be further studied. Akbas (2016) developed both a closed-formed equation and a fibre-based numerical model to describe the lateral behaviour of PT-CLT walls coupling with UFPs. A seismic design criterion was developed where seismic performance objectives are related to structural damage (limit) states, and each design objective is related to a seismic PO with a particular level of seismic hazard intensity (Table 2-2). Archetype buildings of 6 and 11 storeys were developed and examined using NLRHA. Under MCE events, CLT splitting was not reached, and introducing the upper rocking segment for 11-storey helped decrease the roof level floor acceleration. Sarti et al. (2017) adopted the force-based design procedure outlined in Sarti (2015) and determined seismic performance factors for PT-LVL walls following the FEMA P695 approach (FEMA 2009). 22 archetype buildings were developed for each structural configuration (SW, CWC, and CW) to reflect design variability in building and storey height, wall depth, gravity load and seismic design category. NLSA and IDA demonstrate the satisfactory performance of PT-CLT walls and concluded a behaviour factor in Eurocode 8, q, and inelastic spectrum scaling factor, k_μ, to be 2. Pilon et al. (2018) intended to address the potential dynamic amplification of upper-storey responses in tall timber buildings by applying multiple rocking segment systems. NLRHA indicated a 45% reduction in shear and bending moment envelops can be achieved when allowing gap opening between adjacent wall segments. Kovacs and Wiebe (2019) conducted a collapse assessment for 3-, 6-, and 9-storey buildings with PT-CLT walls without EDDs in Montreal, a city of moderate seismicity in Canada. The study set the performance requirement to be 2.5% ISDR. NLRHA showed the median responses were well predicted, and a collapse assessment for 3-, 6-, and IDA indicated that the probability of collapse under MCE ground motions is close to 10%. Sun et al. (2019) correlated PO of IO, LS, and CP with 1%, 1.5%, and 2% ISDR and adopted DDBD to design archetype buildings of 8-, 12-, and 16-storey. NLRHA indicated that for PT-CLT walls

without EDDs, the failure probability decreases with the increase of the storey number from 8 to 12 to 16. Wilson et al. (2020) applied performance-based seismic design for a 5-storey office building and a 12-storey residential building with PT-CLT wall coupling with UFP as SFRS. The performance assessment using 50 ground motions consisting of far-field and near-field events concluded that both buildings met the ISDR limit specified in ASCE 7-16. Furley et al. (2021) assessed the time-to-functionality fragilities of PT-CLT shear wall buildings. The study indicated that the rocking wall system does not reduce damage for non-structural moments, and further study needs to incorporate deformation-compatible non-structural components. Busch et al. (2022) developed a prescriptive design procedure for the Pres-Lams walls aligned with ASCE 7, which can be adopted in typical engineering design offices without the need for advanced nonlinear models and analyses. Ho et al. (2023) adopted the direct displacement-based design (DDBD) and evaluated the seismic performance factors of a 3-storey post-tensioned mass plywood panel (PT-MPP) with coupling UFPs using 44 far-field shallow crustal ground motion from FEMA P695. Wichman (2023) investigated the impact of wall aspect ratio on building performance and its implication for moment amplification independent of the building period by developing six prototype buildings (three 6-storey, and three 12-storey). The study concluded that a higher moment amplification can result in a longer period of PT-CLT shear wall building. Furthermore, moment amplification at mid-height of the building is relatively non-sensitive to low hazard.

Table 2-3. Summary of seismic performance assessment studies for PT-CLT mass timber buildings.

Study	System configuration	Seismic design	Archetypes building	Building location	Modelling strategies	Analyses
Ganey (2015)	PT-CLT wall (CW)	PBD	8, 14	Seattle	MSM	NLRHA
Akbas (2016)	PT-CLT wall (CW)	FBD	6, 11	Seattle	FBM	NLSA, NLRHA
Sarti et al. (2017)	PT-LVL wall (SW, CWC, CW)	FBD	3, 6, 8	Christchurch	MSM	NLSA, NLRHA, IDA
Pilon et al. (2018)	PT-CLT and PT-LVL wall (SW)	DDBD	3, 6, 8, 9	Christchurch	MSM	NLRHA
Kovac and Wiebe (2019)	PT-CLT wall (pure post-tension)	FBD	3, 6, 9	Montreal	MSM	NLRHA, IDA
Sun et al. (2019)	PT-CLT wall (pure post-tension)	DDBD	8, 12, 16	Sichuan	MSM	NLSA, NLRHA
Wilson et al. (2020)	PT-CLT wall (CW)	FBD	5, 12	Seattle	LPM	NLRHA
Furley et al. (2021)	PT-CLT wall (CW)	FBD	2	Seattle	MSM	IDA
Busch et al. (2022)	PT-CLT wall (CWC)	FBD	6	Seattle	LPM	NLRHA
Wichman et al. (2022)	PT-CLT wall (CWC)	FBD and PBD	10	Seattle	MSM	NLRHA
Ho et al. (2023)	PT-MPP wall (CW)	DDBD	3	Seattle	MSM	NLSA, IDA
Wichman (2023)	PT-CLT wall (CW)	FBD	3, 6	Seattle	MSM	NLSA

2.7 Existing Pres-Lam Wall Buildings and Status

With decades of research efforts, the Pres-Lams walls have found themselves in several real-world applications. In 2011, the Art and Media Centre of Nelson-Marlborough Institute of Technology in New Zealand was the first building to use PT-LVL wall panels coupled with UFPs (Figure 2-13). Subsequent projects which use self-centring SFRS in New Zealand and other regions have been complied with in the work of Chen et al. (2024) and re-tabularized in Table 2-4. Notice that most existing buildings are still low-rise (i.e., below 6-storey). Currently, there is a 12-storey tall mixed-use mass timber building to be constructed, including PT-CLT walls with UFPs as SFRS, in a region of high seismicity in the United States (Portland, Oregon). While the construction is on hold, the project-specific testing (fire, acoustic, and structural testing for mass timber) and performance-based design were accomplished and approved in 2016. After the full-scale shaking table test of the 10-storey PT-CLT shear wall building, the NHERI TallWood initiative is conducting a FEMA P695 study to derive the system-specific seismic force modification factors and intend to include PT-CLT walls in ASCE 7-28 as an alternative mass timber lateral system.

Figure 2-13. The Art and Media Centre of Nelson-Marlborough Institute of Technology (Holden et al., 2016).

Table 2-4. Application of self-centring mass timber structures (Adapted from Chen et al. 2024).

Building	Storey	Location	System
NMIT Arts & Media Building (2011)	3	Nelson, New Zealand	PT coupled LVL wall with UFPs
Carterton Events Centre (2011)	1	Carterton, New Zealand	PT-LVL wall with mild steel bars
BRANZ's Nikau building (2011)	1	Judgeford, New Zealand	PT-LVL portal frame and PT columns
EXPAN office (2011)	2	Christchurch, New Zealand	PT-LVL frame & PT-LVL wall
COCA building at Massey University (2012)	3	Wellington, New Zealand	PT frames & PT concrete walls
Young Hunter House - Merritt Building (2013)	3	Christchurch, New Zealand	PT-LVL frames & reinforced concrete wall
Trimble Navigation Offices (2013)	2	Christchurch, New Zealand	PT-LVL coupled walls & PT-LVL frames
St Elmo Courts Building (2013)	5	Christchurch, New Zealand	Base-isolation & PT frames with LVL beams and concrete columns
The ETH HoNR (2014)	3	Zürich, Switzerland	PT ash GLT frames & concrete bottom storey
Sumitomo Forestry Fire Laboratory (2015)	1	Midorigahara Tsukuba City, Japan	PT-LVL wall with mild steel bars in the base
The Kaikoura District Council (2016)	2	Kaikoura, New Zealand	PT-CLT/LVL composite rocking shear walls
The Beatrice Tinsley Building (2019)	4	Christchurch, New Zealand	PT-LVL frame & concentric LVL cross bracing
Peavy Hall (2020)	3	Corvallis, USA	PT single & double CLT walls
Ashburton District Council's new library and civic centre (--)	3	Ashburton, New Zealand	PT-CLT wall with DFFJ

Note: Year of completion labelled as "--" means the building is still under construction.

2.8 Seismic Hazard in Canada

Canada has a vast territory with diverse types of seismic hazards (Figure 2-14). In Southwestern BC, Canada, three different damaging earthquake sources coexist: the shallow crustal, deep-in-slab, and megathrust interface (Goda, 2019). In contrast, a single tectonic regime of the stable crustal dominates the Eastern Canada seismic hazard.
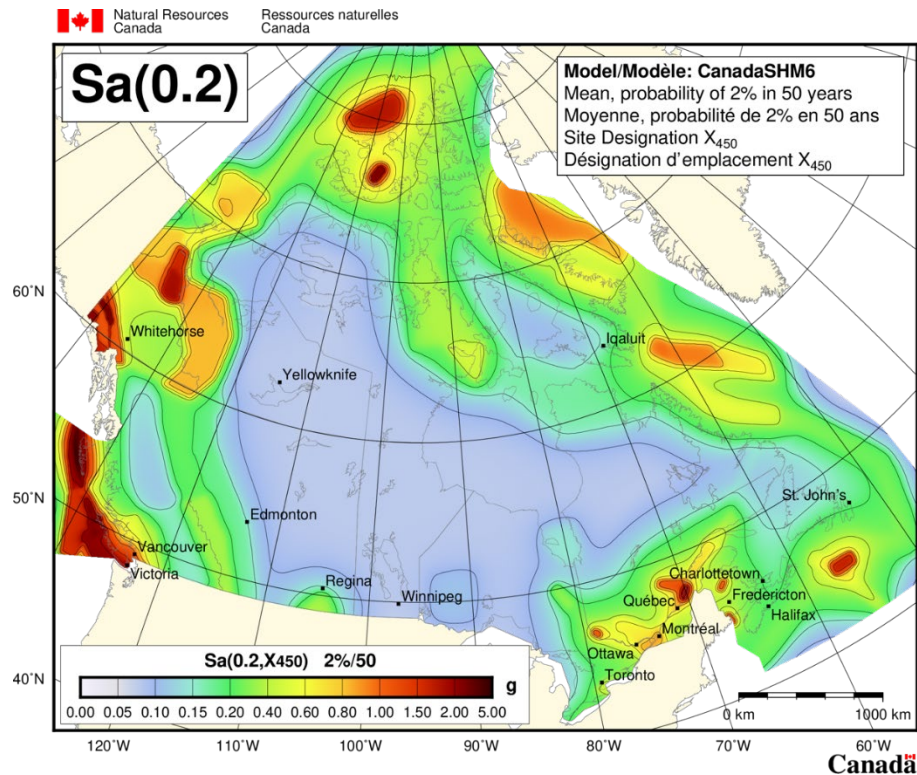
Figure 2-14. Seismic hazard map based on SHM6 in NBCC 2020 with intensity measurement of spectral acceleration at 0.2 s (Kolaj et al., 2020a).

The national seismic hazard model has been developed to support the seismic design of building and infrastructure. In Canada, the adoption of the sixth-generation Seismic Hazard Model (Kolaj et al., 2020a) by NBCC 2020 (NRCC, 2020) resulted in a nationwide increase in seismic hazard (Figure 2-15).
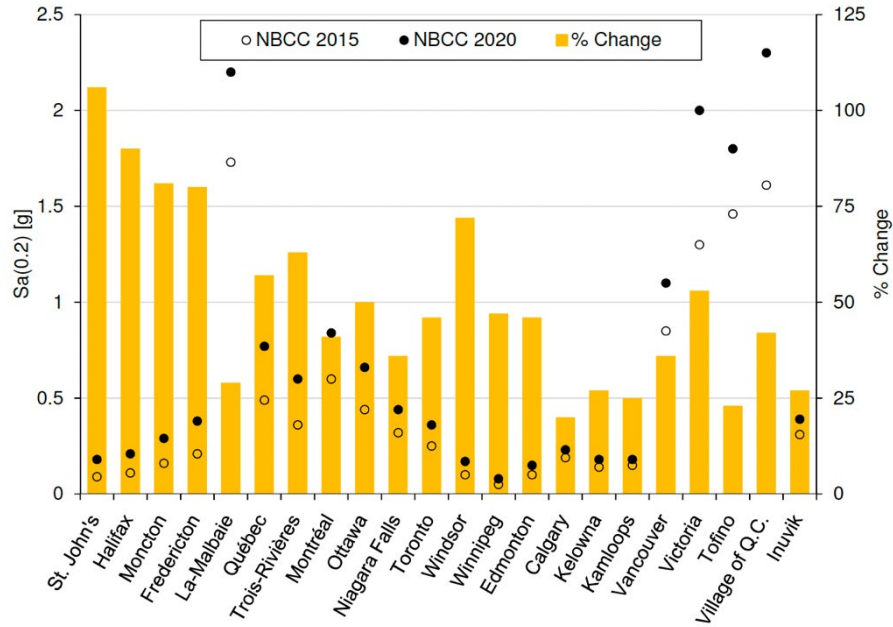
Figure 2-15. Change in seismic hazard from NBCC 2015 to NBCC 2020 for selected locations in Canada. Intensity measure- *Sa* (0.2); Return Period- 2475 years; Site Class- C (*Vs*30=450 m/s) (Odikamnoro et al., 2022).

The observed increase in seismic hazard results from changes in seismic source models (SSM) and ground motion models (GMM), which are summarised below.

- For the Juan de Fuca segment of the Cascadia subduction zone, four extra rupture earthquakes were added in addition to the 18 included in NBCC2015.

- Modification of inslab sources under the Strain of Georgia was made. Specifically, three sources with various depths were adopted to improve the consideration of the dip and spatial activity rate.

- A potentially active crustal fault system was included, i.e., Leech River Valley and Devil's Mountain faults near Victoria.

- GMM in SHM6 adopted the modern ground motion models with a classical weighted approach.

- GMM in SHM6 allows a direct calculation of hazards on various site classes, given Vs30 as input, instead of providing hazard values on a reference class C site and applying the F(T) factor in SHM5 and NBCC 2015.

- Canada's SHM6 was fully implemented with the OpenQuake Engine (Pagani et al., 2014), an open-source software package for seismic hazard and risk analysis.

To quantify project-specific seismic hazards based on SHM6, one can use sample *OpenQuake* compatible command files for probabilistic seismic hazard analysis (PSHA) prepared by NRCan (Kolaj et al., 2020b). Modifications are required to properly define the site of interest, soil condition, annual probability of exceedance, and intensity measurement of interest. Outputs from the calculation include the seismic hazard curves, uniform hazard spectra (UHS) and disaggregation results. Moreover, the NRCan online seismic hazard tool (NRCC 2020) provides spectral acceleration values at only 10 periods, necessitating interpolation if the building's fundamental period falls in between. With *OpenQuake,* spectral accelerations at multiple finite periods can be directly calculated.

2.9 Summary

Chapter 2 offers a comprehensive literature review for mass timber buildings in Canada and PT-CLT walls as SFRS from multiple facets, including experimental testing, numerical modelling, seismic design methods, seismic performance assessment, and existing building using post-tensioned rocking timber walls. While previous studies involving experimental and numerical approaches concluded a satisfactory performance of PT-CLT shear wall buildings in region of low to moderate seismicity, there is clearly a need to assess the performance of such SFRS in high seismic zone susceptible to multiple types of earthquakes. Such a gap motivates this thesis work to investigate the seismic performance and potential application of PT-CLT shear wall building with EDDs in Southwestern BC, Canada. Chapter 3 includes a seismic performance assessment for prototype six-, nine-, and twelve-storey PT-CLT shear wall buildings equipped with BRAFs. Chapter 4 presents a seismic performance assessment for PT-CLT shear wall buildings with coupling UFPs. The conclusion from these studies and research project are summarised in Chapter 5.

Chapter 3 SEISMIC PERFORMANCE ASSESSMENT OF POST-TENSIONED CLT SHEAR WALL BUILDINGS WITH BUCKLING-RESTRAINED AXIAL FUSES

This chapter has been adopted from a published journal paper written by the author. It is published in the Canadian Journal of Civil Engineering:

Zhu, H., Bezabeh, M.A., Iqbal, A., Popovski, M., Chen, Z., 2024. Seismic performance assessment of post-tensioned CLT shear wall buildings with buckling-restrained axial fuses. Can. J. Civ. Eng. cjce-2023-0448. https://doi.org/10.1139/cjce-2023-0448

3.1 Chapter Overview

Post-tensioned cross-laminated timber (PT-CLT) walls have been demonstrated to be a low-damage seismic force-resisting system (SFRS) due to their self-centring capability. However, there is still a need to examine the seismic performance of such SFRS in high seismic risk zones. This study evaluates the seismic performance of 6-, 9-, and 12-storey PT-CLT shear wall buildings in Vancouver, Canada, equipped with Buckling-Restrained Axial Fuses (BRAFs). The prototype buildings were designed using the displacement-based design method, and the assessment considered the most recent seismic hazard model provided in the 2020 National Building Code of Canada. To conduct nonlinear response history analysis (NLRHA) and incremental dynamic analysis (IDA), numerical models were developed in *OpenSeesPy* and calibrated based on component and system-level experimental tests. The NLRHA and IDA results demonstrate that all the studied buildings have adequate collapse margin ratios, with less than a 10% chance of collapsing at maximum considered earthquakes.

3.2 Background

Mass timber buildings have gained popularity in North America due to their attractive architectural appearance, reduced construction time, and inherent material sustainability (NRC & CFS, 2021; Yang et al., 2022; Brown et al., 2022; Daneshvar et al., 2022; Odikamnoro et al., 2022). Mass timber buildings use Cross-laminated timber (CLT) and glued laminated timber (glulam) for load-

bearing walls, columns, beams, floors, and roofs. CLT is an engineered wood product and has been applied in residential and non-residential buildings. With lumber boards positioned in orthogonally alternating directions and bonded with adhesives, CLT features dimensional stability, usage of low-grade timber, and lower weight-strength ratio (Ceccotti et al., 2013; Assadi et al., 2023; Teweldebrhan et al., 2023), and higher in-plane strength and stiffness. Recent advances have led to construction of notable tall timber and hybrid buildings worldwide, such as the 18-storey Mjostarnet in Norway and Tall Wood Building Demonstration Initiative (TWBDI) projects in Canada (i.e., the 18-storey Brock Commons in Vancouver and the 13-storey Origine in Québec) (NRC & CFS, 2021). Approximately 500 mass timber buildings have been constructed in Canada since 2007, and this number is growing exponentially, as is the urge to go taller with timber (NRC & CFS, 2021). In Canada, the latest version of the 2020 National Building Code of Canada (NBCC) (NRCC 2020) has extended the encapsulated mass timber construction height limit to 12 storeys. The US 2021 International Building Code (IBC) (*ICC*, 2020) allowed 18 storeys in mass timber construction.

In mass timber buildings, most of the building flexibility and energy dissipation depends on connectors (Gavric et al., 2015) because mass timber structural components have limited energy dissipation capability (Brown et al., 2022). Under large drift, permanent damage to conventional connectors could result in significant residual drift, posing a risk of aftershock collapse of mass timber buildings with CLT shear walls (Assadi et al., 2023). To enhance seismic performance and reduce structural damage, various innovative and low-damage mass-timber seismic force-resisting systems (SFRSs) have been proposed (Palermo et al., 2005; Bezabeh et al., 2017; Yang et al., 2022; Teweldebrhan et al., 2023). One promising system is post-tensioned cross-laminated timber (PT-CLT) walls, which belong to a broad category of prestressed-laminated timber (Pres-Lam) systems (Palermo et al., 2005). Borrowing the post-tensioned seismic damage-resistant solution from the PREcast Seismic Structural Systems (PRESSS) program (Priestley et al., 1999), such SFRSs integrate mass timber walls with unbonded post-tensioned tendons to create moment-resisting connections (Granello et al., 2020). For a PT-CLT wall, the CLT panel can resist lateral load, whereas the post-tensioned tendon can exert a restoring moment, achieving self-centring of the system. External energy dissipation devices (EDDs) such as buckling-restrained axial fuses (BRAFs) (Sarti et al., 2016b) and U-shaped Flexural Plates (UFPs) (Kelly et al., 1972) are often

coupled with Pres-Lam to increase energy dissipation. The sacrificial energy dissipators will yield at the early stage of seismic excitation, reducing damage to primary structural components (Chen et al., 2020). Such a seismically resilient system is economically appealing because post-earthquake repairs will focus only on replacing the EDDs due to the low damage sustained by the structure (Furley et al., 2021).

Extensive experimental testing has been conducted to investigate the structural performance of hybrid Pres-Lam systems (Palermo et al., 2005; Smith et al., 2007; Iqbal et al., 2015; Sarti et al., 2016a). Early research from the University of Canterbury in New Zealand focused on testing post-tensioned laminated veneer lumber (PT-LVL) walls. Single panels with axial dissipators (Palermo et al., 2005) and coupled wall panels connected by UFPs (Smith et al., 2007) were tested under quasi-static cyclic and pseudo-dynamic testing. Sarti et al. (2016a) investigated the effects of BRAFs arrangement and different levels of initial post-tensioning force in quasi-static cyclic testing of a two-thirds scale PT-LVL wall. Iqbal et al. (2015) also examined the performance of coupled wall systems with UFPs under lateral loading. As similar post-tensioning techniques can also be applied to CLT wall panels, the inherent differences between PT-CLT and PT-LVL walls were explored in a study by Pilon et al. (2019). Brown et al. (2022), based on cyclic testing of single and double PT-CLT walls, concluded that the design method for PT-LVL walls could underpredict the peak compressive strain in CLT walls because of material variability and complexity. Nonetheless, the excellent performance of the self-centring capability of PT-CLT walls was confirmed and assured (Sun et al., 2020). Enhanced strength and stiffness can be achieved when PT-CLT walls are coupled by shear dampers (Pozza et al., 2021), screwed connections (Brown et al., 2022), or BRAFs (Kramer et al., 2016).

In Canada, major testing of PT-CLT walls was initiated and led by FPInnovations (Chen et al., 2018; Chen et al., 2020). In 2019, fourteen full-scale PT-CLT wall specimens in six configurations were tested under monotonic and reversed cyclic loading. In the United States, the National Science Foundation funded a multi-year research project, the NHERI Tallwood Project (Pei 2017), which aimed to develop and validate a seismic design methodology for tall wood buildings. Ganey et al. (2017) performed quasi-static experiments on six PT-CLT walls to investigate structural responses under lateral loading with different design parameters and found that PT-CLT walls possess good self-centring behaviour up to a large drift of 5%. Akbas et al. (2017) identified

structural limit states for PT-CLT walls based on experiments (Ganey et al., 2017) and developed closed-form expressions and fibre-element-based numerical models to predict structural responses. A building-level experimental examination was also performed (Pei et al., 2019), in which a full-scale 2-storey mass timber building with PT-CLT walls as SFRS was tested on the shaking table. After subjecting the test building to a suite of ground motions, the performance goal of no major structural damage was achieved. Currently, by the time of writing of this paper, there is an ongoing full-scale 3-D shaking-table test of a ten-storey mass timber building with PT-CLT walls as SFRS at the University of California in San Diego (Pei et al., 2023).

Various numerical modelling strategies have also been proposed for PT timber walls to predict their structural responses under lateral loading and perform parametric analyses. These strategies include the multi-spring model (Ganey, 2015; Kovacs and Wiebe, 2019; Wichman et al., 2022; Qureshi et al., 2023), the fibre-based model (Akbas et al., 2017; Slotboom, 2020), the lumped plasticity model (Iqbal et al., 2015; Slotboom, 2020), and the finite-element model (Wilson et al., 2019; Chen and Popovski, 2020; Tomei et al., 2023). Among these, the fibre-based model uses vertically distributed fibres at the bottom of the CLT wall to capture the base uplift or gap opening of the wall panel, where large deformation or rocking behaviour is expected within the plastic hinge zone (Akbas et al., 2017). Slotboom (2020) applied results from system-level testing (Chen et al., 2020) and building-level testing (Pei et al., 2019) to calibrate the fibre model. Good agreement was found in the quasi-static cyclic and dynamic responses between the numerical model and experimental results. The fibre model features a simple development process, computational robustness, and its capability to capture the response of PT-CLT walls. Such modelling strategies can further balance accuracy and computational cost and be favourable when performance assessment involves nonlinear response history analysis (NLRHA) and incremental dynamic analysis (IDA) (Vamvatsikos and Cornell, 2002).

Several studies have investigated the seismic performance of buildings equipped with PT timber walls (Akbas, 2016; Sarti et al., 2017; Kovacs and Wiebe, 2019; Furley et al., 2021). Sarti et al. (2017) followed FEMA P-695 (FEMA 2009) to determine the seismic performance factors for PT-LVL walls, and Furley et al. (2021) assessed the time-to-functionality fragilities of PT-CLT shear wall buildings. Akbas (2016) designed 6- and 11-storey buildings using PT-CLT coupled walls with UFPs in Seattle, U.S.A. The NLRHA indicated good seismic performance of the SFRS under

maximum considered earthquake (MCE) events. Kovacs and Wiebe (2019) designed 3-, 6-, and 9-storey PT-CLT shear wall buildings for Montreal, Canada, considering the seismic hazard prescribed in NBCC 2010 (NRCC 2010). The authors reported that, under MCE, the probability of collapse for all prototype buildings was less than 10%. Nonetheless, most of these studies evaluated either low to medium seismicity or simple seismotectonics (e.g., shallow crust), and the performance assessment of PT-CLT wall buildings equipped with BRAFs was limited. With the wide adoption of the sixth generation Seismic Hazard Model of Canada (SHM6) (Kolaj et al., 2020a) in NBCC 2020, there has been a general increase in the estimates of seismic hazards by 25–50% in many regions across Canada. With the complex seismotectonic environment in Southwestern British Columbia (BC), such an increase is expected to affect the seismic design and performance of buildings significantly (Odikamnoro et al., 2022). To further promote development and practical application of PT-CLT shear wall buildings in Canada, a seismic performance study in high seismic-risk zones is necessary.

This study evaluates the seismic performance of PT-CLT shear wall buildings with EDDs, i.e., BRAFs (Figure 3-1a), considering the diverse earthquake types and increased seismic hazard in Southwestern BC, Canada, and is organized as follows. First, the structural mechanics and limit states of PT-CLT walls with BRAFs under lateral loading are described. Displacement-based seismic design and sectional analysis procedures are then outlined and described. Subsequently, the development of two-dimensional fibre-based numerical models of PT-CLT walls with BRAFs using *OpenSeesPy* (Zhu et al., 2018) is presented. The numerical models are calibrated with results from static and quasi-static cyclic component- and system-level experimental tests (Chen et al., 2020). Next, site-specific probabilistic seismic hazard analysis (PSHA) is conducted for Vancouver using the SHM6, and ground motions reflecting regional seismicity are selected and scaled. NLRHA is carried out to examine critical structural responses such as storey drift and shear forces. IDA is used to quantify collapse probabilities.
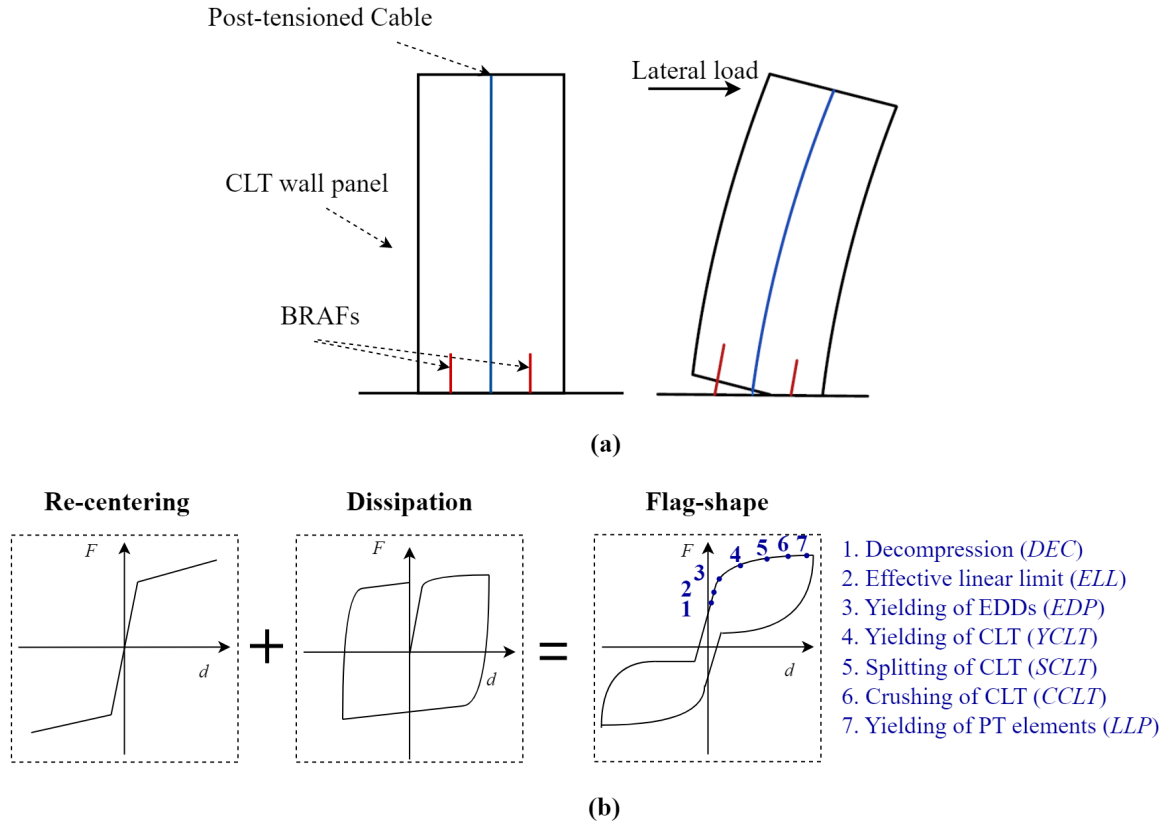
Figure 3-1. (a) PT-CLT single wall with BRAFs under lateral loading. (b) Idealized flag-shaped force-deformation hysteresis of PT-CLT walls with BRAFs.

3.3. Structural Mechanics of PT-CLT Walls with BRAFs

3.3.1. Overall System Response to Lateral Loads

In general, PT-CLT walls are engineered to have a controlled rocking motion at the interface between the wall and the foundation when subjected to lateral loading. Lateral loading in PT-CLT walls results in an overturning moment, leading to a composite deformation with contributions from flexure, shear, and rigid-body rocking (Daneshvar et al., 2022). Figure 3-1 shows the lateral deformation and idealized flag-shaped force-deformation hysteresis behaviour of PT-CLT walls with BRAFs. Several limit states have also been identified in the backbone curve. Initially, the overturning moment in PT-CLT walls is resisted by the decompression moment (DEC) contributed by the self-weight of the panel and the initial post-tensioning force in the tendon and leads to elastic deformations exclusively. As the overturning moment exceeds the DEC, rigid body rocking of the

panel commences, and compressive stress accumulates at the CLT toe. Strain compatibility at the interface is lost, but section equilibrium can still be retrieved, provided that the neutral axis position and CLT stress are known. With increasing imposed rotation, the BRAFs reach the yielding limit state (EDP) and start to dissipate energy. However, the initial geometric and material nonlinearity is limited, and the wall still behaves quasi-elastically until the effective linear limit (ELL), where significant nonlinear behaviour can be observed in the moment-rotation relationship. As the compressive stress in CLT further concentrates, the yielding (YCLT), splitting (SCLT), and crushing (CCLT) limits of the CLT material are sequentially reached, followed by the eventual yielding of PT tendons (LLP). To achieve self-centring, in designing the hybrid PT-CLT wall, it is suggested that the recentring ratio, β_{rc}, should be greater than 0.55 (Sarti et al. 2017).

3.3.2. Buckling-Restrained Axial Fuses

The concept of BRAFs traces back to the early application of buckling restrained braces (BRB) (Sabelli et al., 2003; Black et al., 2004), which effectively enhanced seismic performance for conventional braced frames. In such a system, a steel core encased in a steel tube filled with concrete was utilized, and it can produce ductile and stable hysteretic behaviour. Subsequently, attention was given to applying BRB at the local level (Mojiri et al., 2021) so that the plastic deformation can be concentrated within the system, capacity-protecting the main structure. More recently, replaceable BRAFs were adopted as EDD coupled with self-centring rocking timber walls to increase energy dissipation (Palermo et al., 2005; Sarti et al., 2013; Sarti et al., 2016a; Rahmzadeh and Iqbal, 2018; Chen et al., 2020). BRAFs are typically mild steel bars with reduced diameter in the centre where concentrated and localized tensile and compressive yielding occurs. To prevent buckling, the bars are usually encased in hollow steel tubes filled with epoxy or grout. An alternative way to prevent buckling is to employ two steel half-tubes to cover the portion with reduced diameter (Figure 3-2). A maximum strain of 6% can be achieved in BRAFs using either method (Chen et al., 2018). Sarti et al. (2016b) investigated the failure mechanism of BRAFs by testing samples with various dissipator slenderness, geometry, and differences in fuse versus external diameters. An infill material of either cement grout or epoxy was used. Based on the results, two failure mechanisms were identified. For specimens with a low slenderness ratio, axial low-cycle fatigue leads to fracture after repetitive loading in a manner similar to experimental observations (Chen et al., 2018). The second failure mode is associated with a buckling/sway

54

mechanism, where localized plasticization of the confining tube occurs due to increased unloading force and causes the entire device to sway (Sarti et al., 2016b). A simplified model to capture fuse-tube interaction was also provided, in which the total stiffness of a BRAF with infill material is given by Equation 2-5, Equation 2-6, and Equation 2-7. Kramer et al. (2016) performed panel tension and panel cyclic tests, in which BRAFs were embedded in the CLT panel. In addition to validating the stable energy dissipation of the system, the study showed that no damage occurred to the CLT panel and that the fasteners remained rigidly attached as per the design. Therefore, coupling PT-CLT walls with BRAFs can assist in achieving a low-damage system under seismic events.
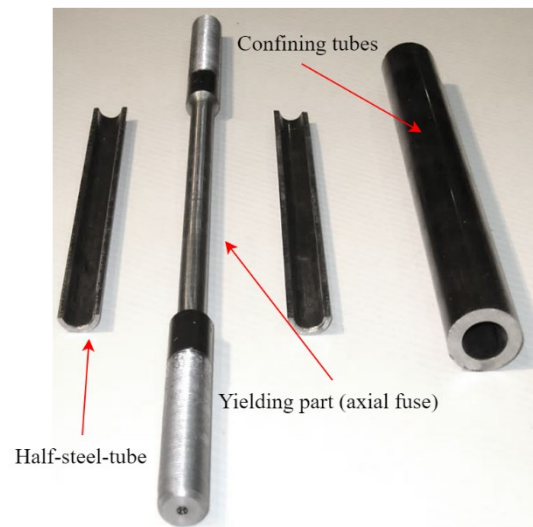
Figure 3-2. Buckling-Restrained Axial Fuses (BRAFs) (Picture courtesy of Zhiyong Chen from FPInnovations).

3.4. Seismic Design of PT-CLT Walls

3.4.1 Seismic Design Approach

Seismic design of PT-CLT walls with EDDs can be carried out using Force-Based Design (FBD) or Displacement-Based Design (DBD) procedures. In FBD, the base shear of the building is obtained by multiplying the spectral acceleration at the building's fundamental period by the seismic mass and other seismic performance and force modification factors. For PT-LVL walls with EDD, a response modification factor (R) of 7 and system overstrength factor (Ω_0) of 3.5 were recommended for ASCE 7 (Sarti et al., 2017). Pei et al. (2019) used an R-factor of 6, which was also suggested by Busch et al. (2022), to design a 2-storey mass-timber building with PT-CLT walls. Nonetheless, in the context of Canada, NBCC 2020 has yet to prescribe ductility (R_d) and overstrength (R_o) factors for PT-CLT walls. Therefore, given the currently unclear R_d and R_o factors, DDBD is a more appealing and rational approach to designing PT-CLT walls.

3.4.2 DDBD Procedure for PT-CLT Walls with BRAFs

In DDBD, the lateral displacement, inter-storey drift ratio, and material strain limit under seismic loading are considered design criteria and are set at the beginning of the design process (Priestley et al., 2007). DDBD has been applied to PT-LVL (Newcombe, 2011; Sarti, 2015) and PT-CLT walls (Sun et al., 2019). DDBD is based on the substitute structure concept, which requires transforming Multi-Degree-Of-Freedom (MDOF) system to an equivalent Single-Degree-Of-Freedom (SDOF) system. The procedure requires accurate estimates of the building's yield displacement, displacement profile, and effective damping to calculate the design shear forces (Pennucci et al., 2009). Figure 3-3 presents the DDBD procedure that is proposed to design PT-CLT walls with BRAFs.

Step 1 : Architectural design
(*e.g. setting number, location, and orientation of PT-CLT walls*) and evaluating the seismic weight $[W]$

$$W = 1.0D + 0.5L + 0.25S$$
(NRCC 2020)

Step 2 : Set the target drift $[\theta_d]$ and identify inter-storey drift ratio limit $[\theta_i]$

Performance criteria: top roof drift ratio not exceeding 2% under MCE event

Step 3 : Specify design ductility $[\mu]$ and evaluate Equivalent Viscous Damping (EVD) $[\xi]$

$$\xi = \xi_{hyst} + \xi_{el}$$

$$\xi_{hyst} = k_{dyn} k_\xi \frac{(2 - 2\beta)(\mu - 1)}{\mu \pi (1 + r(\mu - 1))}$$

$$k_\xi = 0.83 + (\mu - 1) \begin{cases} 0.06 & \text{if} \quad \text{with strain hardening} \\ 0.02 & \text{if} \quad \text{without strain hardening} \end{cases}$$

(Sarti et al., 2015)

Step 4 : Evaluate the displacement profile $[\Delta_i]$

$$\Delta_i = \delta_i \left(\frac{\Delta_c}{\delta_c} \right)$$

$$\delta_i = (1 - k_{el}) \left(\frac{h_i}{h_n} \right) + k_{el} \left[\frac{3h_i^2}{2h_n^2} \left(1 - \frac{h_i}{3h_n} \right) \right]$$

$$k_{el} = 0.1 + \frac{0.6}{\mu}$$
(Sarti et al., 2015)

Step 5 : Determine the equivalent SDOF properties $[\Delta_d], \ [m_e], \ [H_e]$

$$\Delta_d = \sum_{i=1}^n \frac{m_i \cdot \Delta_i^2}{m_i \cdot \Delta_i} \quad m_e = \sum_{i=1}^n \frac{m_i \cdot \Delta_i}{\Delta_d}$$

$$H_e = \frac{\sum_{i=1}^n (m_i \cdot \Delta_i \cdot H_i)}{\sum_{i=1}^n (m_i \cdot \Delta_i)}$$

Step 6 : Determine the displacement design spectrum $[S_d(T)]$

$$S_d(T) = \frac{S_a(T)}{\omega^2} = \frac{S_a(T)}{4\pi^2} \cdot T^2$$

$$R_\xi = \left(\frac{7}{2 + \xi} \right)^\alpha$$

Step 7 : Determine the effective period $[T_e]$ and the effective stiffness $[K_e]$

$$K_e = \frac{4\pi^2 m_e}{T_e^2}$$

Step 8 : Calculate the base shear $[V_b]$ and overturning moment $[M_b]$

$$V_b = K_e \cdot \Delta_d \qquad M_b = V_b \cdot H_e$$

Step 9 : Distribute the base shear to each storey $[F_i]$

$$F_i = (V - F_t) \cdot \frac{W_x h_x}{\sum_{i=1}^n (W_i h_i)}$$

where $F_t = 0.07(T_a)V$ but not exceed $0.25V$
(NRCC2020)

Step 10 : Perform sectional analysis and quantify the moment resistance at the imposed rotation $[M_r]$

Is $M_r > M_b$?
Is preliminary design and detailed design satisfied?

YES

DDBD design finished

Adjust the Architectural design

NO

Figure 3-3. Direct displacement-based design procedure for PT-CLT walls with BRAFs.

With the architectural inputs and the estimated seismic weight (Step 1), DDBD starts by defining the desired performance goal (Step 2). A roof drift ratio of 2% is proposed as the performance criterion for PT-CLT shear wall buildings under MCE events with a return period of 2475 years. The maximum inter-storey drift (MISD) should also not exceed 2.5%, as prescribed in NBCC 2020 (NRCC 2020). System ductility (μ) in the range of 2 to 3 (Sarti, 2015), post-yield stiffness factor (r), and re-centring ratio (β) are then specified to estimate the equivalent viscous damping (EVD) (Step 3), which is the combination of elastic ($\xi_{elastic}$) and hysteretic damping (ξ_{hyst}). Experimental tests (Marriott, 2009; Smith, 2014) reveal that 3% elastic damping is suitable for the Pres-Lam wall systems, and therefore this value was adopted. Priestley et al. (2007) proposed an analytical formula for the area-based hysteretic damping, ξ_{hyst}, of a dissipative post-tensioned rocking system. A correction factor k_{dyn} was used to account for incomplete cycles under real earthquake motions. Sarti et al. (2015) further proposed an additional factor of k_ξ, the area-based hysteretic damping modification factor for PT-LVL walls (Step 3). The storey displacement profile corresponding to the design roof drift was estimated based on the analytical relationships (Step 4). Newcombe (2011) considered a linear displacement profile for PT-LVL walls up to four storeys. Sarti (2015) followed the linear displacement profile(δ_i) and found that the assumption led to overestimation of building displacements and inter-storey drifts for buildings up to nine storeys. A refinement of the displacement profile equation was provided (Sarti et al., 2015). Assuming that mass is lumped at the centre of each storey, the effective mass (m_e), design displacement (Δ_d), and effective building height (H_e) can be calculated for the equivalent SDOF system (Step 5). Subsequently, the 5% damped displacement spectrum is adjusted to a new displacement spectrum at the EVD level (Step 6), and the effective period can be retrieved by tracing Δ_d on the design displacement spectra. The effective stiffness (K_e), base shear (V_b), overturning moment (M_b), and storey force (F_i) (Steps 7–9) are the outcomes of the DDBD. Section analysis is performed (Step 10) to quantify the moment resistance (M_r) at the maximum imposed rotation. If M_r is greater than M_b and if all preliminary and other detailed design criteria, which will be discussed in the next section, are satisfied, DDBD is considered complete. Otherwise, an iterative design is needed with changes, with evaluation proceeding from Step 1.
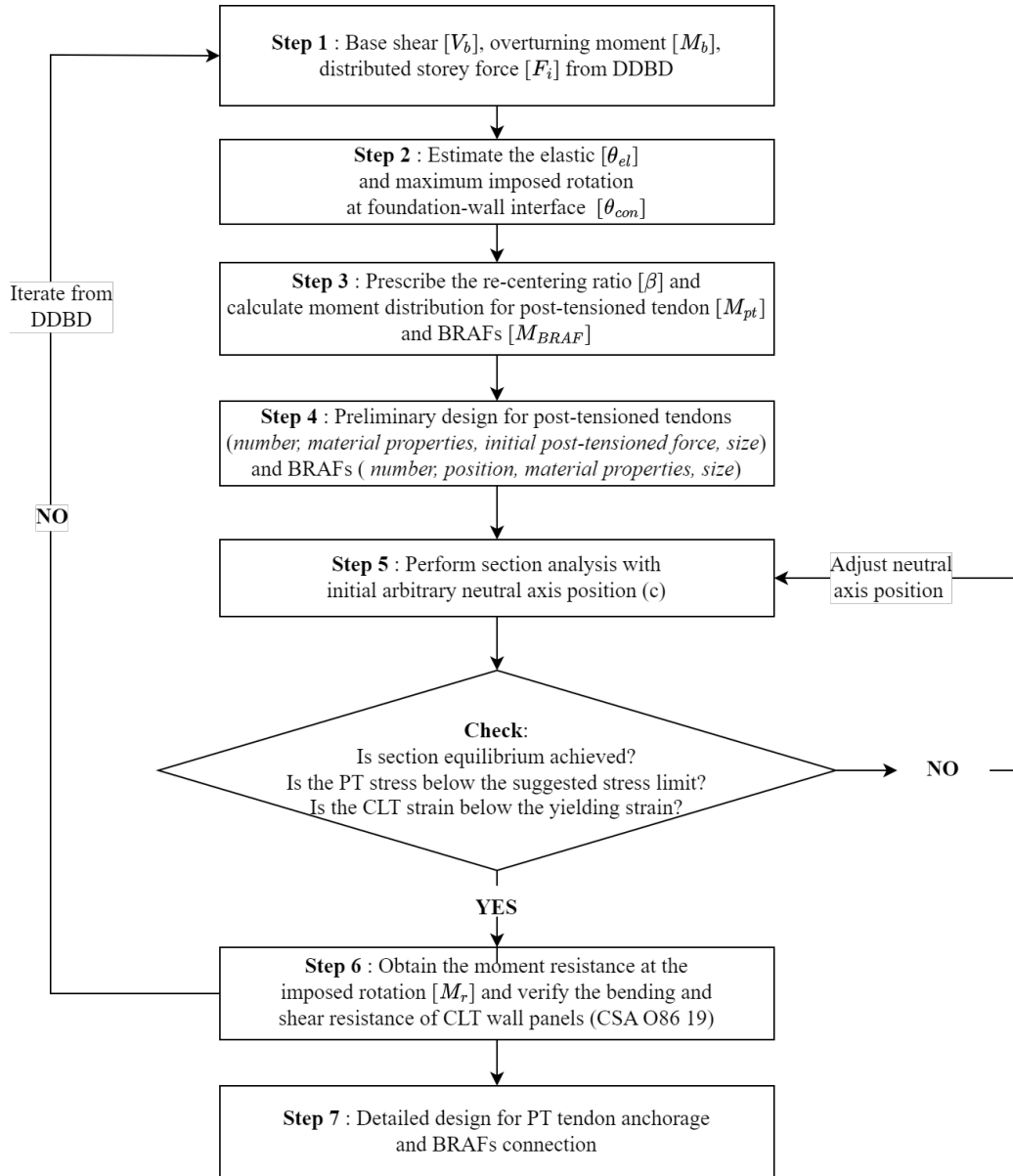
Figure 3-4. Section analysis procedure for PT-CLT walls with BRAFs.

Using the design outcomes (V_b, M_b, F_x) from DDBD, a preliminary sizing for PT-CLT walls with BRAFs can be performed. The procedure is presented in Figure 3-4. Because the overall deformation of the wall under lateral load consists of elastic and inelastic deformations, the maximum imposed rotation (θ_{imp}) can be estimated by subtracting the elastic deformation from the allowable rotation (θ_t):

$$\theta_{\text{imp}} = \theta_t - \theta_{bend} - \theta_{shear} \hspace{3cm} \text{Equation 3-1}$$

where $\theta_{bend}, \theta_{shear}$ are elastic deformation due to bending and shear and are given by:

$$\theta_{bend} = \frac{\sum_{i=1}^{n} F_i h_i^2 (3h_n - h_i)}{6EIh_n} \hspace{3cm} \text{Equation 3-2}$$

$$\theta_{shear} = \frac{\sum_{i=1}^{n} V_i H_i}{GA_{s,w} h_n} \hspace{3cm} \text{Equation 3-3}$$

where h_i is the height at the ith storey, h_n is the building height, and H_i is the ith storey height.

The next step consists of associating the design overturning moment demand with the maximum imposed rotation. Knowing the moment resistance contribution for both post-tensioned tendons and BRAFs, adequate sizing can be performed, and the initial post-tensioning force of the steel tendon can be calculated, as well as the required capacity and number of BRAFs. As mentioned previously, strain compatibility at the wall-foundation interface is lost during rocking of PT-CLT walls, making it challenging to find the section equilibrium. Therefore, an iterative analysis proposed by Pampanin et al. (2001) was used to derive the moment-rotation relationship, including the section moment resistance at the target drift. The procedure was initially developed to describe the post-tensioned dry-jointed ductile connection response and was based on the Monolithic Beam Analogy (MBA), in which the displacement of a post-tensioned connection is equal to that of an equivalent monolithic connection subjected to the same lateral load. Equating the rigid body rotation with the known rotation of a plastic hinge region makes it possible to estimate of the CLT's compressive strain (ε_t)

$$\varepsilon_t = c\left(\frac{3\theta_{imp}}{L_{cant}} + \phi_{dec}\right)\phi_t \qquad \text{Equation 3-4}$$

where ϕ_t is set equal to 1.3 to amplify the CLT strain (Brown et al., 2022) and ϕ_{dec} is the decompression curvature:

$$\phi_{dec} = \frac{M_{dec}}{E_{con}I} \qquad \text{Equation 3-5}$$

where E_{con} is the connection modulus, which is set equal to $0.7E_{CLT}$ to account for the end effect (Newcombe et al., 2008), and I is the section moment of inertia.

The overall sectional analysis starts with a trial value of the neutral axis position at the imposed rotation, after which deformation in the post-tensioned cable and dampers can be evaluated based on the section geometry. Based on the corresponding material properties, the stress of CLT, post-tensioned cables, and BRAFs can be determined at the rocking interface. Simple section equilibrium can be checked by determining whether the net force exceeds the tolerance. If not, iterative adjustment of the neutral axis is required until section equilibrium is achieved. Note that additional checks are necessary to guarantee the adequacy of the design. For example, the stress in the post-tensioned tendon should be less than 70% of the yield strain at the ultimate limit state (ULS) designed for earthquake events with a return period of 500 years (Pampanin et al., 2013). For MCE, a limit of 90% yield strain is assumed for the PT tendon. The CLT strain at the design drift should be less than the yield strain, and the flexural and shear resistance should also be verified following CSA Standard O86 (CSA 2019). The strain limit for BRAFs at MCE is prescribed to be 5–6% (Pampanin et al., 2013).

3.5. Development of a Fibre-based Numerical Model for PT-CLT Walls with BRAFs

3.5.1 Modelling Strategy and Component-level Calibration

Two-dimensional numerical models for PT-CLT walls with BRAFs were developed in *OpenSeesPy* (Zhu et al., 2018) (Figure 3-6a). The modelling strategy consisted of a fibre-based element to simulate the rocking of the CLT panel and *zero-length spring* elements to represent BRAFs' hysteresis. The bottom node of the CLT panel was fully fixed to represent the rigid foundation, and the *force-based beam-column* element was used to connect the bottom node to the node at the plastic hinge height, taken as two times the wall panel thickness as recommended by Akbas et al. (2017). The *fibre section* was discretized into vertically oriented fibres across the length of the wall. Each fibre was assigned *Elastic Perfectly Plastic Gap (EPPGap)* material to idealize the elastic perfectly plastic nature of the CLT's load-deformation response. A zero tensile strength was used to simulate the base uplift or gap opening resulting from rigid body rocking, based on experimental observation (Chen et al., 2018)*.* The portion of the CLT panel above the plastic hinge zone was assumed to be linearly elastic, modelled by an *ElasticTimoshenko* beam to capture shear and bending effects. The post-tensioned tendons were modelled by *corotational trusses* assigned with the *Giuffré-Menegotto-Pinto Model (Steel02) material* to capture the changes in the system geometry (Kovacs and Wiebe, 2019). The top of the PT element was connected to the top of the CLT panel by *rigid link beam* elements. At the fuse location*, zero-length springs* were used and are connected to the CLT panel using *rigid link beam* elements. The *steel02* material was used to model the BRAFs and was calibrated using the component-level experimental results reported by Chen et al. (2018). A (SDOF) oscillator was employed and modelled by a *zero-length spring element* in the vertical direction. The yield strength, initial stiffness, and strain hardening ratio were extracted based on the experiment. Overall, the calibrated material hysteresis (Figure 3-5) achieved a good matching with the experimental testing and is considered satisfactory to represent the actual material property for BRAF.

To model CLT crushing and the maximum strains in PT elements and BRAFs, the *MinMax material* in *OpenSeesPy* was used, which returns zero stress and tangent when the strain limit is reached. To define *EPP Gap material* for CLT in *OpenSeesPy*, one only needs to specify the initial stiffness and yield strength. Hence, to model the strain in the CLT that could cause crushing (one of the criteria for simulated collapse), we coupled the *EPP Gap material* with the *MinMax uniaxial*

material model in *OpenSeesPy*. Based on the experimental test result reported by Ganey et al. (2017), a crushing limit state strain of 4% was assumed for CLT. Maximum tensile strain limit of 2% was used for the PT elements. An experiment test conducted on a two-thirds scale PT-LVL walls equipped with BRAFs (Sarti et al. 2016a) showed that BRAFs developed a maximum strain of 6% at the MCE level. This limit was considered as the suggested maximum strain value to avoid low-cycle fatigue failure. Consequently, a *MinMax material* with a strain limit of 6% was adopted for BRAFs. In this study, it is assumed that the BRAFs have an adequate slenderness ratio, appropriate filling materials, and encasing tubes; therefore, they can be considered not susceptible to fracture failure due to repeated cycles at lower strains.
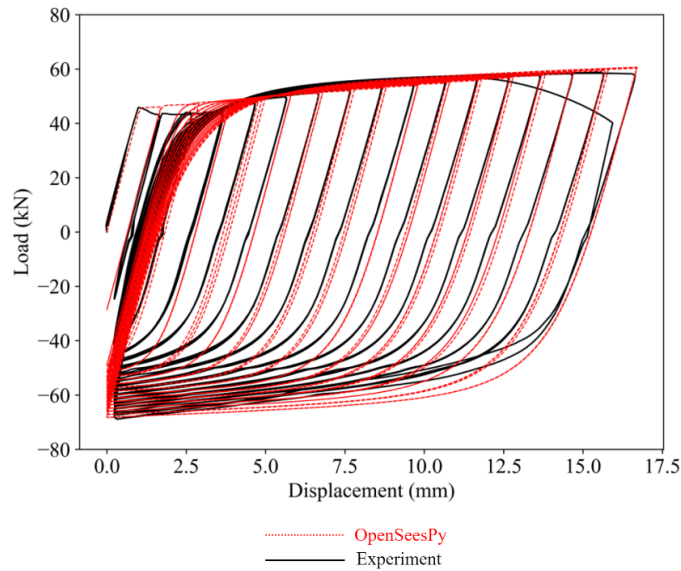
Figure 3-5. Component-level calibration and experimental test for BRAF (Chen et al. 2018).

3.5.2 System-level Calibration

The fibre-based numerical model developed as described in the preceding section was also calibrated at the system level with full-scale experimental tests conducted at FPInnovations (Chen et al., 2020) (Figure 3-6b). Since multiple configurations of PT-CLT walls were tested, only the one with BRAFs was considered for calibration. The individual CLT panel had a length of 1 m, a thickness of 0.143 m, and a height of 3 m. Cyclic loading was exerted at the actuator height of 2.9 m. The post-tensioned cable in the experiment had a diameter of 20 mm, an elastic modulus of 205 GPa, and a yield strength of 900 MPa. The elastic modulus and the compressive yield strength of

CLT were assumed to be 2.6 GPa and 25 MPa (Slotboom, 2020). As part of the investigation, the effects of different initial post-tensioning forces (44.5, 89, and 133.5 kN per cable) and spacings between BRAFs (333and 500 mm) were explored. The calibration results from the three specimens are presented in Figure 3-7.
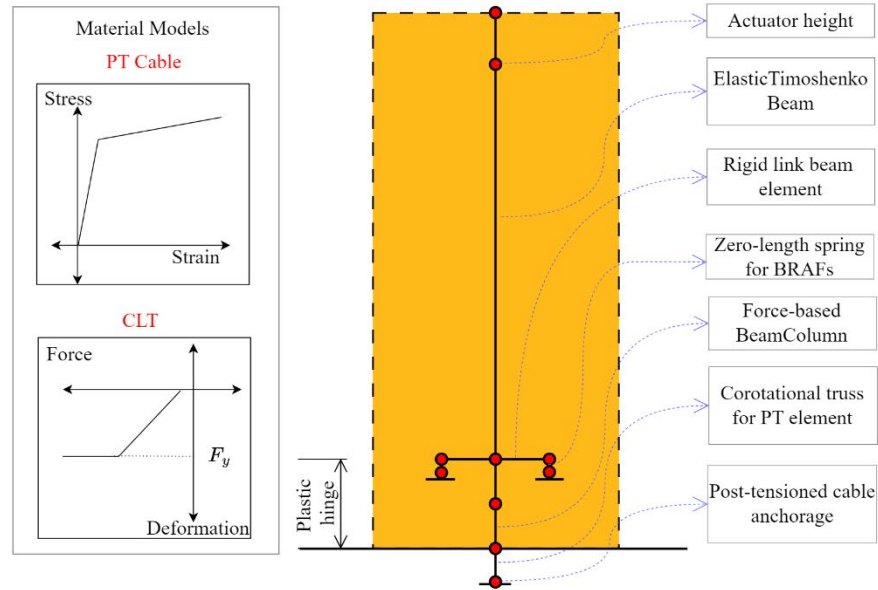
(a)
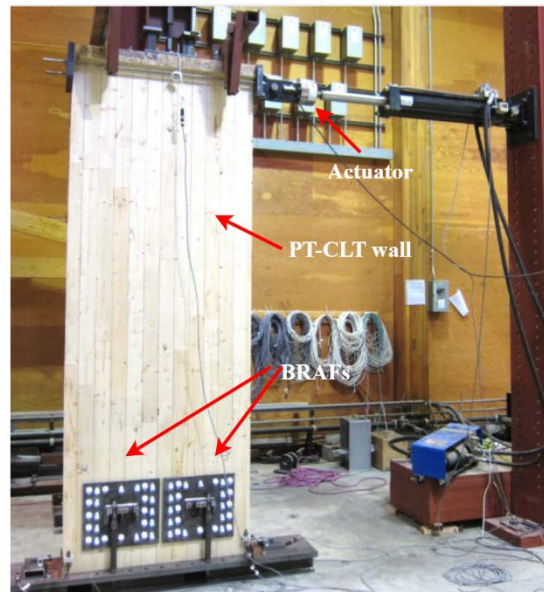
(b)

Figure 3-6. (a) Fibre-based numerical model in *OpenSeesPy*. (b) experimental test layout for a PT-CLT single wall with BRAFs (Picture courtesy of Marjan Popovski from FPInnovations).

Figure 3-7a shows the base shear force versus the horizontal displacement (at the actuator height of the PT-CLT wall panel) with an initial post-tensioning force of 89 kN and a BRAF spacing of 333 mm. The peak horizontal displacement reached 75 mm (equivalent to a 2.67% drift ratio) without strength degradation. The flag-shaped hysteresis signified steady energy dissipation by the BRAFs and self-centring of the system. The initial stiffness and post-yielding stiffness agreed with experimental results. Noticeably, after the initial cycles, the BRAFs experienced significant elongation due to tension, preventing the CLT from returning to its initial position. Such an effect causes the bottom of the V-shaped PT response under cyclic loading to shift upward gradually (Figure 3-7b). However, since the BRAFs are easily replaceable, the low-damage nature of the PT-CLT walls is maintained. Figure 3-7c further presents the calibration of the PT-CLT wall with an initial post-tensioning force of 133kN, and Figure 3-7d shows the hysteresis with an increased BRAF spacing of 500 mm. Overall, the results depicted in Figure 3-7 show the capability of the fibre-based model to capture the peak displacement and energy dissipation of PT-CLT walls under quasi-static cyclic loading.
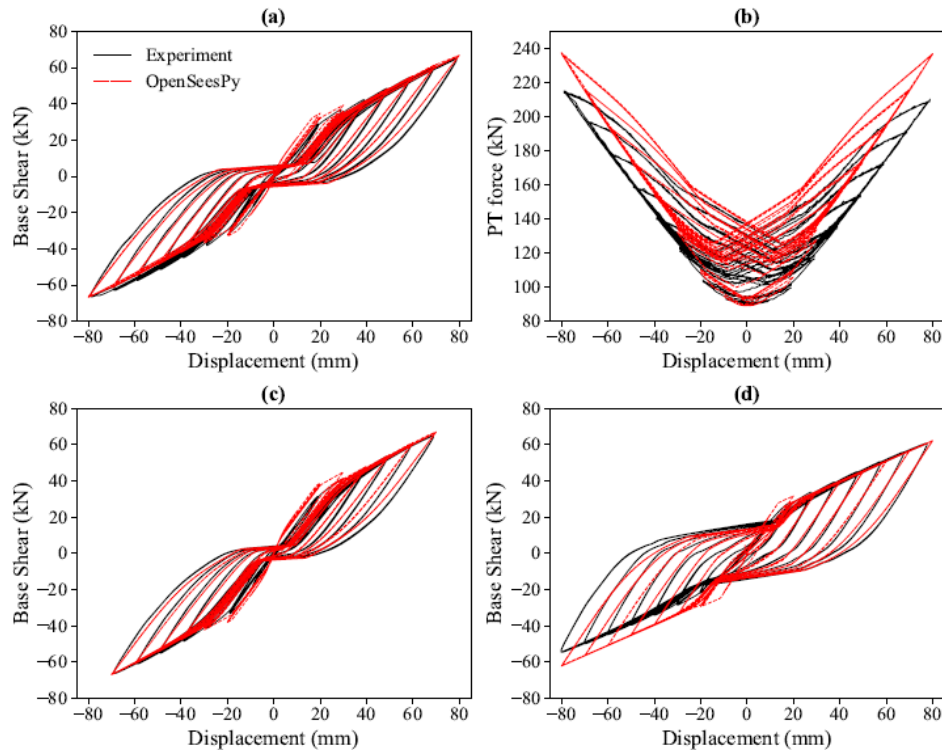
Figure 3-7. Result comparison between *OpenSeesPy* model and experimental test for PT-CLT wall with BRAFs (Chen et al., 2018).

3.6. Seismic Performance Assessment

3.6.1 Details and Design of Prototype Buildings

The DDBD and sectional analysis procedures outlined in Section 3.2 were used to design all the prototype 6-, 9-, and 12-storey PT-CLT shear wall buildings. Each prototype building used PT-CLT walls with BRAFs as SFRS, and all were assumed to be in Vancouver, BC, Canada, with Vs_{30}, in the range between 450 and 600 m/s. The buildings were typical office buildings with a ground floor height of 4 m, a storey height of 3 m, and a floor plan of 21 m × 48 m (Figure **3-8**). For acoustic and vibration control, a 38-mm concrete topping was applied to each floor. The floor had a dead load of 3.5 kPa and a live load of 4.8 kPa, and the roof had a dead load of 1.5 kPa and a snow load of 2.4 kPa. The seismic tributary area for each wall panel was 3% of the floor area. In the East-West direction, a total of 8 PT-CLT single walls with BRAFs were used, and 4 PT-CLT coupled walls were positioned in the North-South direction. The performance of coupled PT-CLT walls is not assessed within the scope of this study. Since there were no irregularities in the buildings, a 2-dimensional numerical model was sufficient for all further numerical analysis, and seismic performance assessment was carried out for only one of the shear walls in the E-W direction. Table 3-1 and Table 3-2 summarise the DDBD and sectional results, respectively.

Table 3-1.Summary of DDBD results for all building prototypes.

	6-STOREY	9-STOREY	12-STOREY
β	0.7	0.7	0.7
μ	3	3	3
r	0.2	0.2	0.2
$\Delta_d\ (m)$	0.25	0.36	0.48
$m_{eff}(kg)$	3.25×10^5	4.90×10^5	6.54×10^5
$h_{eff}(m)$	12.9	19.0	25.1
$\xi_{hyst_{unfactor}}$	9.1	9.1	9.1
k_ξ	0.95	0.95	0.95
k_{dyn}	0.83	0.83	0.83
ξ	10.2	10.2	10.2
R_ξ	0.87	0.87	0.87
$T_{eff}(sec)$	2.21	4	6.27
$K_{eff}(kN/m)$	2620	1200	656
$V_b(kN)$	642	436	312
$M_b(kN \cdot m)$	8310	8270	8710

Table 3-2. Summary of sectional analysis for building prototypes.

	6-storey	9-storey	12-storey
Number of walls in N-S direction	8	8	8
PT bar size	12-strand PT bar (Strand diameter = 15 mm)		
Initial post-tensioning force (per bar)	1350	1340	1410
Number of PT bars	4	4	4
Mild steel fuse size	NO.25 mild steel bar		
Number of fuses	8	8	8
Moment resistance (kNm)	9800	9410	9120

The CLT panels selected for the design complied with the ANSI/APA PRG 320 Standard E1 Grade. All layers had a thickness of 35 mm. The wall base length was 3 m, as limited by manufacturing capability and transportation feasibility (Structurlam, 2021). As prescribed by CSA O86 (CSA 2019), the CLT had a compressive strength of 19.3 MPa and a Young's modulus of 11.7 GPa. The selection of post-tensioned tendons was based on multi-strand post-tensioning steel (CPCI, 2017). The steel yield strength for the PT tendon was 900 MPa, and its Young's modulus is 200 GPa. The mild steel BRAF had a yield stress of 300 MPa and a Young's modulus of 200 GPa, and the fuse size is referred to as Canada's standard reinforcing bars.

The *OpenSeesPy* model for each prototype building was constructed following the strategies in Section 3.4.2. An additional gravity-leaning column representing the gravity system was defined to capture potential P-Delta effects. The leaning column is modelled with elastic beam-column elements with a large cross-sectional area and moment of inertia to incorporate the effect of the gravity columns on the overall system response of the PT-CLT walls. The bottom of the leaning column was pinned at the foundation, and each floor node on the leaning column was rigidly connected to the floor node on the CLT wall. At the joint of the floor node and its adjacent elastic columns, zero-length spring elements with negligible rotational stiffness were defined to simulate

moment release. After the model was constructed, eigen-analysis was performed to obtain the buildings' fundamental period. For the 6-, 9-, and 12-storey, the fundamental periods are 0.67, 1.36, and 2.25 s, respectively. Sarti et al. (2017) suggested using the empirical equation for moment-resisting concrete frames to estimate the periods for PT-LVL walls. Adopting the corresponding equations in NBCC 2020, the estimated periods are 0.68, 0.91, and 1.13 s. While good estimation can be found for 6-storey, large underestimation was observed when the actual period (i.e., based on eigen-analysis) is greater than 1 s, which is consistent with the discussion in Sarti et al. (2017). To accurately predict the period in the future, it is suggested a structure-specific empirical equation should be developed for PT-CLT wall buildings based on full-scale in-situ measurements.
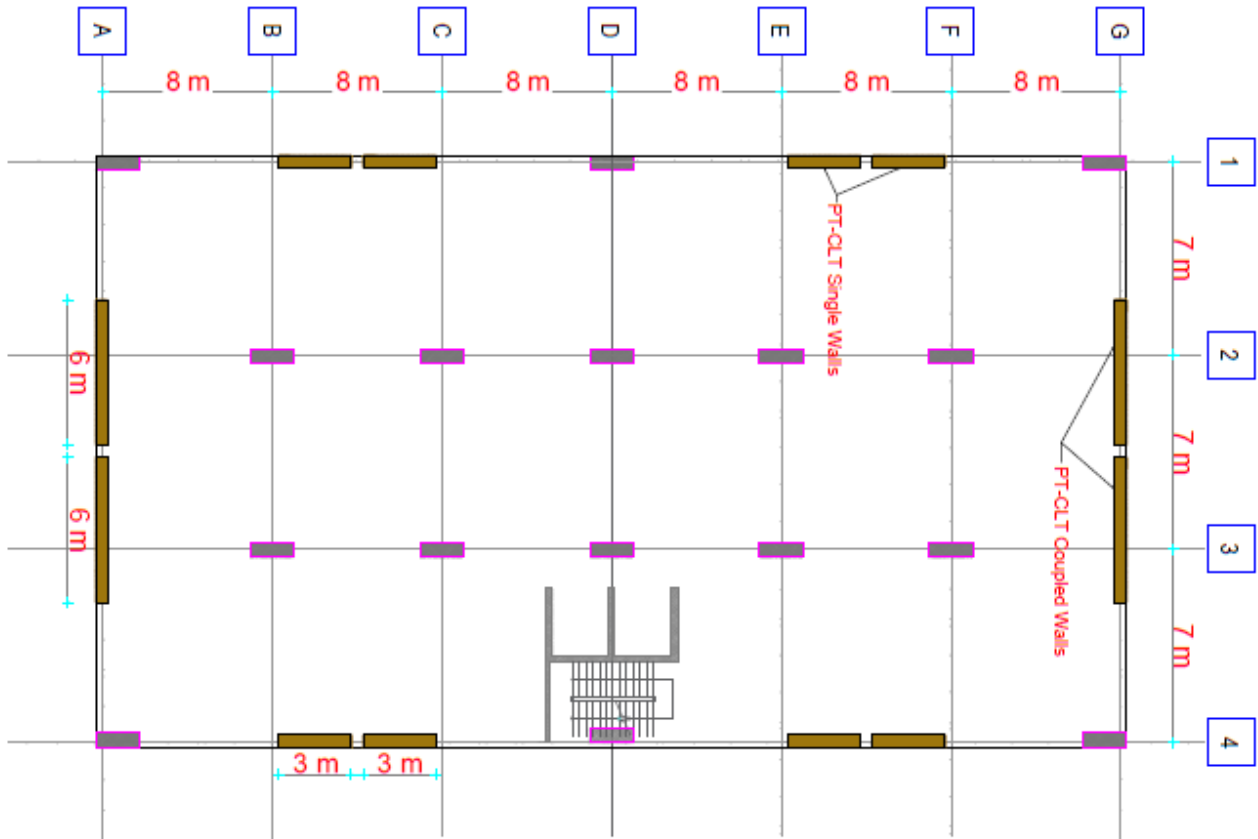
Figure 3-8. Typical floor plan layout of the prototype buildings.

3.6.2 Ground Motion Selection and Scaling

To assess the seismic performance of the prototype PT-CLT shear wall buildings in Vancouver, ground motion records representative of the regional seismicity were selected. In Southwestern BC, due to the complex seismotectonics, seismic hazards from three potential sources of damaging earthquakes (shallow crustal, off-shore mega-thrust interface, and deep in-slab earthquakes) should be considered. The procedure shown in Figure 3-9 was followed to select a suite of hazard-consistent ground motion records.
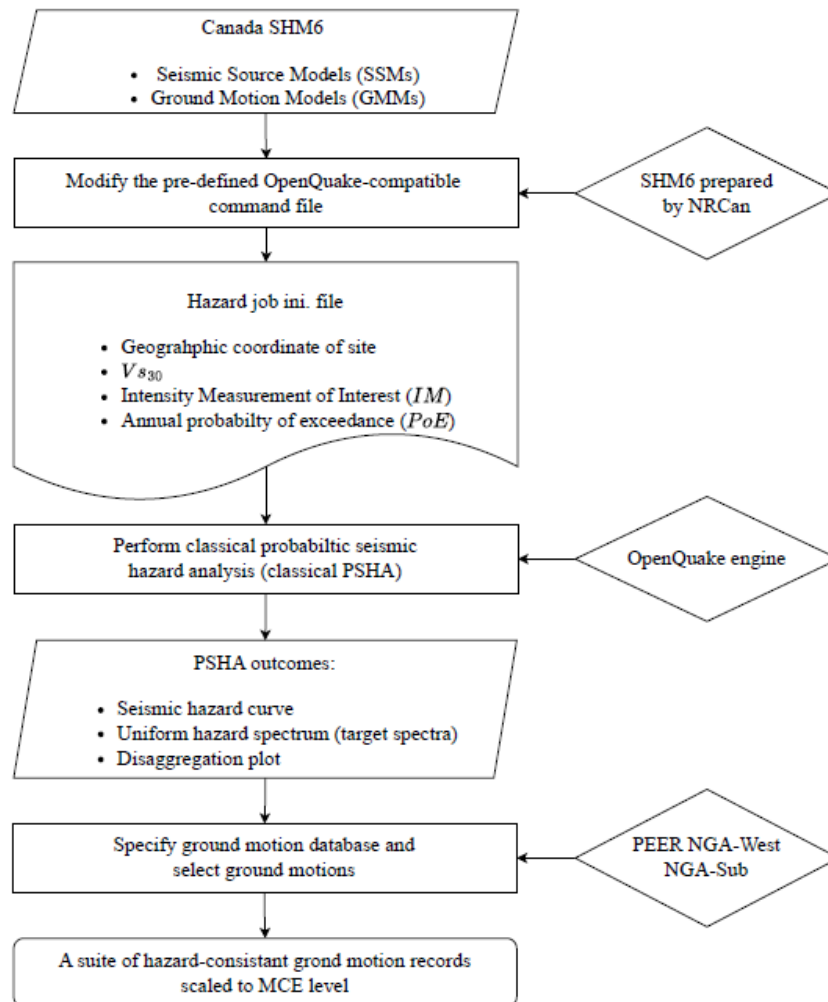
Figure 3-9. Procedure for ground motion selection and scaling.

Canada's SHM6 was fully implemented with the OpenQuake Engine (Pagani et al., 2014), which is an open-source software package for seismic hazard and risk analysis. Natural Resources Canada (NRCan) has prepared sample OpenQuake-compatible command files for PSHA (Kolaj et al., 2020b). Modifications are required to properly define the site of interest, soil condition, annual probability of exceedance, and intensity measurement of interest. Outputs from the calculation include the uniform hazard spectra (UHS) and disaggregation results. The NRCan online seismic hazard tool (NRCC 2020) provides spectral acceleration values at only 10 periods, necessitating interpolation if the building's fundamental period falls in between. The discrete spectral acceleration points may also lead to inaccuracy in calculating the design displacement spectra for DDBD. With OpenQuake, spectral accelerations at multiple finite periods can be directly calculated. In Figure 3-10, the UHS calculated from *OpenQuake* is compared with the UHS (based on linear interpolation) obtained from NRCan, and a good match can be observed between the two curves. The seismic disaggregation analysis was conducted using the average fundamental period of all prototype buildings. The result provided the dominant magnitude and distance pair for each earthquake type, which were input parameters to select site-specific and hazard-consistent ground motions. A total of 33 ground motions were selected, with 11 ground motions for each earthquake type. Crustal and in-slab ground motion records were obtained from the PEER NGA-West2 database (Ancheta et al., 2014), and records for interface events were from the PEER NGA-Sub database (Kishida et al., 2018). Ground motions were scaled following method A of Commentary J of NBCC 2015 (NRCC 2015). All ground motions were scaled over a period range of 0.2–7 sec to cover the fundamental period and effective period of all prototype buildings. To prevent over-scaling, the scaling factors were limited to the range between 0.5 and 4. The mean spectra of all ground motions after scaling achieved a good match with UHS for each earthquake type, as shown in Figure 3-10. To conduct dynamic analysis, a tangent stiffness proportional Rayleigh damping model with a critical damping of 3% was employed. The damping modelling strategy and critical damping level were based on previous studies on the dynamic response of PT-CLT walls (Marriott, 2009; Smith, 2014; Sarti, 2015). The analysis utilized the KrylovNewton algorithm and Newmark-β integration method (average acceleration with $\gamma = 0.5$ and $\beta = 0.25$)
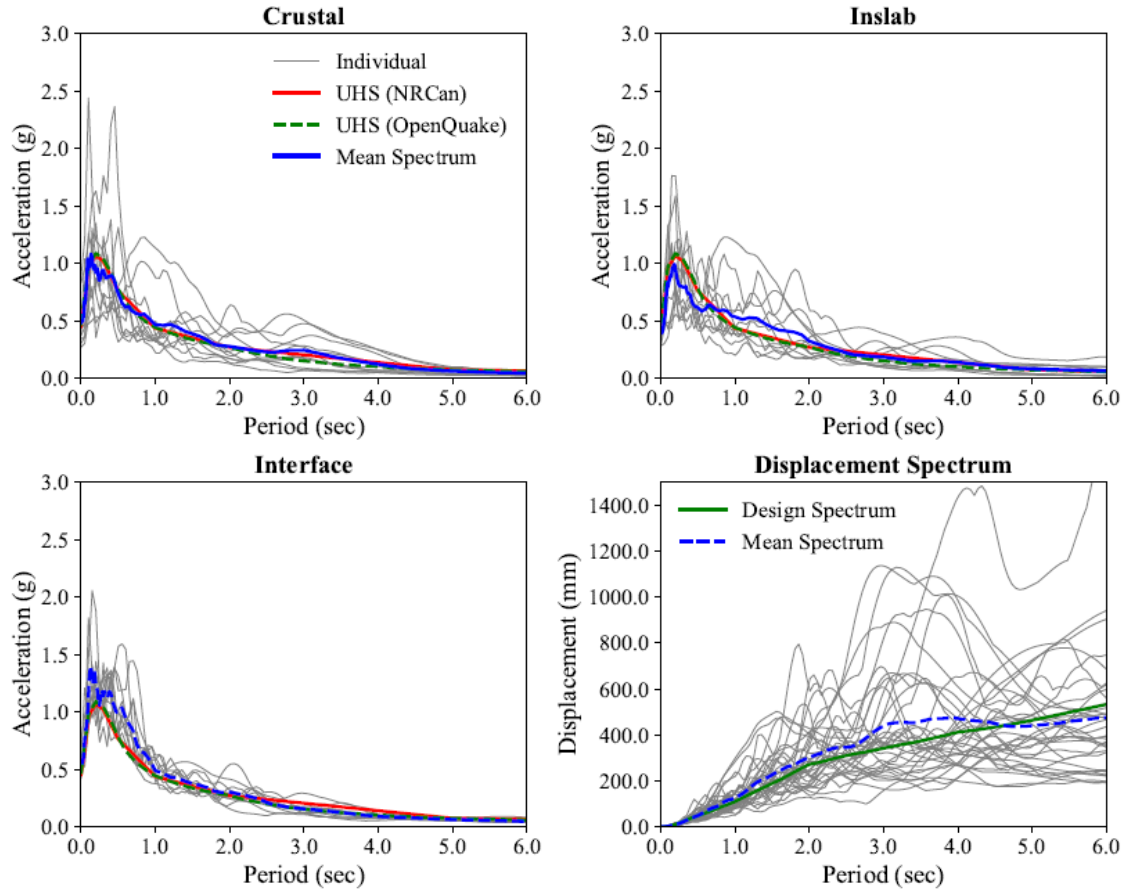
Figure 3-10. Selected and scaled ground motion spectra.

3.6.3 Nonlinear Response History Analysis

NLRHA was performed for all prototype buildings using the selected and scaled ground motions. Peak storey shear force and horizontal displacement responses for each floor under each seismic excitation were extracted. The peak floor displacements for each storey were further normalized by the building's total height to obtain storey drift responses. The peak storey shear forces for all building prototypes are plotted in Figure 3-11.
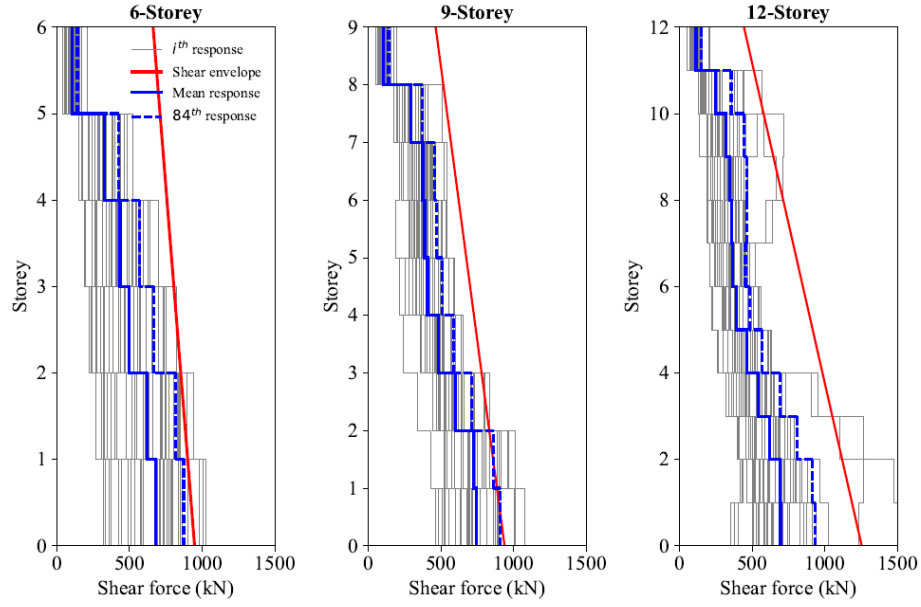
Figure 3-11. Storey shear responses for 6-, 9-, and 12-storey building prototypes.

For all building prototypes, the design storey shear forces from DDBD were amplified to account for higher mode effects and to obtain shear force envelopes (Priestley et al., 2007). Newcombe (2011) and Sarti (2015) applied a similar amplification for PT-LVL walls. The envelope consists of a linear distribution of the design shear force defined by the over-strength design base shear V_{base}° and the over-strength design top shear V_n°.

$$V_{base}^{\circ} = \phi^{\circ}\omega_v V_b \qquad \text{Equation 3-6}$$

$$\omega_v = \frac{\mu}{\phi^{\circ}}C_{2,T} + 1.0 \qquad \text{Equation 3-7}$$

$$V_n^{\circ} = C_{3,T}V_{base}^{\circ} \qquad \text{Equation 3-8}$$

Where $C_{2,T}$ and $C_{3,T}$ are seismic coefficients given by

$$C_{2,T} = 0.062 + 0.4(T_i - 0.5) \leq 1.15 \qquad \text{Equation 3-9}$$

$$C_{3,T} = 0.9 - 0.3T_i \geq 0.3 \qquad \qquad \text{Equation 3-10}$$

where T_i is the building's fundamental period. An over-strength factor (ϕ°) of 1.15 was adopted for the PT timber wall system with a strain-hardening effect (Sarti, 2015). The result indicates that the mean storey shear force is well-bounded within the shear envelope under the MCE, with the 84th percentile response being closest to the design shear envelope.

The peak storey drift responses from NLRHA are depicted in Figure 3-12. The results show that the mean storey drift is less than the design target drift, especially for the 6- and 9-storey buildings, at 0.74% and 1.03%, respectively. At higher storey levels, the 84th percentile response is the closest to the design value. The 12-storey building has reduced stiffness compared to the 6-, and 9-storey buildings and exhibits larger drift, and its 84th percentile response nearly overlaps with the design drift. Noticeably, 12% (4 out of 33) of the ground motion led to an exceedance of the design drift.
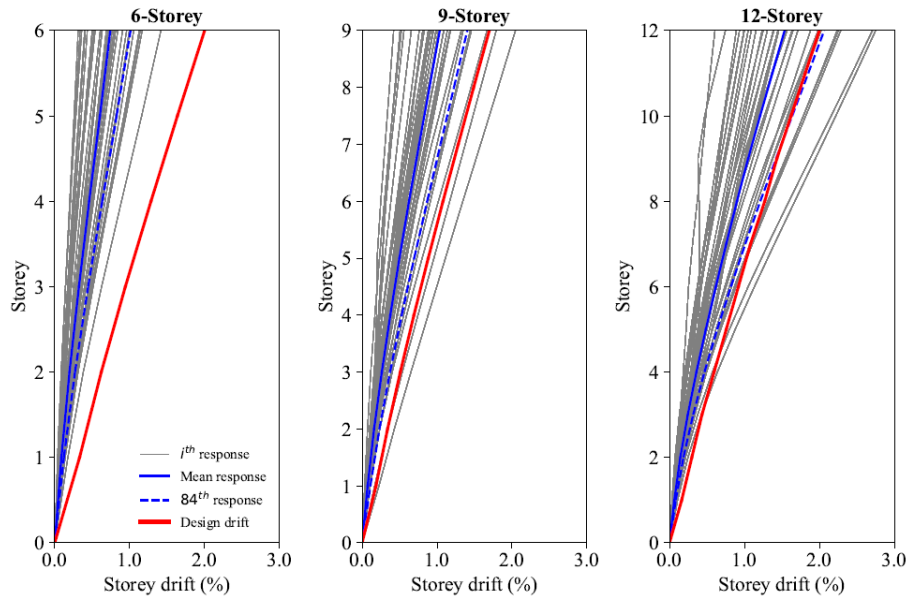
Figure 3-12. Storey drift responses for 6-, 9-, and 12-storey building prototypes.

3.6.4 Incremental Dynamic Analysis and Fragility Assessment

To assess the buildings' fragility, IDA was performed using the *hunt and fill* algorithm (Vamvatsikos and Cornell, 2002) by scaling up each ground motion record until collapse occurred. To capture the collapse appropriately, both simulated and non-simulated collapse mechanisms

were considered. The former entailed a series of strain limits for CLT, PT elements, and BRAFs. When one or more strain limits are exceeded, the material model returns zero stress and tangent, accelerating the building's collapse, which is characterized by flattening of the IDA curve. Since the gravity system was not explicitly modelled, a non-simulated collapse criterion was applied that accounted for the drift capacity of the gravity system. Sarti et al. (2017) performed a parametric analysis, and a roof drift of 5% was recommended as the maximum lateral drift capacity of a timber gravity framing. Therefore, a 5% roof drift was assumed to be a non-simulated collapse criterion. Figure 3-13 shows the IDA curves of the prototype buildings with 16%, 50%, and 84% statistics.
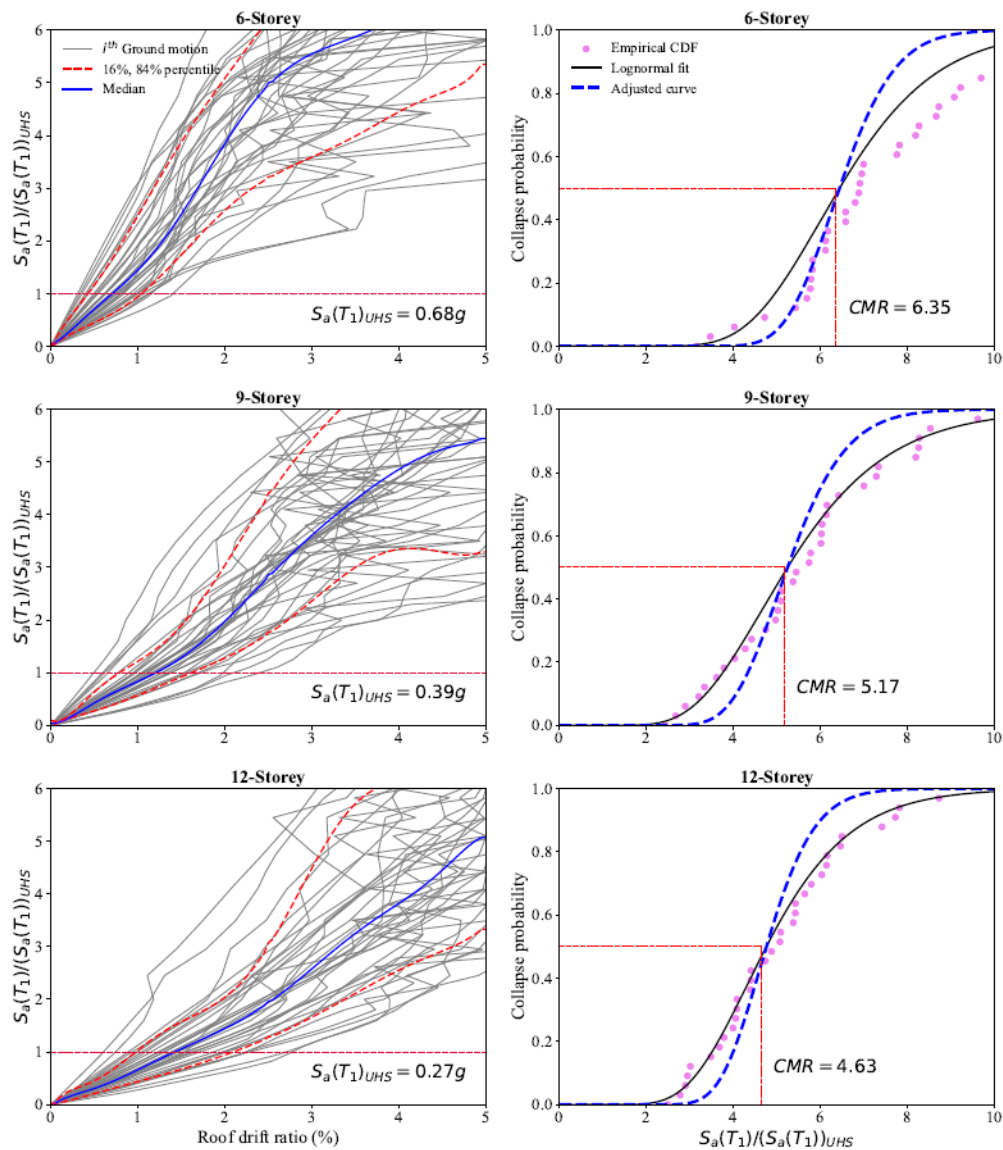
Figure 3-13. IDA results and collapse fragilities for 6-, 9-, and 12-storey building prototypes.

The IDA results indicate that, for PT-CLT walls with BRAFs, significant strain hardening occurs with increasing scaled intensity, which is consistent with the design assumption made in Section 3.2. One of the objectives of IDA is to calculate the collapse margin ratio (CMR):

$$CMR = \frac{S_{CT}}{S_{MT}}$$
Equation 3-11

where S_{CT} is the spectral acceleration resulting in 50% collapse of a building, and S_{MT} is the spectral acceleration at the MCE level. FEMA P695 (FEMA, 2009) further suggests applying the spectral shape factor (SSF) to obtain the ACMR, which accounts for the bias introduced by the spectral shape of the ground motion suite:

$$ACMR = CMR \times SSF$$
Equation 3-12

Since the SSF for the ground motion suite in this study was not available and applying the SSF will would lower the collapse probability (Kovacs and Wiebe, 2019), to remain conservative, the ACMR for each building prototype was assumed to be the same as the CMR and is so labelled in Figure 3-13. Extracting all the collapse points from IDA and fitting the data with a lognormal distribution enable the collapse fragility assessment. To check the CMR again for acceptable values, the total system collapse uncertainty, β_{tot}, must be examined and incorporated:

$$\beta_{tot} = \sqrt{\beta_{RTR}^2 + \beta_{DR}^2 + \beta_{TD}^2 + \beta_{MDL}^2}$$
Equation 3-13

where $\beta_{RTR}, \beta_{DR}, \beta_{TD}, \beta_{MDL}$ are parameters to account for uncertainty in ground motion record variability, system design requirements, test data, and numerical modelling. Given the prescribed upper limit in FEMA P695 (FEMA, 2009), β_{RTR} was assumed equal to 0.4. The design for all building prototypes considered only a heavy floor system with concrete topping, omitting the possibility of a short-period building design scenario. Therefore, β_{DR} was assumed to be 0.35 (fair). β_{MDL} and β_{TD} were both 0.1 (Superior) because numerical calibration from this and previous studies (Akbas, 2016; Slotboom, 2020) indicated that the fibre-based model could capture well the structural response of the PT-CLT wall system with EDDs. A final system collapse

uncertainty of 0.57 was used. The standard deviation-adjusted collapse fragility curves are given in Figure 3-13. Based on the collapse fragility assessment, the calculated ACMR for each prototype building (see Figure 3-13) exceeds the suggested threshold specified in FEMA P695 (ACMR 10% = 2.02). The recommended ACMR 10% threshold was determined based on a collapse probability of 10% and a total system collapse uncertainty of 55% ($\beta_{tot} = 0.55$). In addition, the collapse probability at MCE for all building prototypes is significantly lower than 10%, which is the upper limit prescribed in FEMA P695 (FEMA, 2009). Besides examining collapse fragility, the fragility of drift of exceedance at two ISDR levels (1% and 2.5%) was also evaluated, and the results are presented in Figure 3-14.
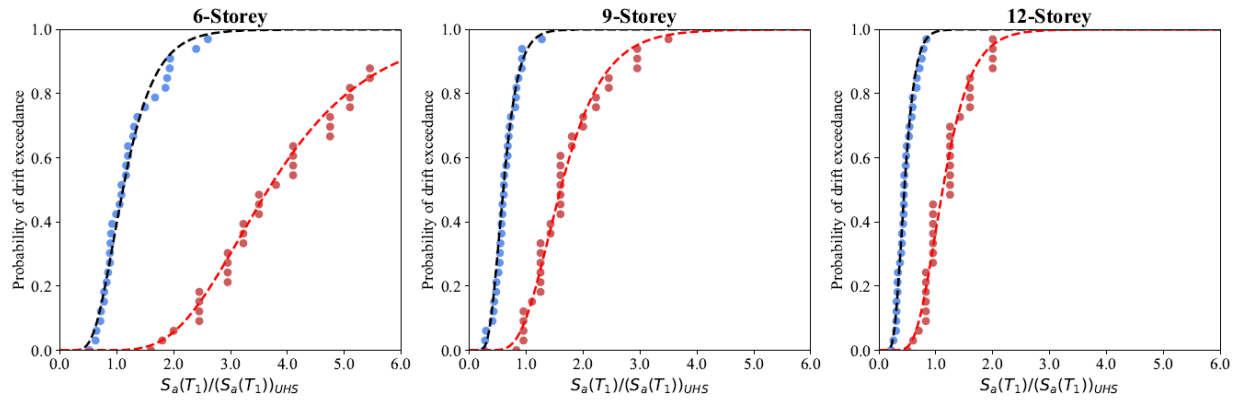
Figure 3-14. Fragility assessment of drift of exceedance at ISDR of 1% and 2.5%.

Yang et al. (2022), when assessing the seismic performance of balloon-type CLT rocking shear walls, proposed a maximum limit on the number of ground motions (i.e., 10%) that cause 2.5% MISD or more at MCE. Based on Figure 3-14, the 6-storey building sustained all ground motion without exceeding 2.5% MISD, and for the 9-storey, the probability of reaching 2.5% MISD is 9.1%. The limit proposed in Yang et al. (2022) is violated for the 12-storey PT-CLT shear wall building at MCE, where 36.4% of the ground motions led to the exceedance of 2.5% of MISD. Since the BRAF dissipates energy primarily at the rocking interface, which is at the bottom of the CLT, energy dissipation of PT-CLT walls at high storey levels is limited and reduced. To improve such design, the PT-CLT single wall may consist of multiple rocking segments (Pilon et al., 2019), or a PT-CLT coupled wall connected by UFPs can be adopted to achieve continuous energy dissipation along the height of the building.

3.7. Summary and Conclusion

In this study, the seismic performance of 6-, 9-, and 12-storey mass timber buildings with PT-CLT shear walls equipped with BRAFs was evaluated using nonlinear dynamic analysis. The studied buildings were assumed to be in the city of Vancouver, Canada, and designed based on the DDBD approach. Fibre-based numerical models were developed in *OpenSeesPy* and calibrated with experimental tests at component and system levels. To assess seismic performance, a suite of site-specific ground motion records best reflecting the regional seismicity of Vancouver, Canada, were selected and scaled considering the SHM6. NLRHA was conducted to compare the peak storey shear force and storey drift demands with the design targets. IDAs were performed to derive the collapse fragilities and calculate the drift of exceedance probabilities. The following conclusions can be drawn from the study:

- The DDBD method demonstrates a relative advantage in overcoming the absence of clear R_d and R_o factors for PT-CLT walls.

- The fibre-based numerical modelling strategy is proven to be capable of accurately capturing the structural response of PT-CLT walls with BRAFs under quasi-static cyclic loading. Such a modelling strategy achieves a balance between computational expense and accuracy and is favourable and efficient when conducting NLRHA and IDA.

- The NLRHA results indicate that the DDBD method produced designs that meet the design target (2% roof drift) and the 2.5% ISDR limits of the NBCC. The mean roof drifts for 6-, 9-, and 12-storey buildings were 0.74%, 1.03%, and 1.53%, and drift response increased with building height. Therefore, it is suggested that PT-CLT wall buildings taller than 12 storeys should incorporate mechanisms to control drift.

- The IDA results reveal that PT-CLT walls with BRAFs possess distinct strain-hardening effects at increased scaling factors. The ACMRs for the 6-, 9-, and 12-storey prototype buildings were 6.35, 5.17, and 4.63 and are considered satisfactory compared to the suggested threshold specified in FEMA P695 (ACMR 10% = 2.02). Based on fragility analysis, it is concluded that all buildings performed well in terms of collapse prevention limit state, as the collapse probabilities at MCE for all buildings were significantly lower than 10%.

- Overall, the 6- and 9-storey PT-CLT shear wall buildings with BRAFs as EDD exhibited good seismic performance and have the potential to be applied in high seismic-risk zones as primary SFRS. However, in a 12-storey prototype building, despite the adequate ACMR, the probability of exceeding the 2.5% ISDR threshold at MCE was 36.4%. The underlying reason was localized and limited energy dissipation. This excessive drift could have been better controlled had the building used a PT-CLT single wall consisting of multiple rocking segments or PT-CLT walls coupled by UFPs.

Chapter 4 SEISMIC DESIGN AND PERFORMANCE EVALUATION OF POST-TENSIONED CLT SHEAR WALLS WITH COUPLING U-SHAPED FLEXURAL PLATES IN CANADA

This chapter has been adopted from a journal paper under review written by the author. It is under review in Earthquake Spectra journal:

Zhu, H., Bezabeh, M., Iqbal, A., Popovski, M., and Chen, Z. (2024). Seismic Design and Performance Evaluation of Post-Tensioned CLT Shear Walls with Coupling U-Shaped Flexural Plates in Canada. Earthquake Spectra. Under Review (*submitted May-18-2024* and *received first round peer review feedback on July-12-2024*).

4.1 Chapter Overview

Post-tensioned cross-laminated timber (PT-CLT) walls coupled with U-shaped Flexural Plates (UFPs) have proved to be a low-damage seismic force-resisting system (SFRS) due to their self-centring capability and stable energy dissipation. Global efforts have been made to explore the applicability of PT-CLT walls as primary SFRSs in mass timber buildings. Adoption of the sixth-generation Seismic Hazard Model (SHM6) in the 2020 National Building Code of Canada resulted in a nationwide increase in seismic hazard. Given the increased popularity of mass timber buildings and the elevated seismic hazard, a comprehensive study is required to examine their performance in high seismic regions with complex seismotectonics, such as southwestern British Columbia, Canada. Therefore, the seismic design and performance evaluation of 3-, 6-, and 9-storey mass timber buildings that use PT-CLT shear walls with coupling UFPs as SFRS for the seismicity of Vancouver, Canada, is presented in this section. The prototype buildings were designed using the direct displacement-based design (DDBD) approach considering the SHM6. Two-dimensional fibre-based numerical models were developed in *OpenSeesPy* and validated with full-scale quasi-static cyclic and shaking table experimental tests. Nonlinear static and response history analyses were carried out to assess the structural responses and validate the DDBD procedure. Incremental dynamic analyses (IDA) were conducted using 80 ground motions selected for each building to develop the buildings' fragilities and estimate collapse margin ratios. The IDA results demonstrate that all the examined buildings have adequate collapse margin ratios compared to the acceptable

limits in the literature. Overall, this study demonstrated that PT-CLT walls with coupling UFPs are a potential SFRS alternative in Canada's high seismic-risk regions.

4.2 Introduction

Buildings account for approximately 24% of global carbon emissions related to energy consumption (Cabeza et al., 2022). In response to concerns about climate change, there has been a growing demand to decarbonize the construction industry. In Canada, efforts are underway to achieve net-zero carbon emissions by 2050. These include advancing performance-based construction codes and promoting digitalization within the construction sector (NRCC-CRC, 2022). As part of these initiatives, a proposed strategy is to prioritize using low-carbon construction materials such as engineering wood products (EWPs) (Bezabeh et al., 2017). Common EWPs include Cross-laminated timber (CLT), Glulam Laminated Timber (Glulam), Nail Laminated Timber (NLT), Dowel Laminated Timber (DLT), Mass Plywood Panel (MPP), and Laminated Veneer Lumber (LVL). Among these, CLT, fabricated from layers of lumber stacked and glued crosswise, features dimensional stability, use of low-grade timber for inner layers, higher strength-to-weight ratio compared to masonry or concrete, and higher in-plane strength and stiffness compared to sawn lumber.

CLT-based mass timber buildings can be built as a platform or balloon-type construction (Karacabeyli and Lum, 2022). In platform construction, each CLT floor panel serves as a platform for the wall panel above. Therefore, gravity load is cumulatively transferred to the lowest storey, and such a design is typically governed by the perpendicular-to-grain compressive resistance of the floor panels at the base storey. The 2020 version of the National Building Code of Canada (NBCC 2020) (NRCC, 2022) prescribes seismic performance factors for moderately ductile and limited-ductility CLT shear walls for platform-type construction. The building height limit for such SRFSs is 30 m for Seismic Categories 1 to 3 (low to medium seismicity) and 20 m for Seismic Category 4 (high seismicity). In balloon-type construction, vertical CLT panels or Glulam columns extend continuously from the foundation to the top of the building. Several studies have been conducted to investigate the application and performance of balloon-type CLT walls (Chen and Popovski, 2020a; Shahnewaz et al., 2021; Hayes et al., 2023; Xing et al., 2023). Nonetheless, in both types of construction, energy dissipation in buildings primarily depends on inelastic

deformation of connections (Lepine-Lacroix and Yang, 2023). Under large drift, permanent damage to conventional connectors in mass timber buildings could result in significant residual drift, posing a risk of aftershock collapse (Assadi et al., 2023). To enhance seismic performance and reduce residual damage, various innovative self-centring balloon-type mass timber SFRSs have been proposed (Pei et al., 2019; Hashemi et al., 2020; Lepine-Lacroix and Yang, 2023). Among them, post-tensioned CLT (PT-CLT) walls (Pei et al., 2019; Chen et al., 2020) (Figure 4-1a) have gained global attention and public awareness due to their self-centring and stable energy dissipation capabilities.

PT-CLT walls adopt the post-tensioned seismic damage-resistant technology from the PREcast Seismic Structural Systems (PRESSS) program (Priestley et al., 1991) and integrate CLT panels with post-tensioned high-strength steel strands or threaded bars across the centre of each panel to develop moment-resisting connections (Busch et al., 2022). CLT panels are allowed to undergo controlled rocking instead of being rigidly fixed to the wall-to-foundation interface. Sliding is prevented using shear keys; although CLT panels can resist lateral loading, post-tensioning bars exert a restoring moment when elongated, attaining self-centring. External energy dissipation devices (EDDs) such as BRAFs (Massari et al, 2017, Rahmzadeh and Iqbal, 2018; Zhu et al., 2024) and U-shaped Flexural Plates (UFPs) (Kelly et al., 1972; Iqbal et al., 2015) are often used to couple PT-CLT walls and provide energy dissipation. The sacrificial EDDs are designed to be activated during seismic excitation and therefore capacity-protect primary structural components (Chen et al., 2020). With limited or negligible residual damage, such a system is economically appealing because building downtime can be significantly reduced, and post-earthquake building repairs will mainly focus on replacing the EDDs (Furley et al., 2021).

Extensive experimental testing has been conducted to investigate the structural performance of PT mass timber rocking walls. Early testing in New Zealand primarily focused on post-tensioned LVL walls with EDDs (Palermo et al., 2005; Smith et al., 2007; Iqbal et al., 2007; Iqbal et al., 2015; Sarti et al., 2016). Due to the relative popularity and availability of CLT in North America, testing was carried out using the PT-CLT wall (Ganey et al., 2017; Chen et al., 2018; Pei et al., 2019; Pei et al., 2023). Ganey et al. (2017) conducted full-scale quasi-static testing for six PT-CLT wall specimens under reversed cyclic loading and parametrically considered the design parameters such as area and initial stress of PT bar and wall boundary conditions. Chen et al. (2018) tested a total

of 17 PT-CLT walls with six different configurations under monotonic and reversed cyclic loading. The occurrence of crushing and splitting of the CLT wall at the compressive edges and the buckling of lumber in the exterior layer of the wall were identified as failure modes, but they were not observed until the roof drift reached or exceeded 2.5%. Building-level experimental examinations were also performed in the United States as part of the NHERI TallWood Project. In 2017, a full-scale two-storey mass timber building with PT-CLT walls coupled with UFPs as SFRS was tested on the shaking table at the University of California San Diego (Pei et al. 2019; Barbosa et al., 2021; Mugabo et al., 2021). After the test building was subjected to a suite of ground motions, the performance goal of no major structural damage was achieved. In 2023, a full-scale ten-storey PT-CLT shear wall building designed using a performance-based approach was tested on a shaking table (Pei et al., 2023). The test was carried out under various suites of ground motions scaled to seven different seismic hazard levels. Preliminary results indicated that building performance exceeded code minimum requirements and that the inter-storey drift ratio (ISDR) was limited to 1.5% at MCE events (Wichman, 2023). Various numerical modelling strategies have also been proposed for PT rocking timber walls to predict their structural responses under lateral loading and perform parametric analyses. These strategies include the multi-spring model (Ganey, 2015; Massari et al, 2017; Kovacs and Wiebe, 2019; Wichman et al., 2022; Qureshi et al., 2023; Ho et al., 2023), the fibre-based model (Akbas et al., 2017; Slotboom, 2020; Zhu et al., 2024), the lumped plasticity model (Iqbal et al., 2015; Wilson et al., 2019; Slotboom, 2020), and the finite-element model (Wilson et al., 2019; Chen and Popovski, 2020; Tomei et al., 2023).

Several studies have assessed the seismic performance of post-tensioned mass timber rocking walls using numerical approaches (e.g., Ganey, 2015; Akbas, 2016; Sarti et al., 2017; Kovacs and Wiebe, 2019; Wilson et al., 2020; Furley et al., 2021; Ho et al., 2023). Akbas (2016) developed 6- and 11-storey prototype buildings equipped with PT-CLT walls with coupling UFPs and examined their performance under a design basis earthquake (DBE) (10% in 50 years) and a maximum considered earthquake (MCE) (2% in 50 years). Performance objectives (POs) of Immediate Occupancy (IO) and Life Safety (LS) were considered in the seismic design and performance assessment. Although the investigation concluded satisfactory performance of the prototype buildings, the exceedance probabilities of POs were not evaluated, and the seismotectonics were limited to crustal events. Following the FEMA P695 (FEMA, 2009) approach, Sarti et al. (2017)

determined seismic performance factors for PT-LVL walls, and recommended a response modification factor (R) of 7 for ASCE 7 (ASCE, 2016). Kovacs and Wiebe (2019) conducted a collapse assessment for 3-, 6-, and 9-storey buildings with PT-CLT walls without EDDs for Montreal, a city of moderate seismicity in Canada, and reported that the probability of collapse under MCE ground motions is less than the 10%. Wilson et al. (2020) applied performance-based seismic design for a 5-storey office building and a 12-storey residential building with PT-CLT wall coupling with UFPs as SFRS. NLRHA was carried out using 50 ground motions consisting of both far-field and near-field events. It was concluded that both buildings met the ISDR limit specified in ASCE 7-16 (ASCE, 2016) and that structural damage was limited to crushing at the CLT wall toe and UFP plastic deformation. Ho et al. (2023) evaluated the seismic performance factors of a 3-storey PT-MPP rocking wall with coupling UFPs and developed limit-state-dependent fragility functions based on truncated incremental dynamic analysis (IDA) using 44 far-field shallow crustal ground motions from FEMA P695. Although a lower bound R of 6.48 was reported, the collapse margin ratio (CMR) was not provided, and the POs considered were not examined in a probabilistic manner based on archetype buildings of various heights.

In Canada, adoption of the sixth-generation Seismic Hazard Model (SHM6) (Kolaj et al., 2020) by NBCC 2020 (NRCC, 2020) resulted in a nationwide increase in seismic hazard. In addition, Canada has regions with complex seismotectonics, such as Southwestern BC, where three different damaging sources of earthquakes coexist: the shallow crustal, deep-in-slab, and interface (Goda, 2019). As a result, seismic design and performance of buildings are anticipated to be greatly impacted (Popovski et al., 2021; Odikamnoro et al., 2022). To further validate the potential application of PT-CLT walls in high seismic risk zones, the seismic performance of 3-, 6-, and 9-storey PT-CLT shear wall buildings with UFPs was assessed, considering diverse earthquake types and increased seismic hazards in southwestern British Columbia (BC), Canada. The performance evaluation considered various POs and used static and nonlinear dynamic analyses.

This paper is organized as follows. First, the lateral responses of PT-CLT walls with UFPs and the structural mechanics of UFPs are illustrated. Seismic POs for PT-CLT shear walls are then defined. Second, the design of the prototype buildings is presented, which was based on the direct displacement-based design (DDBD) approach. Next, a fibre-based numerical modelling strategy for PT-CLT walls with UFPs in *OpenSeesPy* and validation with full-scale quasi-static cyclic and

shaking table experimental tests are presented. Nonlinear static analyses (NLSA) and response history analyses (NLRHA) are then carried out to assess the structural responses and validate the DDBD procedure. Finally, to develop the buildings' fragilities and estimate CMRs, IDA was conducted for each prototype building using 80 ground motion records, which were selected considering the complex seismotectonics in Southwestern BC, following SHM6 and NBCC 2020.

4.3 Lateral Response of PT-CLT Walls with UFPs

PT-CLT walls benefit from controlled rocking and self-centring when subjected to lateral loadings, such as seismic action. Lateral loading leads to a composite deformation of the SFRS with contributions from flexure and shear deformation, as well as rigid-body rocking (Figure 4-1b). Figure 4-1c shows a typical base shear versus roof displacement relationship of PT-CLT walls with UFPs under NLSA. Initially, the overturning moment in PT-CLT walls is resisted by the gravity load and initial post-tensioning force until reaching the decompression (DEC) limit state. Prior to DEC, the wall behaves as a fixed-end cantilever and exhibits exclusively elastic deformation due to flexure and shear. As the DEC is exceeded, rigid body rocking of the panel commences. The base uplift or gap opening at one side of the CLT wall will accumulate compressive stress on the opposite side (Figure 4-1b). Meanwhile, UFPs near the top of the building could reach the yielding limit state (YUFP) and start dissipating energy with increasing imposed rotation at the wall-to-foundation interface. However, the initial geometric and material nonlinearity is limited, and the wall still behaves quasi-elastically until the effective linear limit (ELL). Akbas et al. (2017) quantitatively associated ELL with the contact length between the wall and foundation, defining it as three-eighths of the panel length. As the contact length further reduces due to rocking, the rest of the UFPs yield consecutively, and yielding of CLT (YCLT) can occur at the compressive toe of the wall, followed by the splitting of CLT (SCLT), crushing of CLT (CCLT), and the eventual yielding of PT tendons (YPT). It is to be noted that strength degradation might occur at the onset of CCLT before YPT (see Figure 4-11). To achieve self-centring, when designing PT-CLT walls, it is suggested that the system re-centring ratio, β, be greater than 0.55 (Sarti et al. 2017), which is the ratio of the moment resistance contributed by PT elements and the gravity load to the total moment resistance at the wall-to-foundation interface.

These structural damage states of PT-CLT walls can be associated with different seismic POs. Note that some limit states are either difficult to detect during experiments (e.g., ELL and YCLT) (Furley et al, 2021) or computationally demanding to record the time histories of all component-level responses in numerical analysis, particularly in IDA. Therefore, ISDRs are typically used as a proxy for damage (limit) states based on existing experimental observations (Ho et al., 2023). Table 4-1 summarises the relationship between various POs and the component and system limit states employed in the literature. Wichman (2023), based on full-scale shaking table tests of 2- and 10-storey PT-CLT wall buildings, recommended 1%, 2%, and 3% ISDR limits for IO, LR, and CP respectively, which were adopted as the POs in this study.
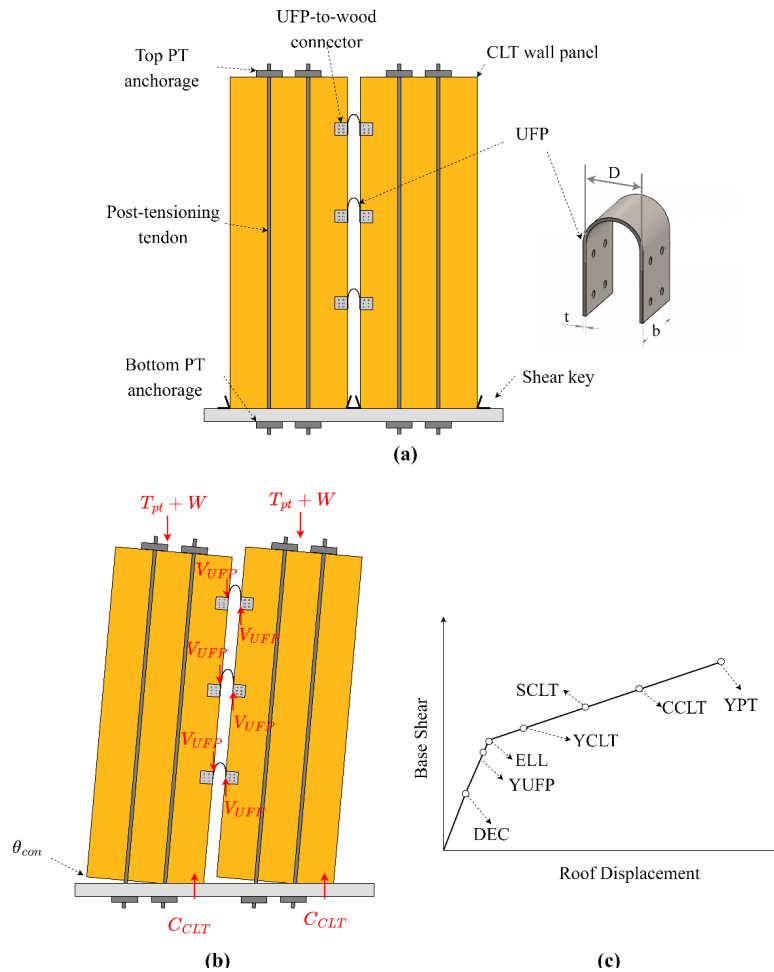
Figure 4-1. (a) PT-CLT walls coupled with UFPs; (b) system deformation and equilibrium under lateral load, (c) base shear versus roof displacement relationship of PT-CLT walls with UFPs outlining limit states.

Table 4-1.Summary of seismic POs and corresponding limit states for PT mass timber buildings.

Reference	System configuration	PO	Hazard level	Component limit states	System limit states
Akbas (2016)	PT-CLT wall coupling with UFPs	IO	DBE	DEC, YUFP, ELL, YCLT [1]	-
		LS	MCE	DEC, YUFP, ELL, YCLT, SCLT [1]	-
Sarti et al. (2017)	PT-LVL rocking walls with EDDs	-	SLE	DEC, YUFP [1]	-
		-	DBE	DEC, YUFP, YCLT [1]	-
		CP	MCE	DEC, YUFP, YCLT, failure of UFP, and YPT [1]	5% roof drift
Ho et al. (2023)	PT-MPP wall coupling with UFPs	IO	SLE	Effective yielding of any component [2]	1% ISDR
		LS	DBE	Crushing of MPP wall and YPT [2]	2% ISDR
		CP	MCE	Ultimate capacity PT element and MPP wall [2]	a) 4% ISDR b) 1.5% residual ISDR
Wichman (2023)	PT mass timber rocking wall with EDDs	OC	SLE	All components remain elastic	-
		IO	DBE	DEC, YUFP [1]	a) 1% ISDR b) 0.2% residual ISDR
		LR	5% in 50 years	DEC, YUFP, YCLT [1]	2% ISDR
		CP	MCE	DEC, YUFP, YCLT, CCLT, YPT [1]	3% ISDR

Note that in Table 4-1, SLE stands for a service level earthquake (50% in 30 years). Superscripts [1] and [2] denote that the system is allowed to reach and not exceed the specified component limit states respectively.

4.4 U-shaped Flexural Plates (UFPs)

In coupled PT-CLT walls, UFPs serve as coupling links and offer energy dissipation in the event of relative vertical movement between adjacent wall panels. Bending a piece of mild steel plate of a certain thickness (t) about a certain diameter (D) can produce a UFP with a semicircle and two equal side plates (Figure 4-1a). The side plates of UFPs can be connected to CLT walls to create coupling. The connection can be either bolted saddle connections for simple post-earthquake replacement of damaged UFPs (Wichman et al., 2022) or metal inert gas welding (Iqbal et al., 2015). UFPs were applied early in precast post-tensioned PT-LVL walls (Iqbal et al., 2015; Sarti et al., 2017). Recently, Ganey et al. (2017), Pei et al. (2019), Chen et al. (2020), and Pei et al. (2023) used UFPs in PT-CLT wall studies.

Baird et al. (2014) reported factors governing failure of UFPs, including stroke and maximum strain. The stroke is related to the dynamic bending deformation of UFPs, whereas the maximum strain is determined by geometry and taken as the ratio between t and D (Skinner et al., 1974). Iqbal et al. (2015) conducted component-level testing for three UFPs under reversed cyclic loading. A 5-mm thickness and a 15-mm radius of curvature were chosen for all UFPs, with widths of 50 mm, 65 mm, and 100 mm, respectively. The test setup and UFP specimens are shown in Figure 4-2. The experiment revealed that UFP hysteresis remained stable, without distinct stiffness and strength degradation (Figure 4-6). The number of cycles leading to UFP failure decreased as strain increased, especially for strokes greater than double the initial bend length. Previous testing by Kelly et al. (1972) indicated that the failure mode of UFPs is dominated by a localized kinking of the plate followed by a complete transverse fracture. Furthermore, UFPs under cyclic loading, exhibit a distinct strain-hardening effect (Kelly et al. 1972). Hence, accurate predictions of initial UFP stiffness and maximum force are important. Baird et al. (2014), based on experimental testing and numerical simulation, provided formulations for UFP yield force and initial stiffness (Equations 4-1 and 4-2) with geometrical parameters (t, b, D) as inputs:

$$F_y = \frac{\sigma_y b t^2}{2D} \qquad\qquad \text{Equation 4-1}$$

$$k_0 = \frac{16Eb}{27\pi}\left(\frac{t}{D}\right)^3 \qquad \text{Equation 4-2}$$

where σ_y and E are the yield stress and Young's modulus of mild steel.
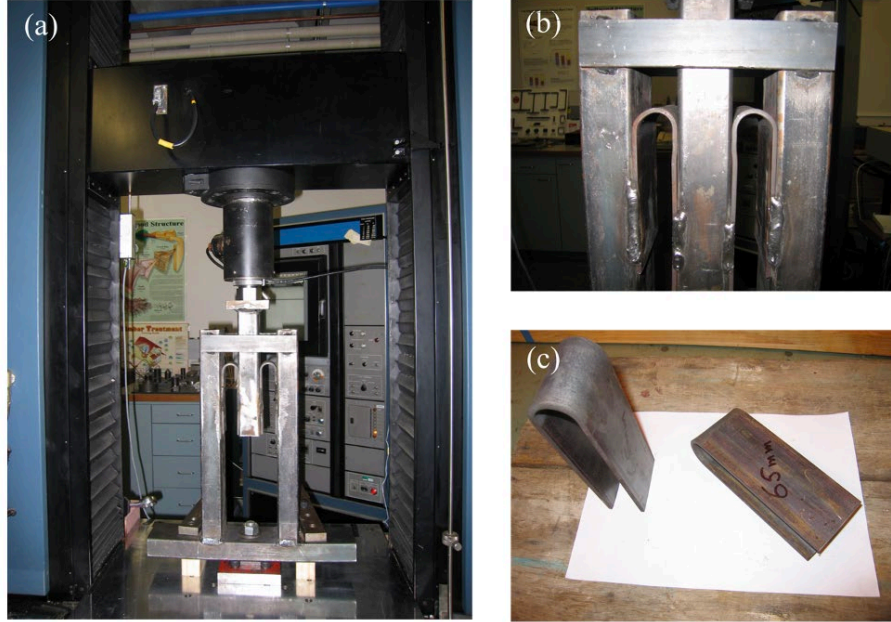
Figure 4-2. Test setup for U-shaped flexural plate (UFP) (Picture courtesy of Asif Iqbal from UNBC).

4.5 Seismic Design of PT-CLT Shear Wall Buildings

Prototype Buildings

Three-, six-, and nine-storey prototype buildings were designed based on the seismic hazard in Vancouver, a metropolitan city in southwestern BC, Canada. All prototype buildings have a floor area of $616\ m^2$ (Figure 4-3), with a ground floor height of 4 m and a typical storey height of 3 m. The buildings are designated as office buildings and are situated on Site Class C soil. The floors consist of 175-mm (5-ply) CLT panels with 38-mm concrete topping. Each floor bears 3.44 kPa dead load and 1.9 kPa live load, and the roof supports 1.76 kPa dead load and 1.64 kPa snow load. Each building, as shown in Figure 4-3, has four PT-CLT coupled walls in each lateral direction.
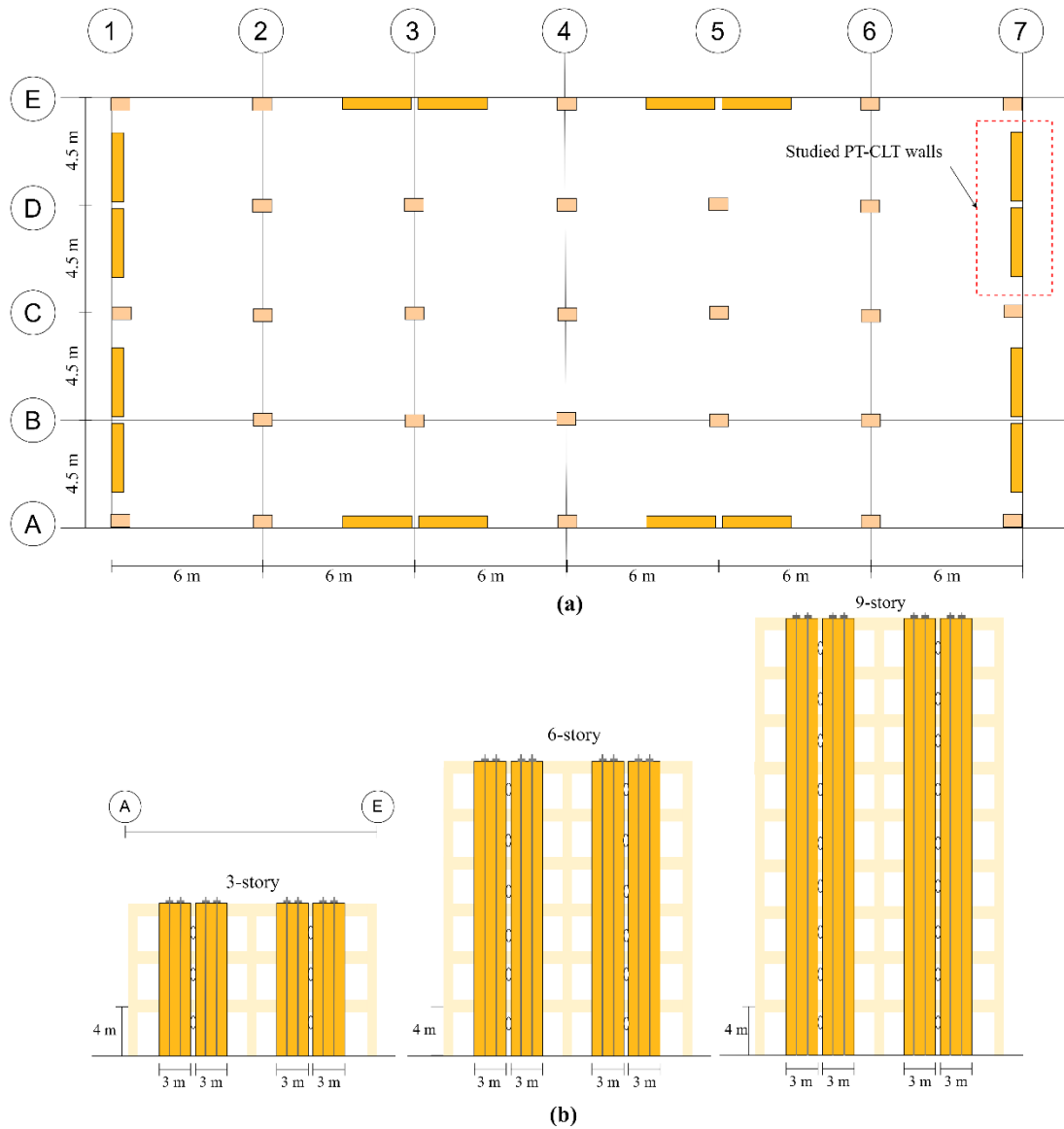
Figure 4-3. (a) Typical floor plan and (b) schematics of 3-, 6-, and 9-storey prototype buildings.

Direct Displacement-Based Design

Currently, PT-CLT walls can be designed only as an alternative solution in Canada. This is due to the absence of seismic force modification factors (R_d and R_o) for PT-CLT shear walls in the NBCC 2020 (NRCC, 2020). Therefore, a DDBD approach was used to design the prototype buildings. Figure 4-4 depicts the DDBD procedure, which combines the design steps for PT-LVL walls proposed by Sarti (2015) (Steps 1-6) and the sectional analysis developed by Pampanin et al. (2001) (Step 7). The following subsections present a complete DDBD process for the 3-storey

PT-CLT shear wall prototype building with UFPs. Since the same procedure was followed for the 6- and 9-storey buildings, only their final design summary is provided in Table 4-3.
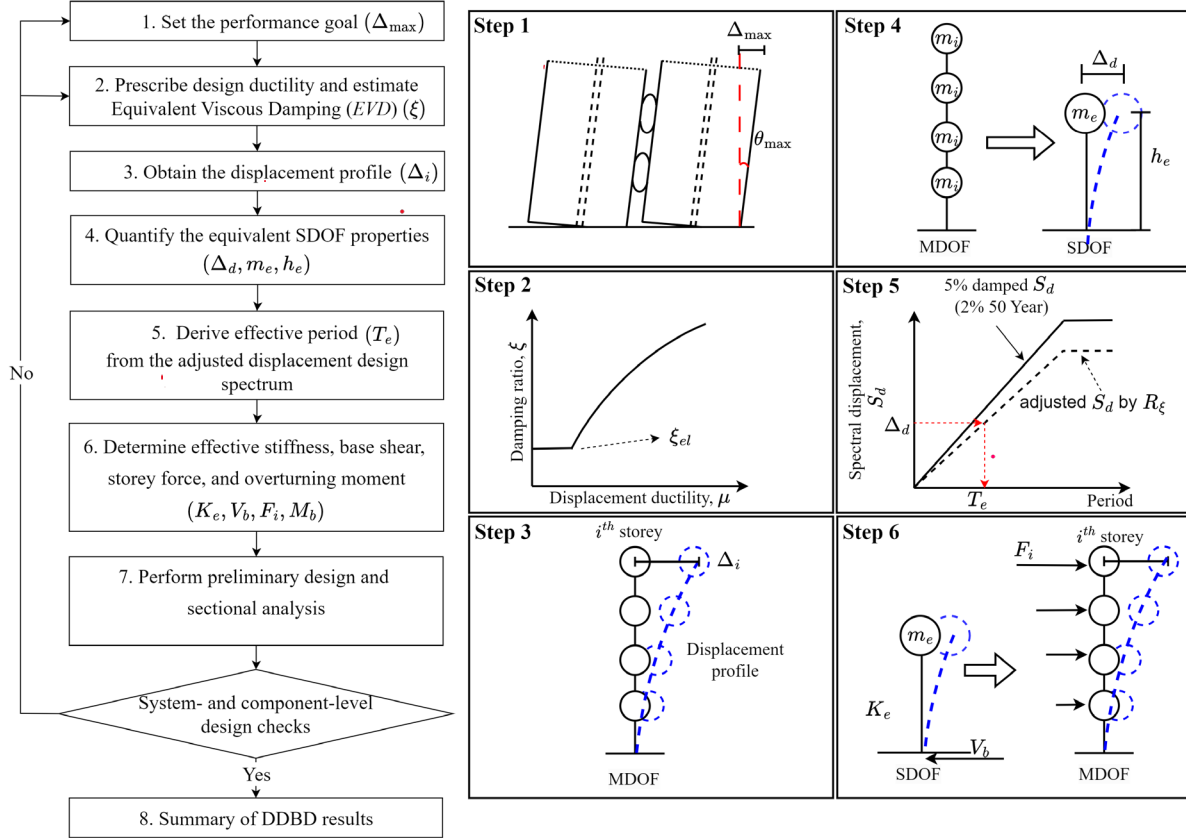
Figure 4-4. DDBD procedure for PT-CLT walls with UFPs.

Step 1: Set the performance goal

A maximum roof drift ratio of 2% was prescribed as the performance criterion for PT-CLT shear wall buildings under MCE events (Sarti, 2015). The maximum ISDR limit of 2.5%, as required in NBCC 2020, must also be satisfied.

Step 2: Prescribe design ductility and calculate equivalent viscous damping

System ductility (μ), post-yielding stiffness factor (r), and re-centring ratio (β) were specified to estimate the equivalent viscous damping (EVD) (ξ), using Equations 4-3 to 4-5 provided by Sarti (2015):

$$\xi = \xi_{hyst} + \xi_{elastic} \qquad\qquad \text{Equation 4-3}$$

$$\xi_{hyst} = k_{dyn}k_\xi \frac{(2-2\beta)(\mu-1)}{\mu\pi(1+r(\mu-1))} \qquad\qquad \text{Equation 4-4}$$

$$k_\xi = 0.83 + 0.06(\mu-1) \qquad\qquad \text{Equation 4-5}$$

where $\xi_{elastic}$ was taken as 3% (Sarti, 2015), ξ_{hyst} was quantified based on the analytical formula for area-based hysteretic damping (Priestley et al. 2007), k_{dyn} is a correction factor to account for incomplete cycles under real earthquake motions, and k_ξ is an area-based hysteretic damping modification factor (Sarti, 2015). For all designed buildings, μ, r, β were assumed to be 3, 0.2, and 0.7, respectively.

Step 3: Obtain the displacement profile

The storey displacement profile corresponding to the design roof drift was estimated using Equations 4-6 to 4-8 (Sarti 2015):

$$\Delta_i = \delta_i \left(\frac{\Delta_c}{\delta_c}\right) \qquad\qquad \text{Equation 4-6}$$

$$\delta_i = (1-k_{el})\left(\frac{h_i}{h_n}\right) + k_{el}\left[\frac{3h_i^2}{2h_i^2}\left(1-\frac{h_i}{3h_n}\right)\right] \qquad\qquad \text{Equation 4-7}$$

$$k_{el} = 0.1 + \frac{0.6}{\mu} \qquad\qquad \text{Equation 4-8}$$

where Δ_c is the design displacement at the critical storey (roof level), δ_i is the inelastic mode shape at storey i, and k_{el} is a calibration factor specifying the ratio of elastic contribution to the total drift. Table 4-2 summarises the design displacement profile and parameters relevant to the properties of the equivalent single-degree-of-freedom (SDOF) system for the 3-storey building in Step 4.

Table 4-2. Summary of parameters for obtaining the equivalent SDOF system for the 3-storey PT-CLT shear wall building.

level	h_i	M_i	δ_i	Δ_i	ISDR	$M_i\Delta_i$	$M_i\Delta_i^2$	$M_i\Delta_i h_i$
	(m)	(kg)		(m)	(%)			
roof	10	33844	1.00	0.20	2.27	6768	1354	67688
2	7	68468	0.66	0.13	2.11	9024	1190	63173
1	4	68468	0.34	0.07	1.71	4689	321	18755

Step 4: Quantify the equivalent SDOF properties

Assuming that mass is lumped at the centre of each storey, the effective mass (m_e), design displacement (Δ_d), and effective building height (H_e) can be calculated for the equivalent SDOF system using Equations 4-9 to 4-11:

$$\Delta_d = \frac{\sum_{i=1}^{n} m_i\Delta_i^2}{\sum_{i=1}^{n} m_i\Delta_i} = 0.140\ m \qquad \text{Equation 4-9}$$

$$m_e = \frac{\sum_{i=1}^{n} m_i\Delta_i}{\Delta_d} = 146461\ kg \qquad \text{Equation 4-10}$$

$$H_e = \frac{\sum_{i=1}^{n} m_i\Delta_i h_i}{\sum_{i=1}^{n} m_i\Delta_i} = 7.30\ m \qquad \text{Equation 4-11}$$

Step 5: Calculate the effective period from the displacement spectrum

The displacement spectrum was derived from Vancouver's Uniform Hazard Spectrum (UHS) (NRCC, 2020) using Equations 4-12 and 4-13. Subsequently, the 5% damped displacement spectrum was adjusted to a new displacement spectrum at the *EVD* level, and the effective period was retrieved by tracing Δ_d on the design displacement spectra (Figure 4-4).

$$S_d(T) = \frac{S_a(T)}{\omega^2} = \frac{S_a(T)}{4\pi^2} \cdot T^2 \qquad\qquad \text{Equation 4-12}$$

$$R_\xi = \left(\frac{7\%}{2\% + \xi}\right)^{0.5} = \left(\frac{7\%}{2\% + 10\%}\right)^{0.5} = 0.77 \qquad\qquad \text{Equation 4-13}$$

Step 6: Determine effective stiffness, base shear, storey force, and overturning moment

The effective stiffness (K_e), base shear (V_b), overturning moment (M_b), and storey force (F_i) are the outcomes of the DDBD and can be calculated using Equations 4-14 to 4-17:

$$K_e = \frac{4\pi^2 m_e}{T_e^2} = 4015 \; kN/m \qquad\qquad \text{Equation 4-14}$$

$$V_b = K_e \cdot \Delta_i = 562 \; kN \qquad\qquad \text{Equation 4-15}$$

$$M_b = V_b \cdot H_e = 4102 \; kN \cdot m \qquad\qquad \text{Equation 4-16}$$

$$F_i = \frac{m_i \Delta_i}{\sum_{i=1}^{n} m_i \Delta_i} V_b \qquad\qquad \text{Equation 4-17}$$

Step 7: Perform preliminary design and sectional analysis

Based on the design outcomes from Step 6, a preliminary design for PT-CLT walls with UFPs was conducted. Because the overall deformation of the wall under lateral load consists of elastic and inelastic deformations, the maximum imposed rotation (θ_{imp}) can be estimated by subtracting the elastic rotation (i.e., the sum of deformation due to bending, θ_{bend} and shear, θ_{shear}) from the total rotation (θ_t) using Equation 4-18 to 4-20:

$$\theta_{imp} = \theta_t - \theta_{bend} - \theta_{shear} = 0.018 \; rad \qquad\qquad \text{Equation 4-18}$$

$$\theta_{bend} = \frac{\sum_{i=1}^{n} F_i h_i^2 (3h_n - h_i)}{6EI h_n} = 0.0013 \; rad \qquad\qquad \text{Equation 4-19}$$

$$\theta_{shear} = \frac{\sum_{i=1}^{n} V_i H_i}{GA_{s,w} h_n} = 0.0007 \ rad \qquad \text{Equation 4-20}$$

where h_i is the height of the ith storey, h_n is the building height, and H_i is the ith storey height.

The next step consists of associating the design overturning moment demand (M_b) with the maximum imposed rotation (θ_{imp}). Knowing the moment resistance contributions of the PT and UFPs in resisting M_b, adequate sizing can be performed, and the initial post-tensioning force as well as the required capacity and number of UFPs can be calculated. Notice that strain compatibility at the wall-to-foundation interface is lost during rocking of the CLT panel, making it challenging to find the section equilibrium. Therefore, a sectional analysis (Pampanin et al. 2001) was used to quantify the system's moment resistance at θ_{imp}. The analysis starts with a trial value of the neutral axis depth, after which deformation in the post-tensioned cable and the UFPs can be evaluated based on the section geometry. To estimate the CLT strain, the Monolithic Beam Analogy (MBA) concept was used (Pampanin et al. 2001). The analogy considers the displacement of a post-tensioned connection equal to that of an equivalent monolithic connection under the same lateral load. Equating the rigid body rotation with the known rotation of a plastic hinge region makes it possible to estimate the CLT's compressive strain (ε_t), given by Equation 4-21 (Newcombe et al., 2008; Wichman, 2023):

$$\varepsilon_t = c \left(\frac{L_{cant} \ \theta_{imp}}{l_p (L_{cant} - \frac{l_p}{2})} + \phi_e \right) \qquad \text{Equation 4-21}$$

where L_{cant} is the effective cantilever height of the wall, l_p is the plastic hinge height, taken as two times the CLT wall thickness (Akbas et al., 2017) and ϕ_e is the elastic curvature. Section equilibrium can be checked based on component deformations by determining whether the net force exceeds the tolerance. If not, iterative adjustment of the neutral axis is required until section equilibrium is achieved. Additional checks shall be performed, such as the strain in the post-tensioned tendon at the design drift. The flexural and shear resistance of the CLT walls shall also be verified following CLT manufacturing standards.

Step 8: Summary of DDBD design results

From Step 7, if the moment resistance at θ_{imp} for the PT-CLT coupled wall is greater than the overturning moment demand and all other checks are satisfied, the DDBD is finished and considered satisfactory. The final design plan for the 3-storey PT-CLT shear wall building adopted 5-ply E1 grade CLT panels with an individual panel width of 3 m. Four tendons with an initial post-tensioning force of 170 kN each were utilized for every single wall panel, and the tendon had a cross-sectional area of $740\ mm^2$. Eleven UFPs were employed ($t = 13\ mm$, $b = 180\ mm$, $D = 110\ mm$) and distributed evenly along the height of the building. The design was repeated for 6- and 9-storey buildings and the results are summarised in Table 4-3.

Table 4-3. DDBD outcomes for prototype buildings.

	3-storey	6-storey	9-storey
$\Delta_d(m)$	0.14	0.25	0.37
$m_e(kg)$	146461	300112	449312
$H_e(m)$	7.30	13.22	19.29
ξ	9.70	9.70	9.70
R_ξ	0.77	0.77	0.77
$T_e(s)$	1.20	1.88	3.41
$K_e(kN/m)$	4015	3349	1525
$V_b(kN)$	562	843	559
$M_b(kNm)$	4102	11145	10790
N_{UFP}	11	30	29
N_{PT}	4	4	4
$A_{PT}\ per\ bar(mm^2)$	740	2000	1945
$T_{PT_{ini}}$	172	717	767
$CLT\ layer$	5	7	7

4.6 Development of Fibre-based Numerical Models for PT-CLT Walls

For performance assessment, two-dimensional numerical models for PT-CLT walls with UFPs were developed in *OpenSeesPy* (Zhu et al., 2018) (Figure 4-5). The key modelling strategies are illustrated in the following subsection, including component-level calibration and model validation at system-, and building-levels.

4.6.1 Modelling Strategy

Force-based beam-column elements with *fibre sections* were used to capture the deformation at the plastic zone of the CLT panel, in which the plastic hinge length is taken as two times the wall panel thickness (Akbas et al., 2017) (Figure 4-5) Each *section* was discretized to vertically oriented fibres across the length of the wall. *Elastic Perfectly Plastic Gap (EPPGap)* material with no tensile strength was assigned to *fibres* to idealize the stress and strain relationship of the CLT based on experimental observation (Chen et al., 2018) and to simulate the base uplift. The portion above the plastic hinge zone was assumed to be linearly elastic and modelled by the *ElasticTimoshenko* beam. The PT elements were modelled by corotational trusses assigned with the *Giuffré-Menegotto-Pinto Model (Steel02)* material. The top of the PT tendon was connected to the upper portion of the CLT panel using *rigid beam elements*. The *initial stress* function of the material was used and iteratively adjusted to attain the target initial PT force after wall precompression (Kovac and Wiebe, 2019; Slotboom, 2020). It is assumed that CLT walls have negligible compression due to the prestressing of PT elements and lateral load between two wall panels was transferred using a rigid link element. *Zero-length elements* with calibrated uniaxial material properties in the vertical direction were used to model UFPs. At each UFP location, the *zero-length elements* were rigidly connected to the nodes at CLT walls at the same height to account for the offset between the CLT wall and the UFPs (Sarti, 2015; Akbas, 2016; Wichman et al., 2022).
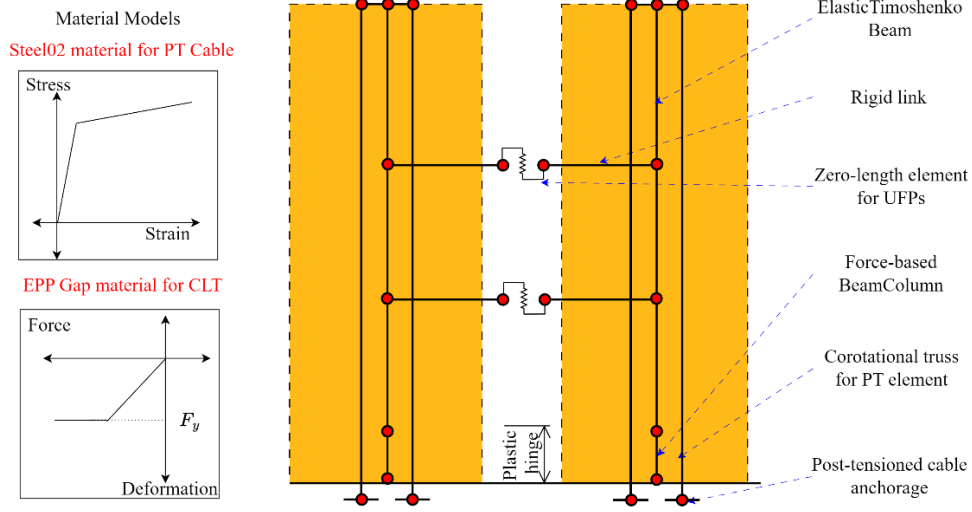
Figure 4-5. Fibre-based numerical model in *OpenSeesPy*.

4.6.2 Component-level Calibration for the UFPs

The *Steel02 uniaxial material model* coupled with *low-cycle fatigue* material was adopted to model the UFPs (Sarti, 2015). The material model was calibrated using the component-level experimental results reported in Iqbal et al. (2015). An SDOF oscillator was employed and modelled by a zero-length spring element in the vertical direction. The yield strength, initial stiffness, and strain hardening ratio were extracted based on the experiment. The transition parameters were adjusted until they closely matched the experimental hysteresis. The calibrated and experimental hysteresis are depicted in Figure 4-6, which shows good agreement for the three tested UFPs.
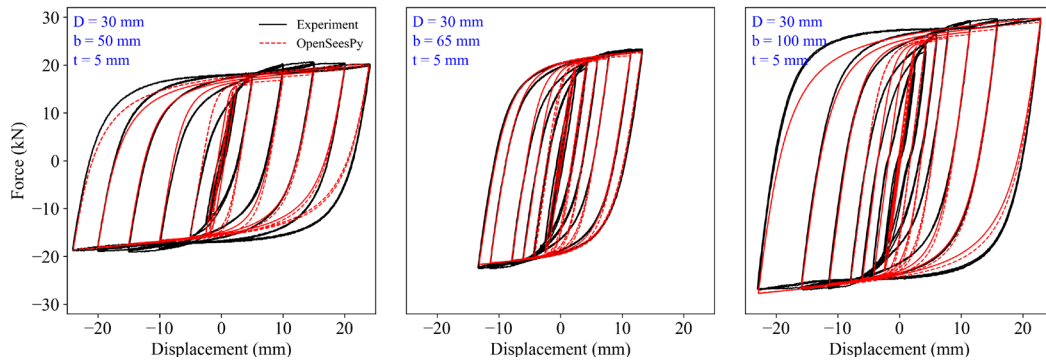
Figure 4-6. Comparison between the cyclic responses of numerical model and experiments (Iqbal et al., 2015).

4.6.3 System-level Validation

The fibre-based numerical model was validated with full-scale quasi-static experimental tests conducted at FPInnovations (Chen et al., 2020) (Figure 4-7a). The experiment was conducted under reverse cyclic loading until the roof drift reached 2.67%. The dimensions of the tested CLT panels were 1 m long, 0.143 m thick, and 3 m tall. The loading was exerted at an actuator height of 2.9 m. A single post-tensioned cable with a diameter of 20 mm was used. The initial post-tensioning force was 89 kN. The elastic modulus and the compressive yield strength of CLT were taken as 2.6 GPa and 25 MPa, respectively (Slotboom, 2020). Figure 4-7b shows the base shear force versus the horizontal displacement at the top of the CLT wall panel from the experiment and numerical simulation. A good agreement was found between the two curves regarding initial stiffness, post-yielding stiffness, and energy dissipation under each cycle. The peak roof horizontal displacement reached 75 mm without structural failure or strength degradation. As shown in Figure 4-7b, the flag-shaped hysteresis curve represents the distinct energy dissipation of UFPs and the self-centring nature of the system.

(a)   (b)

Figure 4-7. (a) Experimental testing setup (Picture courtesy of Zhiyong Chen from FPInnovations); (b) Comparison between the *OpenSeesPy* model results and the cyclic responses from the experimental test (Chen et al., 2018).

4.6.4 Building-level Validation based on Shaking Table Tests
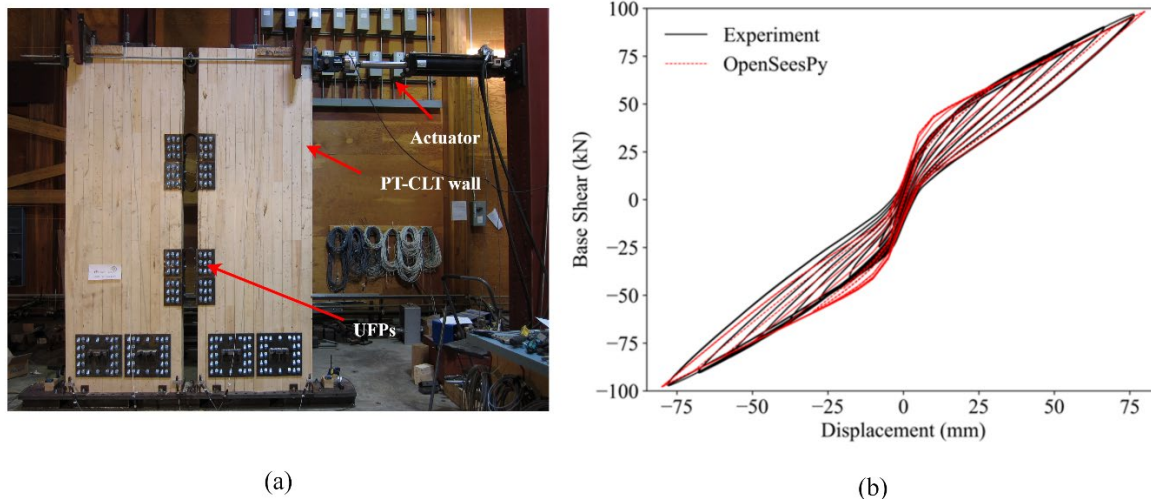
Building-level validation was also performed to verify the robustness of the fibre-based numerical model in predicting the nonlinear dynamic response of PT-CLT walls. The target was the NHERI shaking table test of a 2-storey mass timber building (Pei et al., 2019), which consisted of two coupled PT-CLT walls with UFPs in the same shaking direction. The building was tested under fourteen ground motions, including four ground motions scaled to three hazard intensity levels, namely SLE (50% in 30 years), a DBE (10% in 50 years), and an MCE (2% in 50 years). The detailed descriptions of the building, materials, and ground motions can be found elsewhere (Wichman, 2018; Pei et al., 2019; Barbosa et al., 2021; Mugabo et al., 2021; Wichman et al., 2022). The PT-CLT wall panels were positioned on a steel foundation beam to achieve a rigid foundation. However, significant flexible foundation effects were observed during the test, impacting the overall structural dynamics (Wichman et al., 2022). Therefore, while adopting the same fibre-based modelling strategy, additional considerations proposed by Slotboom (2020) were followed to account for the foundation's flexibility. A 2D numerical model (Figure 4-8) was developed for one of the two walls because the structure is symmetric, and negligible torsion was observed during the experiment (Wichman et al., 2022). It is assumed that each individual panel resists a quarter of the overall seismic force for the rigid diaphragm (Pei et al., 2019), and the corresponding seismic mass was defined at the floor nodes on CLT walls. An additional gravity-leaning column representing the gravity system was defined in *OpenSeesPy* to capture potential P-Delta effects. The leaning column was modelled with *elastic beam-column elements* and was pinned at the foundation (Figure 4-8). Each floor node on the leaning column was rigidly connected to the floor node on the CLT wall. *Zero-length elements* with negligible rotational stiffness were defined at the junction of the floor node and its adjacent elastic columns to simulate moment release. Two more nodes (W1 and W2) and the elements shown in Figure 4-8 were defined below the bottom node at the CLT wall panel (W3). The first node (W1) was defined at the height of the steel foundation beam below the bottom node of the CLT panel and was fully fixed. A rigid link element connected W1 and W2 to model the foundation beam. To capture flexible deformation of the beam, a second node (W2) was defined at the same position as W3, and a *zero-length section element* was used to connect both nodes (Figure 4-8). The *zero-length section* was discretized into vertically distributed fibres, each assigned with elastic bilinear material. Elastic moduli calibrated

by Slotboom (2020) were used to account for the pre-yielding and post-yielding behavior of the foundation beam.

Eigen-analysis was first performed to obtain the period of the system. The fundamental period of the *OpenSeesPy* numerical model is 0.84 s and is considered acceptable compared to the actual period range (0.73 – 0.98 s) based on *in-situ* white noise analysis (Wichman, 2018). The white noise analysis also yielded an average damping coefficient of 1.92%. Hence, 2% mass and tangent stiffness-proportional Rayleigh damping was applied in subsequent analysis. NLRHA was conducted for all fourteen ground motions non-sequentially, and the results were compared with the raw time histories of structural responses from the shaking table test. Time histories of the roof drift ratio from three ground motions were presented and compared with the shaking table test, as shown in Figure 4-9. Figure 4-9 indicates that the model predicted displacement demands in terms of pattern and peak values with accuracy, especially under SLE events. Slight underpredictions for both responses at DBE and MCE levels are observed, similar to those observed in Wichman et al. (2022). Given that the system endured all ground motions during the shaking table test, it is possible that cumulative damage in the CLT walls and PT occurred but was overlooked by the numerical model, potentially resulting in the observed underestimation.

Because the shaking table test revealed a significant flexible foundation effect, the structural performance of the 2-storey PT-CLT wall building, if tested on a rigid foundation, was also investigated by removing the *zero-length fibre section element*. NLRHA for all ground motions was repeated, and the hysteresis plots showing the base shear force versus the roof drift ratio of nine ground motions are presented in Figure 4-10. As expected, the building with a rigid foundation exhibited higher initial and post-yielding stiffness. Under both MCE and DBE, the overall flag-shaped hysteresis and recentring capability were more distinct. To conclude, the fibre-based numerical modelling strategy demonstrated its robustness in capturing the nonlinear dynamic behavior of PT-CLT shear walls and can be used for subsequent performance assessment of the prototype buildings.
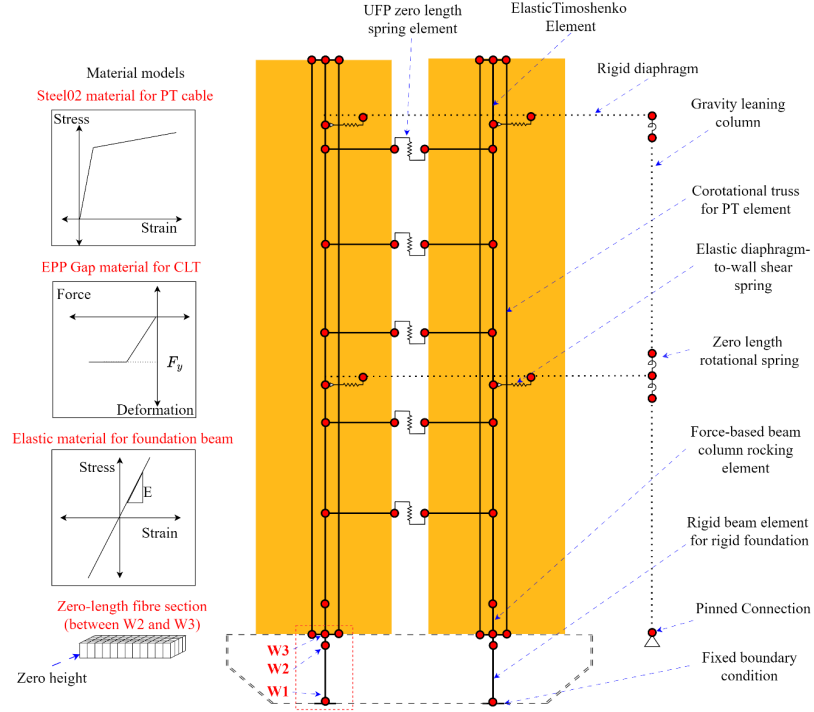
Figure 4-8. Fibre-based numerical model with a flexible foundation.
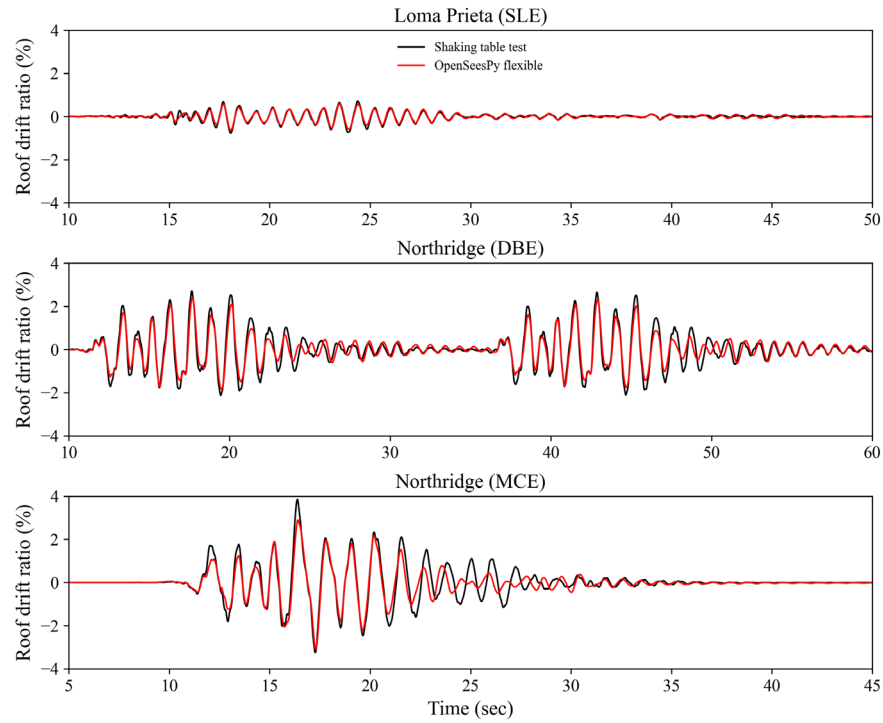
Figure 4-9. Comparison of the time history of roof drift between *OpenSeesPy* flexible foundation model and the shaking table test (Pei et al. 2019).
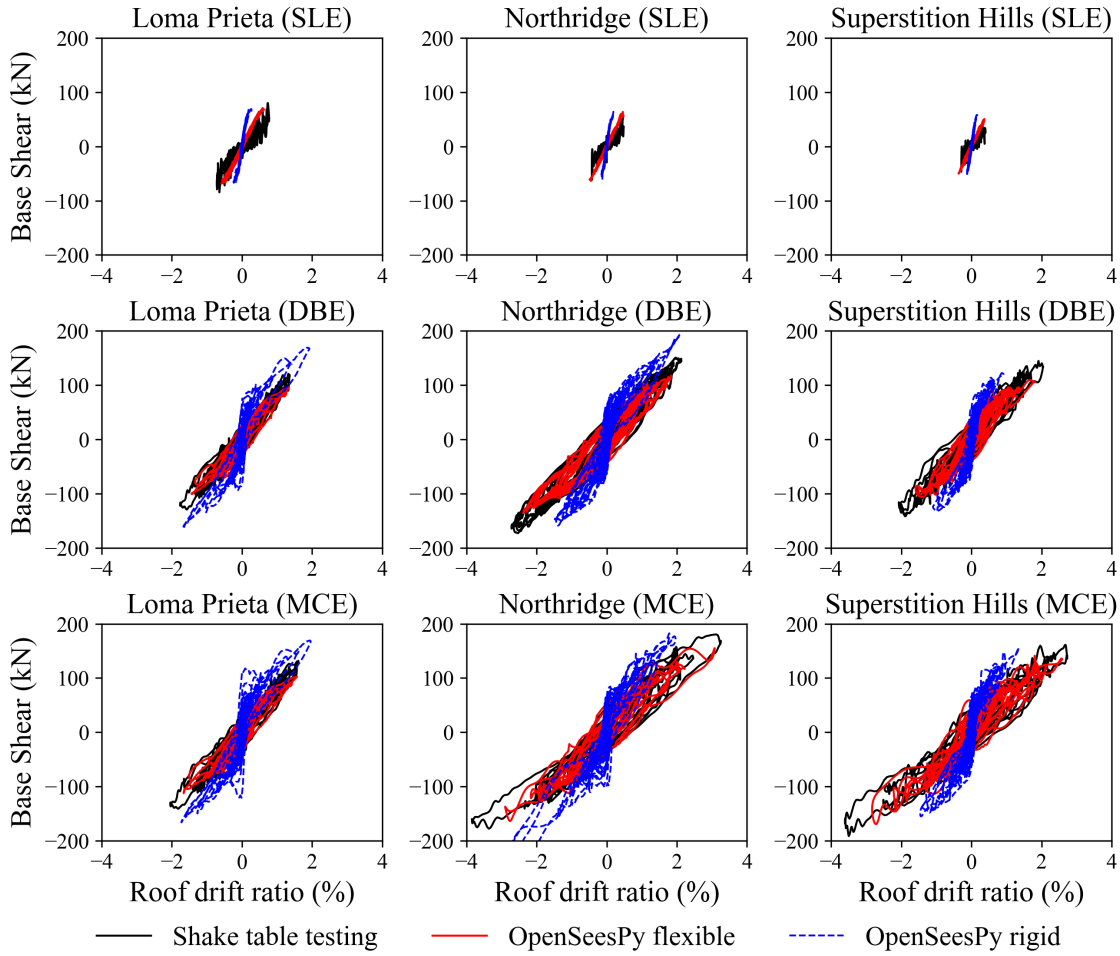
Figure 4-10. Comparison of the hysteretic responses from the shaking table test, the *OpenSeesPy* flexible foundation model, and the *OpenSeesPy* rigid foundation model (Pei et al. 2019).

4.7 Seismic Performance Assessment

In this section, a seismic performance evaluation of the prototype buildings designed in the preceding sections using validated numerical models was presented. Eigen-analysis was first conducted to quantify the prototype buildings' fundamental periods, which are 0.35 s, 0.78 s, and 1.31 s for the 3-, 6-, and 9-storey buildings, respectively. Sarti et al. (2017) reported that the period for PT-CLT walls can be well predicted using the empirical equation for moment-resisting concrete frames up to 1.5 s. However, for structures with longer periods, the equation tends to result in underestimations. Using the corresponding equation from NBCC 2020, the predicted

periods are 0.42, 0.68, and 0.91 s. Although slight period differences were observed for 3- and 6-storey buildings, the expected underestimation for taller PT-CLT walls was noted.

4.7.1 Nonlinear Static Analysis

NLSA was performed for each of the prototype buildings with storey forces determined from the DDBD procedure. Sarti et al. (2017) concluded a 5% roof drift ratio as the maximum drift capacity of mass timber gravity frames. Pei et al. (2019) also reported that gravity connection details can withstand an ISDR up to 5% without compromising stability or causing damages. Hence, each building was monotonically pushed using a displacement-control integrator until a 5% of the roof drift ratio (a non-simulated collapse mechanism). To consider the impact of CLT crushing and the large tensile strain of PT, simulated collapse mechanisms were included through material strain limits for both CLT and PT elements. Using the *MinMax* material model in *OpenSeesPy*, it was possible to incorporate material strain limits. When these limits are exceeded, zero tangent and stiffness are returned, accelerating building collapse. Similar practices can be found in Sarti et al. (2017), in which 1% ultimate compressive strain for LVL was assumed and implemented using the *MinMax* material. Kovac and Wiebe (2019) used a multi-spring modelling approach and removed the individual CLT spring element when twice the yield strain was reached, and Ho et al. (2023) incorporated *MinMax* material into their numerical model to consider the limit states of MPP walls. Inherent conservatism should be recognized since residual strength for CLT and PT elements remains even when the considered limit has been reached (Ganey et al., 2017; Chen et al., 2018). It is expected that CCLT precedes YPT, in which the system's strength degradation is governed by the CCLT.

Two pushover curves are presented in Figure 4-11 for each prototype building. These curves correspond to models with material strain limits for CLT and PT (broken line) and without such limits (solid line). With the inclusion of the *MinMax* material, strength degradation was observed upon reaching the CLT crushing strain at the extreme fibre under compression and NLSA was terminated due to numerical instability. The figures also incorporated a series of component limit states. The stress-strain relationship of each CLT fibre was monitored, and the first onsets of CLT yielding, splitting, and crushing were identified. The CLT yielding strain was based on the value reported by Chen and Popovski (2020b), and the splitting and crushing strains were taken as 0.02

and 0.05, respectively (Akbas et al., 2017). Figure 4-11indicates that CCLT occurred at 3% roof drift for 3- and 6-storey and 2.4% for 9-storey buildings. Since the DDBD approach considered 2% roof drift as the design target under the MCE event, satisfactory structural performance of the prototype building can be demonstrated as damages due to CLT crushing can be effectively limited.
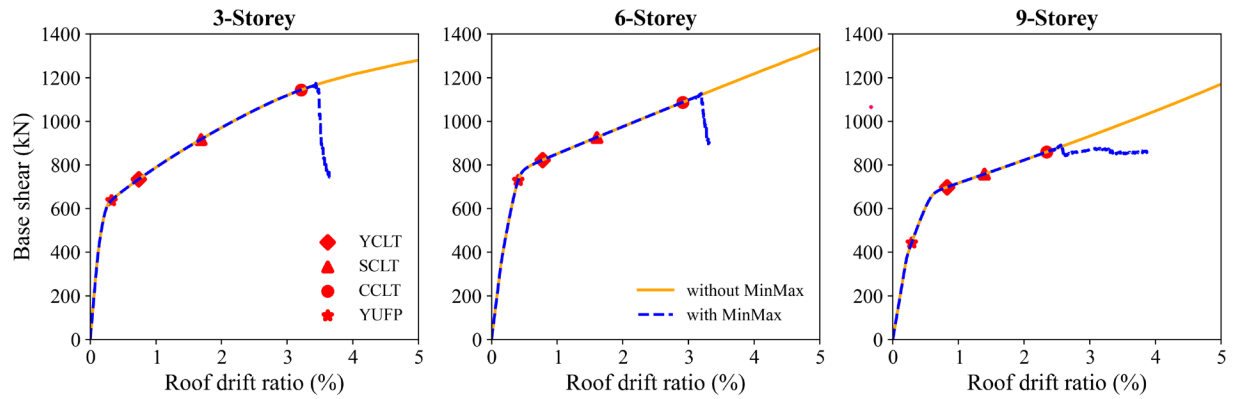
Figure 4-11. Nonlinear static analysis results for the three analyzed buildings.

4.7.2 Nonlinear Response History Analysis under MCE

To validate the DDBD procedure and evaluate the seismic performance of the prototype buildings, NLRHA was conducted. For this purpose, suites of site-specific ground motions consisting of 11 records for each earthquake type scaled to Vancouver's UHS as defined in (NRCC, 2020) were used (Zhu et al., 2024). To perform NLRHA, a transient analysis solver was configured in *OpenSeesPy*. The solver considers a 3% tangent stiffness proportional Rayleigh damping (Sarti, 2015). Structural responses (i.e., storey displacement normalized by building height and the storey shear force) were extracted from each individual NLRHA. The design storey shear forces from DDBD were amplified to a linear shear force envelope to account for higher mode effects (Priestley et al., 2007; Sarti, 2015; Zhu et al., 2024). Figure 4-12 presents the ISDR response for all prototype buildings. The performance is satisfactory because both the mean and 84% quantile responses for all buildings are lower than the 2.5% ISDR limit prescribed in NBCC 2020, with only one out of 33 ground motions causing exceedance of this limit for each of the 6- and 9-storey buildings. Figure 4-13 shows that the design shear envelope bounded the individual and median shear force responses well at each storey. Overall, the adopted DDBD procedure is considered

adequate to ensure acceptable seismic performance of PT-C LT shear wall buildings subjected to MCE level ground motions.

Figure 4-12. Comparison of storey drift responses with design target drift.

Figure 4-13. Comparison of storey shear responses with target shear envelope.

4.7.3 Ground Motion Selection and Scaling for IDA
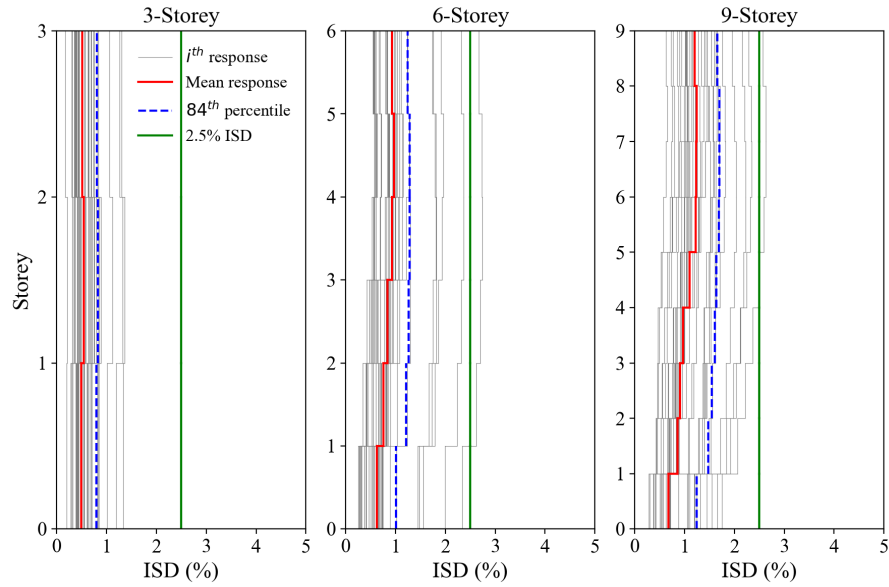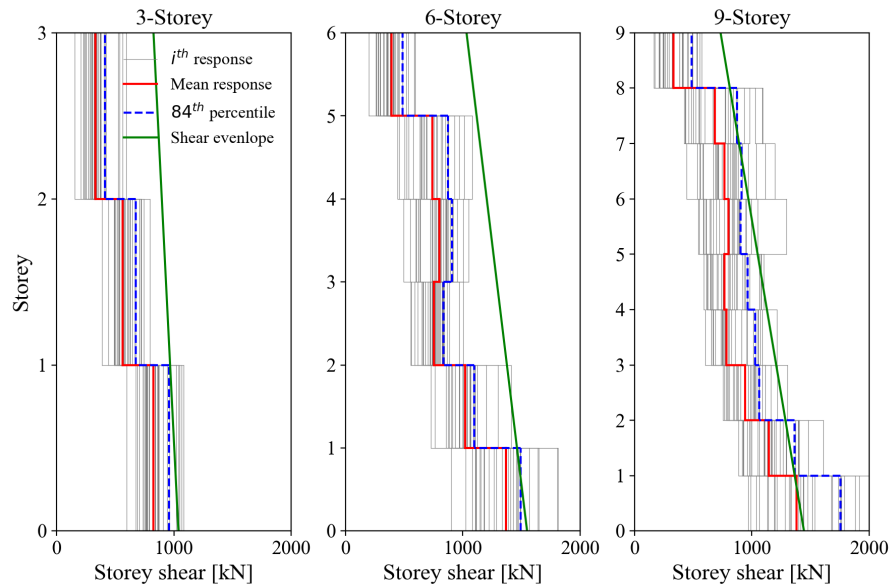
To conduct incremental dynamic analysis (IDA), hazard-specific ensembles of ground motions were selected to best capture the tectonic characteristics of southwestern BC. They covered three contributing regimes: active shallow crust, subduction interface, and deep in-slab (Goda, 2019; Tesfamariam et al. 2023). For ground motion selection, structural- and site-specific conditional spectra (CS) were used as targets (Baker, 2011; Baker and Lee 2018). Probabilistic seismic hazard analyses (PSHA) were first carried out using the *OpenQuake Engine* (Pagani et al. 2014) and the command files for SHM6 prepared by Natural Resources Canada (NRCan) (Kolaj et al. 2020). After the location of interest, soil condition, annual probability of exceedance, and the desired intensity measurement were specified in the command file, PSHA produced the seismic hazard curve, the UHS and the disaggregation. A ground motion selection and scaling tool developed in the study by Tesfamariam et al. (2023), which is based on SHM6 and NBCC 2020, was utilized. The input for this tool includes the return period, the required number of ground motions, an anchoring period (T_1) (i.e., the buildings' fundamental period) and the period range for matching spectral values. The number of records for each tectonic regime is proportional to its relative contribution to the regional seismic hazard based on seismic disaggregation results (Table 4-4) and should contain at least 11 records according to Method B in Appendix J of the NBCC 2015 Commentary (NRCC, 2015). Records for subduction were selected from the KiK-net database (Okada et al. 2004), and the PEER NGA West-2 database (Ancheta et al., 2014) was used for crustal and in-slab records. The matching period is bounded by (T_{min}, T_{max}) (Table 4-4). The upper limit T_{max} is the maximum of 1.5 s and $2T_1$. T_{min} is taken as the minimum of $0.15T_1$ and $T_{90\%}$, which is the lowest period of vibration achieving a cumulative mass participation greater than 90% (NRCC, 2015) and is based on modal analysis of prototype buildings. $R_{JB} > 20km$ was imposed to prevent selection of near-field records, and the scaling factor limit was between 0.5 and 5. In total, 40 pairs of horizontal ground motion components were selected for each prototype building, resulting in 80 records, which were used for IDA. The selected records and target spectrum for each type of earthquake are presented in Figure 4-14. The agreement between the target and achieved mean and covariance of the three conditional spectra (Figure 4-14) demonstrates the acceptability of the ground motion selection process.

Table 4-4. Ground motion selection based on relative contribution to seismic hazard.

Prototype building	Sa(T₁) 2% 50 years	No. of Crustal records	No. of Interface record	No. of In-slab record	T_{min} (s)	T_{max} (s)
3-storey	0.96	16	11	53	0.05	1.50
6-storey	0.64	25	18	37	0.11	1.50
9-storey	0.39	34	27	20	0.20	2.70
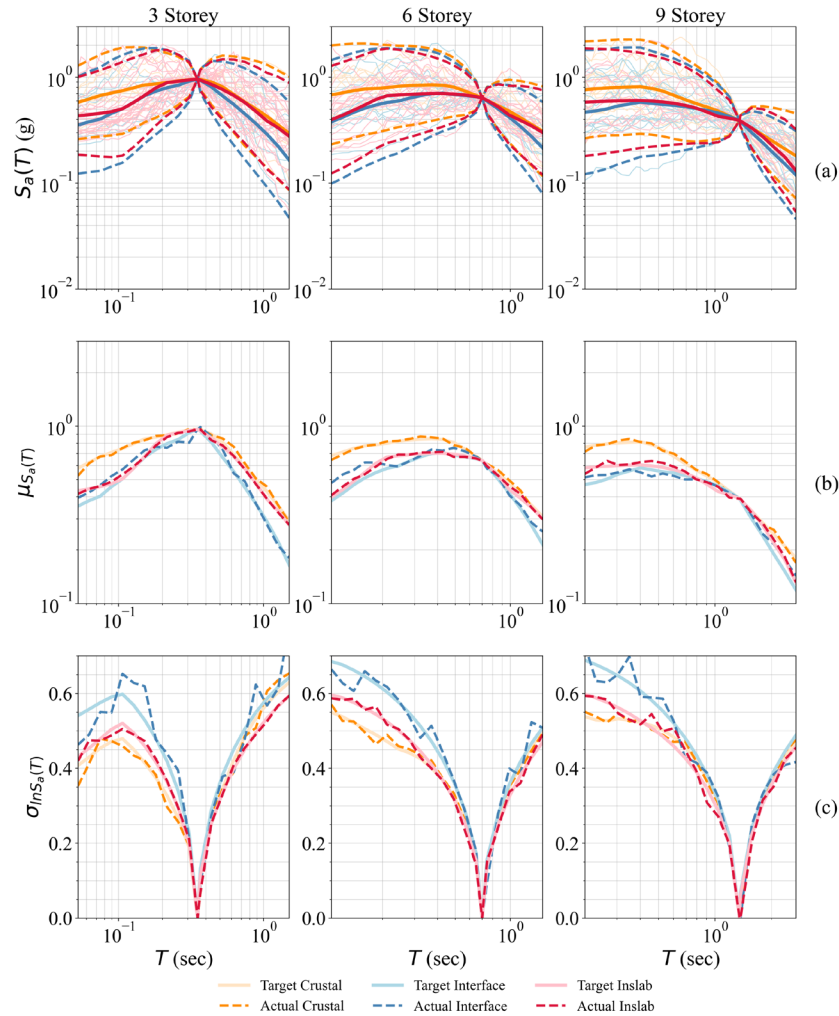
Figure 4-14. Scaled records for each prototype building: (a) pseudo-response spectra of individual records; (b) target and achieved conditional means (c) target and achieved covariances for the conditional spectra.

4.7.4 Incremental Dynamic Analysis and Collapse Fragility Assessment

IDA was performed to assess the building's fragility by scaling up each ground motion record until any one of the considered simulated and non-simulated collapse criteria was triggered (i.e., the occurrence of building collapse) (Vamvatsikos and Cornell, 2002). To enhance computational efficiency, the *hunt and fill algorithm* was used. Figure 4-15 presents the IDA results with 16%, 50%, and 84% statistics.
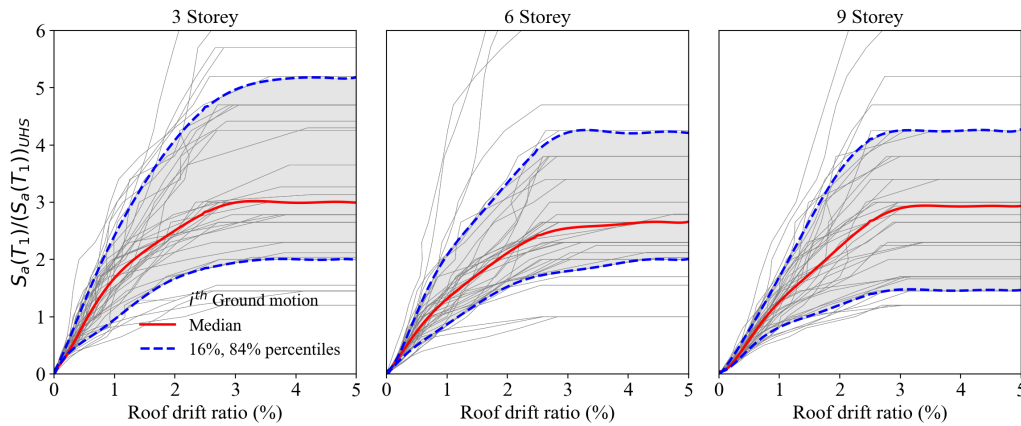
Figure 4-15. Incremental dynamic analyses results for the three analyzed buildings.

Fragility assessment was carried out based on the IDA results by fitting the building collapse at each intensity measurement level to a lognormal distribution (Figure 4-16). The CMR, which is the ratio spectral acceleration resulting in 50% collapse of a building and the spectral acceleration at the MCE level, was quantified based on IDA results. For 3-, 6-, and 9- storey prototype buildings, the CMR values are 3.4, 3.12, and 2.71. Note that FEMA P695 (FEMA, 2009) further suggests applying the spectral shape factor (SSF) to obtain the adjusted CMR (ACMR), which accounts for the bias introduced by the spectral shape of the ground motion suite. However, the SSF for the ground motion suite in this study was not available, and applying the SSF would have lowered the collapse probability (Kovacs and Wiebe, 2019). Therefore, the ACMR for each building prototype was assumed to be conservatively the same as the CMR.

To check the CMR again for acceptable values, the total system collapse uncertainty, β_{tot}, must be examined and incorporated. It accounts for uncertainty in ground motion record variability, system design requirements, test data, and numerical modelling. Given the prescribed upper limit in FEMA P695 (FEMA, 2009), β_{RTR} was assumed equal to 0.4. The design for all building prototypes considered only a heavy floor system with concrete topping, omitting the possibility of a short-period building design scenario. Therefore, β_{DR} was assumed to be 0.35 (fair). β_{MDL} and β_{TD} were both 0.1 (superior) because numerical calibration from this study demonstrated that the fibre-based model could capture well the structural response of the PT-CLT wall system with UFPs. A final system collapse uncertainty of 0.57 was used. The adjusted collapse fragility curves are also included in Figure 4-16. The calculated ACMR for each prototype building exceeds the suggested threshold specified in FEMA P695 (ACMR 10% = 2.09) determined based on a collapse probability of 10% and a total system collapse uncertainty β_{tot} = 0.57. In addition, the collapse probability at MCE for all prototype buildings is significantly lower than the 10% upper limit prescribed by FEMA P695 (FEMA, 2009).

Figure 4-16 presents drift of exceedance (DoE) fragilities for each prototype building related to three POs. The figure also included a DoE fragility of 2.5% ISDR as collapse prevention criteria outlined in NBCC, identified as CP-NBCC, distinguished from the CP PO proposed in Wichman (2023), denoted as CP-W. At 100% MCE, the probabilities of exceeding CP-NBCC are 1.6%, 4.6%, and 5% for 3-, 6-, and 9-storey prototype buildings. Yang et al. (2022), when assessing the seismic performance of balloon-type CLT rocking shear walls, proposed a maximum limit on the number of ground motions (i.e., 10%) that cause 2.5% ISDR or more at MCE. Given that the rates of exceeding such a threshold are below 10% for all cases, the performance can be considered satisfactory. Furthermore, the probability of exceeding the 3% ISDR associated with CP-W for the 3-, 6-, and 9-storey prototype buildings were 1.2 %, 2%, and 4.5%, respectively. These probabilities underscore that the designed structures met the seismic PO under MCE events and PT-CLT walls have the potential to be applied in high seismic-risk zones as primary SFRS.
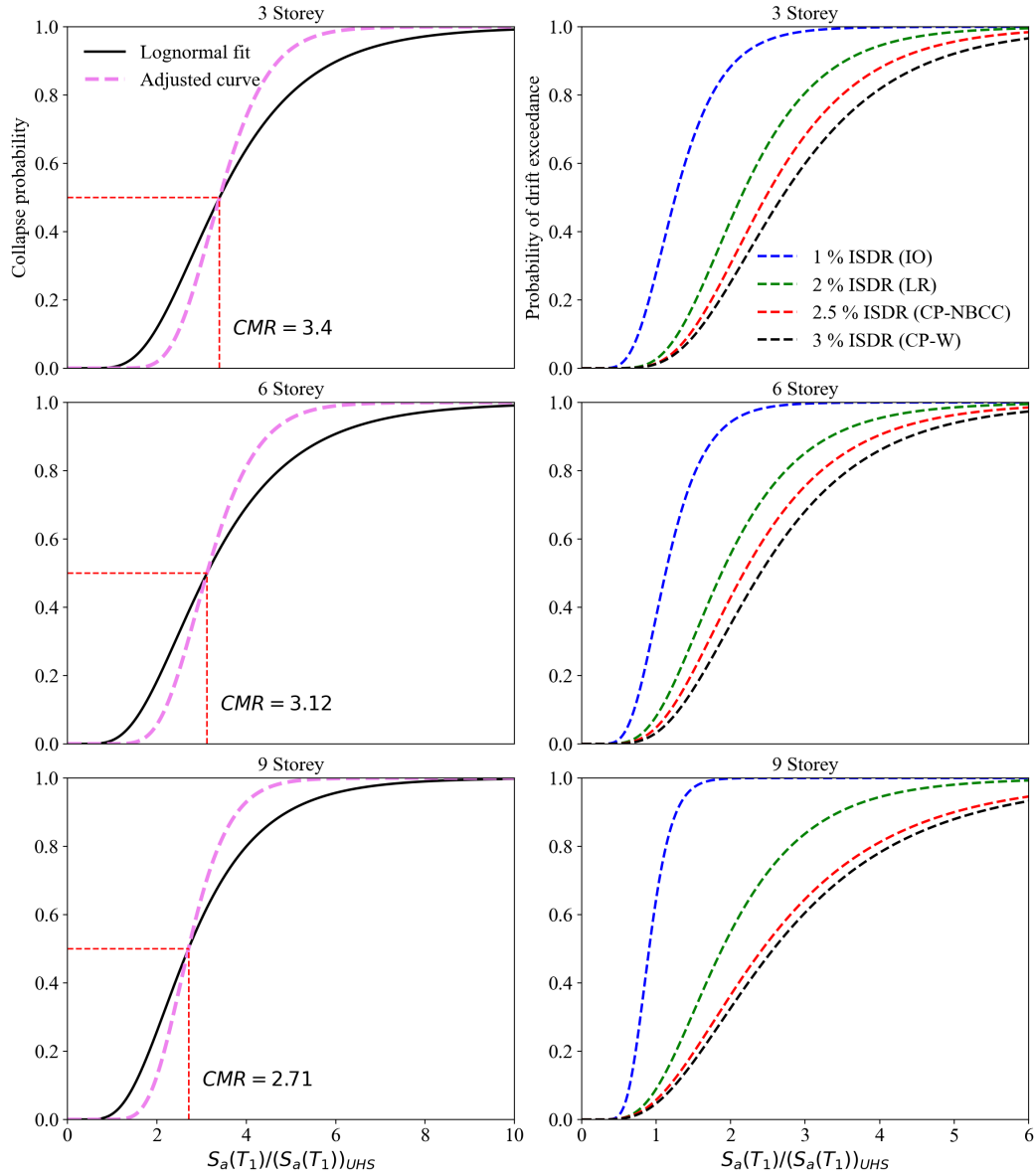
Figure 4-16. Collapse fragilities (left) and fragilities for drift of exceedance (right).

4.8 Summary and Conclusion

In this study, 3-, 6-, and 9-storey mass timber buildings with PT-CLT shear walls coupled with UFPs were designed and their seismic performance was examined. The DDBD approach was applied to design the prototype buildings for the seismicity of Vancouver (metropolitan city in Southwestern British Columbia, Canada), where three tectonic regimes coexist and increased

seismic hazard resulted from the adoption of SHM6 in NBCC 2020. Two-dimensional fibre-based numerical models were developed in *OpenSeesPy* and validated to perform NLSA, NLRHA and IDA. To perform collapse fragility assessment, IDA was conducted using 80 ground motions that were selected for each building and scaled to each seismotectonic regime's CS. The following conclusions can be drawn from this study:

- The 2D fibre-based numerical models were proven to be robust. Validations using full-scale quasi-static and shaking table experimental tests revealed their capability in capturing the response of PT-CLT walls with UFPs.

- NLSA indicated that satisfactory structural performance of the prototype buildings. According to NLSA results, for 3- and 6-storey buildings, the incipient crushing of CLT occurred at 3% roof drift and for 9-storey buildings, at 2.4%. Since the DDBD approach considered 2% roof drift as the design target under the MCE event, satisfactory structural performance of the prototype building can be demonstrated as damages due to CLT crushing can be effectively limited.

- The NLRHA results indicate that the DDBD method resulted in designs that met the design target (2% roof drift) at the MCE level. Moreover, none of the ground motions resulted in an ISDR surpassing the 2.5% limit from NBCC 2020 for the 3-storey building. For the 6-storey and 9-storey buildings, only one instance out of 33 led to exceeding this limit.

- From IDA, the CMRs for the 3-, 6-, and 9-storey buildings were 3.4, 3.12, and 2.71, respectively. All values are considered satisfactory compared to the suggested threshold specified in FEMA P695. Based on fragility analysis, the collapse probabilities for all buildings were significantly lower than 10% under MCE. The probabilities of exceeding the CP-NBCC for the 3-, 6-, and 9-storey buildings were 1.6%, 4.6%, and 5% respectively, and were 1.2 %, 2%, and 4.5% for CP-W. Overall, the studied PT-CLT shear wall buildings exhibited good seismic performance and have the potential for application in Canada's high seismic-risk zones as a primary SFRS.

Chapter 5 CONCLUSION

In this thesis work, seismic performance assessment of PT-CLT shear wall buildings was carried out in high seismic zones in Canada. Fibre-based numerical modelling strategies were adopted and proven to be robust based on validation with system-level quasi-static reversed cyclic and building-level shaking table testing. Initially, prototype buildings of various numbers of storeys with either BRAFs or UFPs as EDDs were designed using the DDBD approach. Employing ensembles of ground motion considering the increased seismic hazard and complex seismotectonics of the City of Vancouver in Southwestern BC, NLRHA were carried out to validate the DDBD design approach and examine the performance of the prototype buildings. From various building performance indicators and collapse probabilities, PT-CLT shear wall buildings exhibited promising potential for adoption in high seismic regions in Canada. For each portion of the analyses described above, key findings are discussed in the following Section. Recommendations are also presented for future work.

5.1 Research Findings

In Chapters 3 and 4, an effective fibre-based numerical modelling strategy was explored, developed, and validated. The key findings are summarised below.

- The 2D fibre-based models were proven to be robust in capturing and predicting the cyclic and dynamic behaviour of PT-CLT shear walls. Validations using full-scale quasi-static cyclic and shaking table experimental tests revealed their capability in capturing the response of PT-CLT walls with EDDs in terms of initial and post-yielding stiffness and of energy dissipation.

- The fibre-based model can be easily modified to incorporate the foundation flexibility effect resulting from either foundation yielding or soil-structure interaction, as evidenced from validation with shaking table testing of a two-storey PT-CLT shear wall building.

- The fibre-based model captures cumulative damage at CLT compressive edges and cyclic responses of PT elements, as well as the gradual shifting of the neutral axis position. This can be significant for PT-CLT walls because CLT panels and PT elements are capacity-protected components in the system. Damage to them is usually associated with different

structural limit states and being able to trace the load or deformation in these elements can facilitate accurate performance assessment and a seismic-resilient design.

In Chapters 3 and 4, prototype buildings with BRAFs and UFPs were designed using DDBD and their seismic performance was examined. The key findings are summarised below.

- From both studies, the adopted DDBD method demonstrated a relative advantage in overcoming the absence of clear R_d and R_o factors for PT-CLT walls in NBCC. The analytical relationships to predict displacement profile and equivalent viscous damping for PT-LVL walls can be adopted for PT-CLT walls. Using ensembles of ground motion scaled to the uniform hazard spectrum, NLRHA results indicated that the DDBD method produced designs that meet the design target (2% roof drift) and the 2.5% ISDR limits of the NBCC.

- For PT-CLT shear wall buildings with BRAFs, the mean roof drifts for 6-, 9-, and 12-storey buildings were 0.74%, 1.03%, and 1.53%, and the drift response increased with building height. Therefore, it is suggested that PT-CLT wall buildings taller than 12 storeys should incorporate mechanisms to control drift. The IDA results revealed that PT-CLT walls with BRAFs possess distinct strain-hardening effects at increased scaling factors. The ACMRs for all prototype buildings were considered satisfactory compared to the suggested threshold specified in FEMA P695. Based on fragility analysis, it is concluded that all buildings performed well in terms of collapse prevention limit state, as the collapse probabilities at MCE for all buildings were significantly lower than 10%.

- For PT-CLT shear wall buildings with UFPs, NLSA indicated that at the design target (2% roof drift ratio prescribed in DDBD), buildings were unlikely to be damaged due to CLT crushing. From IDA, sufficient collapse margin ratios were identified compared to the acceptable limit in FEMA P695. Based on fragility analysis, the collapse probabilities for all buildings were significantly lower than 10% under MCE.

- Overall, the studied PT-CLT shear wall buildings exhibited good seismic performance and have potential for application in Canada's high seismic-risk zones as a primary SFRS.

5.2 Recommendation for Future Research

Based on the research outcome, the following recommendations for future studies are proposed.

- **Development of Canadian seismic force modification factors**. Currently, PT-CLT shear wall buildings can be designed in Canada only as alternative solutions due to the absence of the overstrength-related factor (R_o) and the ductility-related factor (R_d). To facilitate the practical adoption of PT-CLT walls as SFRSs in Canada, future study should aim to determine the R_o and R_d factors for PT-CLT walls following either the FEMA P695 or the Canadian Performance-based Unified (PBU) procedures.

- **Further CLT testing to derive a material-specific constitutive law.** In seismic performance assessment of PT-CLT shear wall buildings, damage to CLT (yielding, splitting, and crushing) is a critical performance indicator. Hence, being able to accurately model the progressive strength and stiffness degradation of CLT is important. This can be achieved by adopting higher-order modelling and a representative constitutive law for CLT. As indicated in Chapter 2, development of a unified material model for CLT is a developing research topic. Most existing nonlinear modeling approaches for CLT, although based on experimental observations, make several assumptions about post-yielding behaviour of CLT. For instance, the *EPP Gap* material assumes perfectly plastic behaviour after yielding. *Conc01* material assumes perfectly plastic behaviour after CLT crushing. Therefore, it is recommended that future research aim to develop a unified constitutive model for numerical modelling of CLT that can capture yielding, splitting, and crushing of CLT.

- **Multi-hazard design and performance for PT-CLT shear wall buildings.** Although many studies have focused on seismic design of PT-CLT walls, the design and performance assessment of PT-CLT walls under wind loading have not been investigated. This can be vital in regions where wind load governs and for flexible and tall mass timber buildings. In addition, in regions where wind and seismic loads are comparable, a multi-hazard design guideline is required. Hence, future research should develop a wind and multi-hazard design guide for PT-CLT shear wall buildings.

- **Seismic performance assessment using near-field and mainshock-aftershock ground motions**. One of the limitations of this thesis work is that all ground motions adopted for

performance assessment belong to far-field categories. Studies on other type of SFRS demonstrate that pulse-like near-field ground motions can have different impacts on building performance. Furthermore, ground motions with long duration and including aftershock events can have significant effects on the structural collapse mechanism due to cumulative damage. Therefore, future studies should characterize building performance and lateral behaviour under near-field and mainshock-aftershock ground motions.

Chapter 6 BIBLIOGRAPHY

Akbas, T., 2016. *Seismic Response Analysis of Structures with Nonlinear Mechanisms Using a Modal Approach* (Doctoral dissertation). Lehigh University.

Akbas, T., Sause, R., Ricles, J.M., Ganey, R., Berman, J., Loftus, S., Dolan, J.D., Pei, S., van de Lindt, J.W., Blomgren, H.-E., 2017. Analytical and Experimental Lateral-Load Response of Self-Centering Posttensioned CLT Walls. J. Struct. Eng. 143, 04017019. https://doi.org/10.1061/(ASCE)ST.1943-541X.0001733.

Allan B. and Eaton, D., 2024. The Mass Timber Roadmap: an Integrated Forest-to-Buildings Value Chain. The Transition Accelerator.

Amaris Mesa, A.D., 2010. Developments of Advanced Solutions for Seismic Resisting Precast Concrete Frames.

Amer, A., Sause, R., Ricles, J., 2024. Experimental Response and Damage of SC-CLT Shear Walls under Multidirectional Cyclic Lateral Loading. J. Struct. Eng. 150, 04023215. https://doi.org/10.1061/JSENDH.STENG-12576

Ancheta, T.D., Darragh, R.B., Stewart, J.P., Seyhan, E., Silva, W.J., Chiou, B.S.J., Wooddell, K.E., Graves, R.W., Kottke, A.R., Boore, D.M. and Kishida, T., 2014. NGA-West2 Database. Earthquake Spectra, 30(3), pp. 989-1005.

APA., 2017. Standard for Performance-Rated Cross-Laminated Timber. ANSI/APA PRG 320-2017, APA - The Engineered Wood Association, Tacoma, WA, USA.

ASCE. 2016. Minimum Design Loads and Associated Criteria for Buildings and Other Structures. ASCE 7-16. Reston, VA: ASCE.

Assadi, S., Hashemi, A., Quenneville, P., 2023. High-Performance Rocking Timber Wall with Innovative Low-Damage Floor Connections. Structures 57, 105075. https://doi.org/10.1016/j.istruc.2023.105075.

Baird, A., Smith, T., Palermo, A., Pampanin, S. 2014. Experimental and Numerical Study of U-Shaped Flexural Plate (UFP) Dissipators. New Zealand Society for Earthquake Engineering Annual Conference, Auckland, New Zealand.

Baker, J.W., 2011. Conditional Mean Spectrum: Tool for Ground-Motion Selection. J. Struct. Eng. 137, 322–331. https://doi.org/10.1061/(ASCE)ST.1943-541X.0000215

Baker, J.W., Lee, C., 2018. An Improved Algorithm for Selecting Ground Motions to Match a Conditional Spectrum. Journal of Earthquake Engineering 22, 708–723. https://doi.org/10.1080/13632469.2016.1264334.

Barbosa, A.R., Rodrigues, L.G., Sinha, A., Higgins, C., Zimmerman, R.B., Breneman, S., Pei, S., Van De Lindt, J.W., Berman, J., McDonnell, E., 2021. Shake-Table Experimental Testing and Performance of Topped and Untopped Cross-Laminated Timber Diaphragms. J. Struct. Eng. 147, 04021011. https://doi.org/10.1061/(ASCE)ST.1943-541X.0002914

Bezabeh, M.A., Tesfamariam, S., Popovski, M., Goda, K., Stiemer, S.F., 2017. Seismic Base Shear Modification Factors for Timber-Steel Hybrid Structure: Collapse Risk Assessment Approach. J. Struct. Eng. 143, 04017136. https://doi.org/10.1061/(ASCE)ST.1943-541X.0001869.

Black, C.J., Makris, N., Aiken, I.D., 2004. Component Testing, Seismic Evaluation and Characterization of Buckling-Restrained Braces. J. Struct. Eng. 130, 880–894. https://doi.org/10.1061/(ASCE)0733-9445(2004)130:6(880)

British Columbia Building Code (BCBC), 2024. Victoria, BC: King's Printer of British Columbia. Retrieved from: https://www2.gov.bc.ca/assets/download/58703F3809B74A8B8937426AA76736CF

Brown, J.R., Li, M., Palermo, A., Pampanin, S., Sarti, F., Nokes, R., 2022. Experimental Testing and Analytical Modelling of Single and Double Post-Tensioned CLT Shear Walls. Engineering Structures 256, 114065. https://doi.org/10.1016/j.engstruct.2022.114065.

Busch, A., Zimmerman, R.B., Pei, S., McDonnell, E., Line, P., Huang, D., 2022. Prescriptive Seismic Design Procedure for Post-Tensioned Mass Timber Rocking Walls. J. Struct. Eng. 148, 04021289. https://doi.org/10.1061/(ASCE)ST.1943-541X.0003240.

Cabeza, L.F., Q. Bai, P. Bertoldi, J.M. Kihila, A.F.P. Lucena, É. Mata, S. Mirasgedis, A. Novikova, Y. Saheb, 2022: Buildings. In IPCC, 2022: Climate Change 2022: Mitigation of Climate Change. Contribution of Working Group III to the Sixth Assessment Report of the Intergovernmental Panel on Climate Change. Cambridge University Press, Cambridge, UK and New York, NY, USA. doi: 10.1017/9781009157926.011.

Canadian Standards Association (CSA), 2019. Standard CSA 086-19: Engineering Design in Wood. Canadian Standards Association, Mississauga, Canada.

Ceccotti, A., Sandhaas, C., Okabe, M., Yasumura, M., Minowa, C., Kawai, N., 2013. SOFIE project - 3D Shaking Table Test on a Seven-storey Full-Scale Cross-laminated Timber Building: 3D Shaking Table Test on a Seven-Storey Full-Scale X-Lam Building. Earthquake Engng Struct. Dyn. 42, 2003–2021. https://doi.org/10.1002/eqe.2309

Chen, F., Li, M., Li, Z., 2024. Self-centering mass timber structures: A Review on Recent Research Progress. Engineering Structures 303, 117474. https://doi.org/10.1016/j.engstruct.2024.117474

Chen, Z., M. Popovski, and P. Symons. 2018. *Advanced Wood-based Solutions for Mid-rise and High-rise Construction: Structural Performance of Post-tensioned CLT Shear Walls with Energy Dissipators*. Vancouver, BC, Canada: FPInnovations.

Chen, Z., Popovski, M., & Iqbal, A., 2020a. Structural Performance of Post-Tensioned CLT Shear Walls with Energy Dissipators. Journal of Structural Engineering, 146(4), 04020035. https://doi.org/10.1061/(ASCE)ST.1943-541X.0002569.

Chen, Z., Popovski, M., 2020. Mechanics-Based Analytical Models for Balloon-Type Cross-Laminated Timber (CLT) Shear Walls under Lateral Loads. Engineering Structures 208, 109916. https://doi.org/10.1016/j.engstruct.2019.109916.

Chen, Z., Popovski, M., 2020b. Material-Based Models for Post-Tensioned Shear Wall System with Energy Dissipators. Engineering Structures 213, 110543. https://doi.org/10.1016/j.engstruct.2020.110543.

CPCI, 2017. CPCI Design Manual: Precast and Prestressed Concrete.

Daneshvar, H., Niederwestberg, J., Letarte, J.-P., Hei Chui, Y., 2022. Yield Mechanisms of Base Shear Connections for Cross-Laminated Timber Shear Walls. Construction and Building Materials 335, 127498. https:// doi.org/ 10.1016/ j. conbuildmat.2022.127498.

FEMA, 2009. Quantification of Building Seismic Performance Factors. FEMA P-695. Applied Technology Council for the Federal Emergency Management Agency, Washington, DC.

Furley, J., Van De Lindt, J.W., Pei, S., Wichman, S., Hasani, H., Berman, J.W., Ryan, K., Daniel Dolan, J., Zimmerman, R.B., McDonnell, E., 2021. Time-to-Functionality Fragilities for Performance Assessment of Buildings. J. Struct. Eng. 147, 04021217. https://doi.org/10.1061/(ASCE)ST.1943-541X.0003195.

Ganey, R., Berman, J., Akbas, T., Loftus, S., Daniel Dolan, J., Sause, R., Ricles, J., Pei, S., Lindt, J. van de, & Blomgren, H.-E., 2017. Experimental Investigation of Self-Centering Cross-Laminated Timber Walls. Journal of Structural Engineering, 143(10), 04017135. https:// doi.org/ 10.1061/ (ASCE)ST. 1943-541X.0001877.

Ganey, R.S., 2015. *Seismic Design and Testing of Rocking Cross Laminated Timber Walls* (Master's Thesis). University of Washington.

Gavric, I., Fragiacomo, M., Ceccotti, A., 2015. Cyclic Behaviour of Typical Metal Connectors for Cross-Laminated (CLT) Structures. Mater. Struct. 48, 1841–1857. https://doi.org/10.1617/s11527-014-0278-7.

Goda, K., 2019. Nationwide Earthquake Risk Model for Wood-Frame Houses in Canada. Front. Built Environ. 5, 128. https://doi.org/10.3389/fbuil.2019.00128.

Granello, G., Palermo, A., Pampanin, S., Pei, S., Van De Lindt, J., 2020. Pres-Lam Buildings: State-of-the-Art. J. Struct. Eng. 146, 04020085. https:// doi.org/ 10.1061/ (ASCE)ST.1943-541X.0002603.

Hashemi, A., Bagheri, H., Yousef-Beik, S.M.M., Darani, F.M., Valadbeigi, A., Zarnani, P., Quenneville, P., 2020. Enhanced Seismic Performance of Timber Structures Using Resilient Connections: Full-Scale Testing and Design Procedure. J. Struct. Eng. 146, 04020180. https://doi.org/10.1061/(ASCE)ST.1943-541X.0002749.

Hayes, B.N., Koliou, M., Van De Lindt, J.W., 2023. Seismic Behavior of Balloon Frame Cross-Laminated Timber Connections. J. Struct. Eng. 149, 04023115. https://doi.org/10.1061/JSENDH.STENG-11984.

Ho, T.X., Uarac, P., Barbosa, A.R., Sinha, A., Simpson, B., A. Araújo, G., F. Orozco, G., 2023. Evaluation of Seismic Performance Factors and Fragility Functions for Post-Tensioned Mass Ply Panel Rocking Walls. Presented at the World Conference on Timber Engineering 2023 (WCTE2023). Oslo, Norway, pp. 2562–2569. https://doi.org/10.52202/069179-0337

Holden, T., Devereux, C., Haydon, S., Buchanan, A., Pampanin, S., 2016. NMIT Arts & Media Building—Innovative Structural Design of a Three Storey Post-Tensioned Timber Building. Case Studies in Structural Engineering 6, 76–83. https://doi.org/10.1016/j.csse.2016.06.003

Hossain, K., Aaleti, S., Dao, T.N., 2021. Experimental Investigation and Finite-Element Modeling of an Aluminum Energy Dissipater for Cross-Laminated Timber Walls under Reverse Cyclic Loading. J. Struct. Eng. 147, 04021025. https://doi.org/10.1061/(ASCE)ST.1943-541X.0002978

ICC (International Code council). 2020. *International Building Code, 2021*, 2021 edition. International Code Council, Country Club Hills, IL.

Iqbal, A., Pampanin, S., Buchanan, A.H., Palermo, A., 2007. Improved Seismic Performance of LVL Post-Tensioned Walls Coupled with UFP devices. In 8th Pacific Conference on Earthquake Engineering, Singapore.

Iqbal, A., Pampanin, S., Palermo, A., Buchanan, A.H., 2015. Performance and Design of LVL Walls Coupled with UFP Dissipaters. Journal of Earthquake Engineering 19, 383–409. https://doi.org/10.1080/13632469.2014.987406.

Karacabeyli, E., Lum, C. (Eds.), 2022. Technical Guide for the Design and Construction of Tall Wood Buildings in Canada, Second edition. ed. FPInnovations, Pointe-Claire, QC.

Kelly, J.M., Skinner, R.I., Heine, A.J., 1972. Mechanisms of Energy Absorption in Special Devices for Use in Earthquake-Resistant Structures. BNZSEE 5, 63–88. https://doi.org/10.5459/bnzsee.5.3.63-88.

Kishida, T., Contreras, V., Bozorgnia, Y., Abrahamson, N.A., Ahdi, S.K., Ancheta, T.D., Boore, D.M., Campbell, K.W., Chiou, B., Darragh, R. and Gregor, N., 2018. *NGA-Sub Ground Motion Database*. In *11th National Conference in Earthquake Engineering*, Earthquake Engineering Research Institute, Los Angeles, CA. 2018.

Kolaj, M., Adams, J., Halchuk, S., 2020a. The 6th Generation Seismic Hazard Model of Canada. In *17th World Conference on Earthquake Engineering*, (pp. 1-12).

Kolaj, M., Halchuk, S., Adams, J., & Allen, T. I., 2020b. Sixth Generation Seismic Hazard Model of Canada: Input Files to Produce Values Proposed for the 2020 National Building Code of Canada (No. 8630; p. 8630). https:// doi.org/ 10.4095/327322.

Kovacs, M.A., Wiebe, L., 2019. Controlled Rocking CLT Walls for Buildings in Regions of Moderate Seismicity: Design Procedure and Numerical Collapse Assessment. Journal of Earthquake Engineering 23, 750–770. https://doi.org/10.1080/13632469.2017.1326421

Kramer, A., Barbosa, A.R., Sinha, A., 2016. Performance of Steel Energy Dissipators Connected to Cross-Laminated Timber Wall Panels Subjected to Tension and Cyclic Loading. J. Struct. Eng. 142, E4015013. https:// doi.org/ 10.1061/(ASCE)ST.1943-541X.0001410.

Lepine-Lacroix, S., Yang, T.Y., 2023. Seismic Design and Performance Evaluation of Novel Dual-Pinned Self-Centering Coupled CLT Shear Walls. Engineering Structures 279, 115547. https://doi.org/10.1016/j.engstruct.2022.115547.

Marriott, D.J., 2009. *The Development of High-Performance Post-Tensioned Rocking Systems for the Seismic Design of Structures*. (Doctoral Thesis). University of Canterbury. https://doi.org/10.26021/2391.

Massari, M., Savoia, M. and Barbosa, A.R., 2017. Experimental and Numerical Study of Two-Storey Post-Tensioned Seismic Resisting CLT Wall with External Hysteretic Energy Dissipaters. Atti del XVII Convegno ANIDIS L'ingegneria Sismica in Italia: Pistoia, 17-21 settembre 2017.-(Studi in tema di internet ecosystem), pp.72-82.

Meta, B., 2024. Ontario Expanding Mass Timber Construction Up to 18 Storeys. URL https://news.ontario.ca/en/release/1004272/ontario-expanding-mass-timber-construction-up-to-18-storeys

Mitchell, D., Paultre, P., 1994. Ductility and Overstrength in Seismic Design of Reinforced Concrete Structures. Can. J. Civ. Eng. 21, 1049–1060. https://doi.org/10.1139/l94-109

Mojiri, S., Mortazavi, P., Kwon, O., Christopoulos, C., 2021. Seismic Response Evaluation of a Five-Storey Buckling-Restrained Braced Frame Using Multi-Element Pseudo-Dynamic Hybrid Simulations. Earthq Engng Struct Dyn 50, 3243–3265. https://doi.org/10.1002/eqe.3508

Mugabo, I., Barbosa, A.R., Sinha, A., Higgins, C., Riggio, M., Pei, S., Van De Lindt, J.W., Berman, J.W., 2021. System Identification of UCSD-NHERI Shake-Table Test of Two-Storey Structure with Cross-Laminated Timber Rocking Walls. J. Struct. Eng. 147, 04021018. https://doi.org/10.1061/(ASCE)ST.1943-541X.0002938

National Research Council of Canada (NRCC). 2010. *National Building Code of Canada 2010*. Canada Commission on Building and Fire Code, Ottawa, Canada.

National Research Council of Canada (NRCC). 2015. *National Building Code of Canada 2015*. Canada Commission on Building and Fire Code, Ottawa, Canada.

National Research Council of Canada (NRCC). 2020. National Building Code of Canada 2020. Canada Commission on Building and Fire Code, Ottawa, Canada.

Natural Resources Canada (NRC) & Canadian Forest Service (CFS). 2021. The State of Mass Timber in Canada. Ottawa. 54 p.

Newcombe, M.P., 2011. *Seismic Design of Post-Tensioned Timber Frame and Wall Buildings*. (Doctoral dissertation). University of Canterbury. https://doi.org/10.26021/2808

Newcombe, M.P., Pampanin, S., Buchanan, A., Palermo, A., 2008. Section Analysis and Cyclic Behavior of Post-Tensioned Jointed Ductile Connections for Multi-Storey Timber Buildings. Journal of Earthquake Engineering 12, 83–110. https://doi.org/10.1080/13632460801925632

NRCC-CRC, 2022. Platform to Decarbonize the Construction Sector at Scale. National Research Council of Canada (NRCC). Construction Research Centre. https://publications.gc.ca/collections/collection_2023/cnrc-nrc/NR16-413-2022-eng.pdf.

Odikamnoro, I., Badal, P.S., Burton, H., Tesfamariam, S., 2022. Seismic Collapse Risk of RC-Timber Hybrid Building with Different Energy Dissipation Connections Considering NBCC 2020 Hazard. J Infrastruct Preserv Resil 3, 14. https://doi.org/10.1186/s43065-022-00061-6.

Okada, Y., Kasahara, K., Hori, S., Obara, K., Sekiguchi, S., Fujiwara, H., and Yamamoto, A. (2004). Recent Progress of Seismic Observation Networks in Japan—Hi-net, F-net, K-NET and KiK-net. Earth, Planets and Space, 56(8):xv– xxviii.

Pagani, M., Monelli, D., Weatherill, G., Danciu, L., Crowley, H., Silva, V., Henshaw, P., Butler, L., Nastasi, M., Panzeri, L., Simionato, M., Vigano, D., 2014. OpenQuake Engine: An Open Hazard (and Risk) Software for the Global Earthquake Model. Seismological Research Letters 85, 692–702. https://doi.org/10.1785/0220130087.

Palermo, A., Pampanin, S., Buchanan, A., and Newcombe, M. 2005. Seismic Design of Multi-Storey Buildings Using Laminated Veneer Lumber (LVL). In NZ Society of Earthquake Engineering, Annual National Conference, Wairakei, New Zealand.

Pampanin, S., Ciurlanti, J., Bianchi, S., Perrone, D., Granello, G., Palmieri, M., Grant, D.N., Palermo, A., Costa, A.C., Candeias, P.X., Correia, A.A., 2023. Triaxial shake table testing of an integrated low-damage building system. Earthq Engng Struct Dyn 52, 2983–3007. https://doi.org/10.1002/eqe.3906

Pampanin, S., Nigel Priestley, M.J., Sritharan, S., 2001. Analytical Modelling of the Seismic Behaviour of Precast Concrete Frames Designed with Ductile Connections. Journal of Earthquake Engineering 5, 329–367. https://doi.org/10.1080/13632460109350397.

Pampanin, S., Palermo, A., Buchanan, A., 2013. Post-Tensioned Timber Buildings—Part 2: Seismic Design. *Christchurch, New Zealand: Structural Timber Innovation Company.*

Pei, S., 2017, April. Development and Full-Scale Validation of Resilience-Based Seismic Design of Tall Wood Buildings: the NHERI Tallwood Project. In *NZ Society of Earthquake Engineering*, Annual National Conference, Wellington, New Zealand.

Pei, S., Van de Lindt, J. W., Barbosa, A. R., Berman, J. W., McDonnell, E., Daniel Dolan, J., Blomgren, H.-E., Zimmerman, R. B., Huang, D., & Wichman, S., 2019. Experimental Seismic Response of a Resilient 2-Storey Mass-Timber Building with Post-Tensioned Rocking Walls. Journal of Structural Engineering, 145(11), 04019120. https://doi.org/10.1061/(ASCE)ST.1943-541X.0002382.

Pei, S., Van De Lindt, J.W., Berman, J., Ryan, K., Dolan, J.D., Pryor, S., Wichman, S., Busch, A., Zimmerman, R., 2023. Full-scale 3-D Shake Table Test of a Ten-Storey Mass Timber Building. *In World Conference on Timber Engineering*, Oslo, Norway, pp. 2084–2089. https://doi.org/10.52202/069179-0276.

Pei, S., Van De Lindt, J.W., Popovski, M., 2013. Approximate R-Factor for Cross-Laminated Timber Walls in Multistorey Buildings. J. Archit. Eng. 19, 245–255. https://doi.org/10.1061/(ASCE)AE.1943-5568.0000117

Pennucci, D., Calvi, G.M., Sullivan, T.J., 2009. Displacement-Based Design of Precast Walls with Additional Dampers. Journal of Earthquake Engineering 13, 40–65. https://doi.org/10.1080/13632460902813265.

Pilon, D.S., Palermo, A., Sarti, F., Salenikovich, A., 2019. Benefits of Multiple Rocking Segments for CLT and LVL Pres-Lam Wall Systems. Soil Dynamics and Earthquake Engineering 117, 234–244. https:// doi.org/ 10.1016/ j.soildyn. 2018. 11. 026.

Popovski, M., Eng, P., Bagheri, M., Chen, E.Z. and Ni, C., 2021. Expanding Wood Use Towards 2025: Increased Seismic Loads in the 2020 National Building Code.

Pozza, L., Benedetti, L., Tomei, V., Ferracuti, B., Zucconi, M., Mazzotti, C., 2021. Cyclic Response of CLT Post-Tensioned Walls: Experimental and Numerical Investigation. Construction and Building Materials 308, 125019. https://doi.org/10.1016/j.conbuildmat.2021.125019.

Priestley, M.J.N., 1991. Overview of PRESSS Research Program. PCIJ 36, 50–57. https://doi.org/10.15554/pcij.07011991.50.57.

Priestley, M.J.N., Calvi, G.M., Kowalsky, M.J., 2007. Displacement-Based Seismic Design of Structures. IUSS Press: Distributed by Fondazione EUCENTRE, Pavia, Italy.

Priestley, M.J.N., Sritharan, S. (Sri), Conley, J.R., Stefano Pampanin, S., 1999. Preliminary Results and Conclusions from the PRESSS Five-Storey Precast Concrete Test Building. pcij 44, 42–67. https://doi.org/10.15554/pcij.11011999.42.67.

Qureshi, I., Acuña, G., Dolan, D., 2023. Development of a Numerical Model to Consider the Foundation Flexibility Effects in CLT Rocking Walls. *In World Conference on Timber Engineering*, Oslo, Norway, pp. 2627–2632. https://doi.org/10.52202/069179-0345.

Rahmzadeh, A. and Iqbal, A., 2018. Study of Replaceable Energy Dissipators for Self-Centering Structures. *In Eleventh US National Conference on Earthquake Engineering, Integrating Science, Engineering & Policy.*

Sabelli, R., Mahin, S., Chang, C., 2003. Seismic Demands on Steel Braced Frame Buildings with Buckling-Restrained Braces. Engineering Structures 25, 655–666. https://doi.org/10.1016/S0141-0296(02)00175-X

Sarti, F., 2015. *Seismic Design of Low-Damage Post-Tensioned Timber Wall Systems*. (Doctoral dissertation). University of Canterbury.

Sarti, F., Palermo, A., Pampanin, S., 2015. Comparison of Force-Based and Displacement-Based Seismic Design of Dissipative Post-Tensioned Rocking Timber Wall Systems. In *NZ Society of Earthquake Engineering*, Annual National Conference, Rotorua, New Zealand

Sarti, F., Palermo, A., Pampanin, S., 2016a. Development and Testing of an Alternative Dissipative Posttensioned Rocking Timber Wall with Boundary Columns. J. Struct. Eng. 142, E4015011. https://doi.org/10.1061/(ASCE)ST.1943-541X.0001390

Sarti, F., Palermo, A., Pampanin, S., 2016a. Quasi-Static Cyclic Testing of Two-Thirds Scale Unbonded Posttensioned Rocking Dissipative Timber Walls. J. Struct. Eng. 142, E4015005. https://doi.org/10.1061/(ASCE)ST.1943-541X.0001291.

Sarti, F., Palermo, A., Pampanin, S., Berman, J., 2017. Determination of the Seismic Performance Factors for Post-Tensioned Rocking Timber Wall Systems: Seismic Performance Factors for Post-Tensioned Timber Wall Systems. Earthquake Engng Struct. Dyn. 46, 181–200. https://doi.org/10.1002/eqe.2784.

Sarti, F., Palermo, A., Pampanin, S., Carradine, D., 2013. Experimental and Analytical Study of Replaceable Buckling-Restrained Fused-type (BRF) Mild Steel Dissipaters. New Zealand Society for Earthquake Engineering Annual Conference, Wellington, New Zealand.

Shahnewaz, M., Dickof, C., Tannert, T., 2021. Seismic Behavior of Balloon Frame CLT Shear Walls with Different Ledgers. J. Struct. Eng. 147, 04021137. https://doi.org/10.1061/(ASCE)ST.1943-541X.0003106

Skinner, R.I., Kelly, J.M., Heine, A.J., 1974. Hysteretic Dampers for Earthquake-Resistant Structures. Earthquake Engng. Struct. Dyn. 3, 287–296. https://doi.org/10.1002/eqe.4290030307

Slotboom, C., 2020. *Numerical Analysis of Self-Centring Cross-Laminated Timber Walls.* (Master's thesis). University of British Columbia. https://doi.org/10.14288/1.0392505.

Smith, T., 2014. *Post-tensioned Timber Frames with Supplemental Damping Devices.* (Doctoral dissertation). University of Canterbury. https://doi.org/10.26021/2400.

Smith, T., Ludwig, F., Pampanin, S., Fragiacomo, M., Buchanan, A., Deam, B., and Palermo, A., 2007. Seismic Response of Hybrid-LVL Coupled Walls under Quasi-Static and Pseudo-Dynamic Testing. In NZ Society of Earthquake Engineering, Annual National Conference, Palmerston North, New Zealand.

Structurlam, 2021. Structurlam Mass Timber Technical Guide for Cross Lam® clt and Glulamplus®, Canadian Version.

Sun, X., He, M., Li, Z., 2020. Experimental and Analytical Lateral Performance of Posttensioned CLT Shear Walls and Conventional CLT Shear Walls. J. Struct. Eng. 146, 04020091. https://doi.org/10.1061/(ASCE)ST.1943-541X.0002638

Sun, X., He, M., Li, Z., Lam, F., 2019. Seismic Performance Assessment of Conventional CLT Shear Wall Structures and Post-Tensioned CLT Shear Wall Structures. Engineering Structures 196, 109285. https:// doi.org/ 10.1016/ j. ngstruct. 2019.109285.

Sun, X., He, M., Li, Z., Lam, F., 2020. Seismic performance of energy-dissipating post-tensioned CLT shear wall structures I: Shear wall modeling and design procedure. Soil Dynamics and Earthquake Engineering 131, 106022. https://doi.org/10.1016/j.soildyn.2019.106022

Tesfamariam, S., Badal, P.S., & Goda, K., 2023. Seismic Hazard and Ground Motion Selection for Response History Analysis Based on the National Building Code of Canada 2020. UBC Faculty Research and Publications. https://dx.doi.org/10.14288/1.0431445.

Teweldebrhan, B.T., Popovski, M., McFadden, J.B.W., Tesfamariam, S., 2023. Development of ductility-related modification factor for CLT-coupled wall buildings with replaceable shear link coupling beams. Can. J. Civ. Eng. 50, 362–374. https://doi.org/10.1139/cjce-2022-0257

Tomei, V., Zucconi, M., Ferracuti, B., 2023. Post-Tensioned Rocking Dissipative Timber Wall Systems: Numerical Prediction. Journal of Building Engineering 66, 105897. https://doi.org/10.1016/j.jobe.2023.105897.

Vamvatsikos, D., Cornell, C.A., 2002. Incremental Dynamic Analysis. Earthquake Engng. Struct. Dyn. 31, 491–514. https://doi.org/10.1002/eqe.141.

Wichman, S., 2018. *Large-Scale Dynamic Testing of Rocking Cross Laminated Timber Walls* (Master's dissertation). University of Washington.

Wichman, S., 2023. *Seismic Behavior of Tall Rocking Mass Timber Walls* (Doctoral dissertation). University of Washington.

Wichman, S., Berman, J.W., Pei, S., 2022. Experimental Investigation and Numerical Modeling of Rocking Cross Laminated Timber Walls on a Flexible Foundation. Earthq. Engng. Struct Dyn 51, 1697–1717. https://doi.org/10.1002/eqe.3634.

Wilson, A.W., Motter, C.J., Phillips, A.R., Dolan, J.D., 2019. Modeling Techniques for Post-Tensioned Cross-Laminated Timber Rocking Walls. Engineering Structures 195, 299–308. https://doi.org/10.1016/j.engstruct.2019.06.011.

Wilson, A.W., Motter, C.J., Phillips, A.R., Dolan, J.D., 2020. Seismic Response of Post-Tensioned Cross-Laminated Timber Rocking Wall Buildings. J. Struct. Eng. 146, 04020123. https://doi.org/10.1061/(ASCE)ST.1943-541X.0002673.

Xing, D., Casagrande, D., Doudak, G., 2023. Investigating the Deformation Characteristics of Balloon-Type CLT Shear Wall. Can. J. Civ. Eng. cjce-2023-0233. https://doi.org/10.1139/cjce-2023-0233.

Yang, T.Y., Lepine-Lacroix, S., Guerrero, J.A.R., McFadden, J.B.W., Al-Janabi, M.A.Q., 2022. Seismic Performance Evaluation of Innovative Balloon Type CLT Rocking Shear Walls. Resilient Cities and Structures 1, 44–52. https://doi.org/10.1016/j.rcns.2022.03.004.

Zhu, H., Bezabeh, M., Iqbal, A., Popovski, M., Chen, Z., 2024. Seismic Performance Assessment of Post-Tensioned CLT Shear Wall Buildings with Buckling-Restrained Axial Fuses. Can. J. Civ. Eng. cjce-2023-0448. https://doi.org/10.1139/cjce-2023-0448.

Zhu, M., McKenna, F., Scott, M.H., 2018. OpenSeesPy: Python Library for the Opensees Finite Element Framework. SoftwareX 7, 6–11.https://doi.org/10.1016/j.softx.2017.10.009.

APPENDIX

Table A1. Ground motion records selected and scaled to UHS in Vancouver for NLRHA (employed in Chapter 3 and 4).

Record NO	Record ID in Ground motion database	Record type
1	2111	Crustal
2	2618	Crustal
3	2623	Crustal
4	3637	Crustal
5	4054	Crustal
6	4225	Crustal
7	4350	Crustal
8	5668	Crustal
9	5800	Crustal
10	5803	Crustal
11	5807	Crustal
12	78	Inslab
13	506	Inslab
14	880	Inslab
15	885	Inslab
16	2113	Inslab
17	2893	Inslab
18	3854	Inslab
19	4183	Inslab
20	4857	Inslab
21	5780	Inslab
22	6976	Inslab
23	3000395	Interface
24	3001964	Interface
25	4028568	Interface
26	4028592	Interface
27	6001228	Interface
28	6001373	Interface
29	6001811	Interface
30	6001823	Interface
31	6001824	Interface
32	6002707	Interface
33	6002719	Interface

Table A2. Ground motion records selected and scaled to CS in Vancouver for IDA of 3-storey prototype building (employed in Chapter 4).

Record NO	Record ID in Ground motion database	Record type
1	324	Crustal
2	3568	Crustal
3	510	Crustal
4	5284	Crustal
5	3027	Crustal
6	68	Crustal
7	3503	Crustal
8	602	Crustal
9	2619	Inslab
10	1294	Inslab
11	5780	Inslab
12	1286	Inslab
13	3679	Inslab
14	3674	Inslab
15	1427	Inslab
16	1288	Inslab
17	2615	Inslab
18	3640	Inslab
19	1292	Inslab
20	6059	Inslab
21	1258	Inslab
22	1315	Inslab
23	5267	Inslab
24	5291	Inslab
25	166	Inslab
26	3020	Inslab
27	999	Inslab
28	930	Inslab
29	570	Inslab
30	362	Inslab
31	3566	Inslab
32	3269	Inslab
33	6878	Inslab
34	990	Inslab
35	IWTH111103111446	Interface
36	YMTH071611220559	Interface
37	FKSH121103111446	Interface
38	IWTH281103111446	Interface
39	TCGH101103111446	Interface
40	YMTH141103111446	Interface

Table A3. Ground motion records selected and scaled to CS in Vancouver for IDA of 6-storey prototype building (employed in Chapter 4).

Record NO	Record ID in Ground motion database	Record type
1	1766	Crustal
2	2744	Crustal
3	1166	Crustal
4	3758	Crustal
5	1057	Crustal
6	902	Crustal
7	890	Crustal
8	602	Crustal
9	1281	Crustal
10	3649	Crustal
11	987	Crustal
12	1144	Crustal
13	1313	Inslab
14	884	Inslab
15	5776	Inslab
16	1260	Inslab
17	762	Inslab
18	1810	Inslab
19	6949	Inslab
20	3667	Inslab
21	1478	Inslab
22	3678	Inslab
23	1030	Inslab
24	324	Inslab
25	756	Inslab
26	3849	Inslab
27	352	Inslab
28	1436	Inslab
29	2383	Inslab
30	5588	Inslab
31	1829	Inslab
32	IWTH051103111446	Interface
33	HDKH061103111446	Interface
34	CHBH161103111446	Interface
35	YMTH141103111446	Interface
36	SITH031103111446	Interface
37	IWTH161103111509	Interface
38	IWTH111103111446	Interface
39	FKSH031103111446	Interface
40	HDKH070309260450	Interface

Table A4. Ground motion records selected and scaled to CS in Vancouver for IDA of 9-storey prototype building (employed in Chapter 4).

Record NO	Record ID in Ground motion database	Record type
1	1575	Crustal
2	1487	Crustal
3	1762	Crustal
4	1236	Crustal
5	68	Crustal
6	1043	Crustal
7	973	Crustal
8	5777	Crustal
9	5780	Crustal
10	352	Crustal
11	522	Crustal
12	1433	Crustal
13	1177	Crustal
14	3269	Crustal
15	835	Crustal
16	4893	Crustal
17	356	Crustal
18	508	Inslab
19	1282	Inslab
20	1450	Inslab
21	3278	Inslab
22	5796	Inslab
23	900	Inslab
24	1436	Inslab
25	1523	Inslab
26	1166	Inslab
27	6060	Inslab
28	IBRH171103111515	Interface
29	IWTH111103111446	Interface
30	FKSH161103111446	Interface
31	IKRH030309260450	Interface
32	HDKH020309260450	Interface
33	IWTH161103111446	Interface
34	TKYH121103111446	Interface
35	HDKH060309260450	Interface
36	CHBH161103111515	Interface
37	NIGH081103111446	Interface
38	NIGH021103111446	Interface
39	SITH031103111446	Interface
40	IWTH241103111509	Interface